TESIS DE LA UNIVERSIDAD DE ZARAGOZA
2022
1

Iris Plá Palacín

Ex vivo revascularization in liver bioengineering. A critical first step towards effective transplantation of bioengineered livers.

Director/es
BAPTISTA, PEDRO
GARCÍA AZNAR, JOSÉ MANUEL

ISSN 2254-7606

Prensas de la Universidad
Universidad Zaragoza

ISSN 2254-7606

Universidad Zaragoza
1542

Tesis Doctoral

EX VIVO REVASCULARIZATION IN LIVER BIOENGINEERING. A CRITICAL FIRST STEP TOWARDS EFFECTIVE TRANSPLANTATION OF BIOENGINEERED LIVERS.

Autor

Iris Plá Palacín

Director/es

BAPTISTA, PEDRO
GARCÍA AZNAR, JOSÉ MANUEL

UNIVERSIDAD DE ZARAGOZA
Escuela de Doctorado

2020

Biomedical Engineering PhD Program

Instituto de Investigación en Ingeniería de Aragón (I3A)

Ex vivo re-vascularization in liver bioengineering. A critical first step towards effective transplantation of bioengineered livers.

Iris Pla Palacín

Thesis to obtain PhD degree by Universidad de Zaragoza

March 2020

Director: Dr. Pedro M. Baptista

El desarrollo y ejecución de esta Tesis Doctoral se han enmarcado dentro de los proyectos de investigación: “Ex vivo re-vascularization in porcine liver bioengineering - A critical first step towards effective transplantation of bioengineered livers” y “Development of transplantable bioengineered human livers in immunodeficient pigs with acute liver failure”, financiados por el Instituto de Ciencias de la Salud Carlos III (PI15/00563 y PI18/00529, respectivamente). Iris Pla Palacín ha disfrutado de una beca i-PFIS: doctorados IIS-Empresa en Ciencias y Tecnologías de la Salud, financiada por el Instituto de Salud Carlos III, expediente IFI15/00158.

Asimismo, agradecemos la generosa aportación de los pacientes en el estudio y la colaboración del Instituto Aragonés de Ciencias de la Salud en el marco del Biobanco del Sistema de salud de Aragón y a la Fundación IIS Aragón, en el marco del personal del Hospital Clínico Universitario Lozano Blesa, pertenecientes al área de Anatomía Patológica y al grupo de Patología Digestiva.

ÍNDICE

AGRADECIMIENTOS

En primer lugar, quisiera agradecer al Dr. Ángel Lanas, porque sin ti no hubiera conseguido la beca predoctoral y probablemente me hubiera ido de Zaragoza. Y a Pedro, por confiar en mí desde el minuto cero, por saber calmarme en momentos de ansiedad y por haberme brindado todo el conocimiento científico del que hoy dispongo.

También a todos los profesionales que han colaborado con nosotros. A la Dra. Lourdes Bengochea y Emma Olmedo, del servicio de Anatomía Patológica del HCULB, que siempre que os he necesitado habéis estado dispuestas a dedicarme unos minutos. A los doctores Agustín García y Trinidad Serrano, por vuestro apoyo recibido con los trasplantes, así como a Pablo, Helen, Cristina, Aurora, Mamen, Marisa, Ricardo, Alicia y Luis, por todos los momentos de quirófano. A César y Mark, porque siempre habéis estado dispuestos a ayudarme en lo que fuera.

A mis Ciberos. Pilar, Natalia, Sofía, Eduardo, Samanta, María Jesús, Joana, Sara, Marisa, Ruth, Manuel, Daniela, Raúl y Nacho, último fichaje de la temporada. Por ser verdaderos compañeros de trabajo, de copas y cenas y por todas las risas y postres que nos hemos echado. Me ha encantado formar parte de este equipazo y no se puede pedir más!!!

A mi cuadrilla del Bajo Aragón. Por todas las escapadas, rutas con la bici, meriendas, noches de fiesta y desconexión. En especial a Jorge S. y David, por sacar tardes de vuestro tiempo para ayudarme con algunas figuras de este trabajo; y a Leo, Raúl, Jorge A. y Juan E., por esos ratillos que habéis dedicado a la ciencia.

A Pablo, por retransmitirme tu fuerza. Y a Elena, por mantener vivas las oficinas de Correos.

A mis padres y mi hermana, por vuestros sabios consejos y apoyo incondicional.. A Éder, por tu contribución con la portada.

En general, por todos los buenos momentos compartidos (han sido muchos) y por los ánimos en ciertas ocasiones.

¡¡¡MUCHAS GRACIAS!!!

RESUMEN

Hasta la fecha, el trasplante de hígado es la única opción disponible para pacientes con enfermedad hepática terminal. El problema es la gran falta de órganos para trasplante. Por lo tanto, nuevas terapias emergentes, como la medicina regenerativa y la bioingeniería de órganos, esperan resolver este problema de escasez. Sin embargo, hasta la fecha nadie ha podido generar hígados de bioingeniería que puedan ser trasplantados con éxito, debido a la falta de permeabilidad vascular lo que conduce a trombosis en el animal receptor.

Por lo tanto, el objetivo principal de esta tesis era el de generar una vasculatura ensamblada *in vitro* que fuera estable y funcional. Paralelamente, también hemos trabajado en la creación de un modelo animal de regeneración hepática, en el que las piezas de bioingeniería revascularizadas pueden ser trasplantados. Además, en colaboración con el grupo de investigación del Dr. Bart Spee y del Dr. Hans Clevers de la Universidad de Utrecht, probamos a sembrar hepatocitos derivados de células somáticas y células madre hepáticas adultas Lgr5 + en ECM descelularizada hepática, mejorando su destino y función hepática cuando se siembran en estos *scaffolds*. Esto puede permitir la posibilidad de obtener una fuente de células hepáticas que se puede expandir para obtener los grandes números requeridos para la bioingeniería de órganos, aumentando la complejidad estructural y anatómica de nuestros hígados de bioingeniería.

En resumen, estos resultados pueden proporcionar las herramientas necesarias (una vasculatura funcional estable, una nueva fuente de hepatocitos y un modelo animal para trasplante) para generar hígados de bioingeniería adecuados para su futura traslación a la clínica.

SUMMARY

To date, liver transplantation is the only available option for patients with terminal liver disease. The problem is the huge lack of organs for transplantation. Therefore, new emerging therapies such as regenerative medicine and organ bioengineering present hope to solve this problem of organ shortage. However, to date no one has been able to generate bioengineered livers that can successfully be transplanted, due to lack of vascular patency in these bioengineered organs, leading to thrombosis in the receptor animal.

Thus, the main objective of this thesis was to generate an *in vitro* assembled vasculature that was stable and functional. In parallel, we have also worked on the creation of an animal model of liver regeneration, in which the revascularized bioengineering grafts can be transplanted.

In addition, in collaboration with the research group of Dr. Bart Spee and Dr. Hans Clevers from the University of Utrecht, we tested seeding hepatocytes derived from somatic cells and Lgr5+ adult liver stem cells in liver decellularized ECM, enhancing their hepatic fate and function when seeded in these scaffolds. This may allow the possibility of obtaining a source of hepatic cells which can be expanded into the large numbers required for organ bioengineering, increasing the structural and anatomical complexity of our bioengineering livers.

In summary, these results can provide the necessary tools (stable functional vasculature, a novel source of hepatocytes and an animal model for transplantation) to generate bioengineered livers suitable for future translation into the clinic.

Prometheus myth and liver regeneration metaphor

According to Greek mythology, the Titan Prometheus, son of Iapetus and Clymene, was a great benefactor of humanity that did not fear any other god.

Thus, he tried to deceive Zeus by sacrificing a great ox that he divided into two parts: he put the skin, the flesh and the viscera in one of them, which he hid in the animal's womb; and he put in the other part the bones, covered with appetizing fat. He let Zeus choose which of the two parts would be tasted by the gods, opting for the fat layer. Such was his anger when he discovered that he had actually chosen the bones that he forbade men from fire.

Prometheus then challenged all the gods and climbed Mount Olympus to steal the fire from the forge of the Hephaestus himself, to return it to men on the stem of a reed, which burns slowly, so that they could warm up again.

This feat caused the wrath of Zeus, who wanted to punish him harshly. Thus, he had the titan taken to the Caucasus, where he was chained with the help of Hephaestus and Kratos and sent an eagle to devour his liver. This organ grew again every night, so the bird returned every day to fulfill its mission.

LIST OF ABBREVIATIONS

AA: abdominal aorta

AL: artificial livers

ALD: alcoholic liver disease

ALT: alanine aminotransferase

AST: aspartate aminotransferase

BAL: bioartificial liver

BM: bioreactor media

CV: central vein

CYP: cytochrome P450

DLD: decellularized liver disc

DM: differentiation medium

DPBS: Dulbecco's phosphate buffered saline

EC: endothelial cell

ECM: extracellular matrix

EGF: epidermal growth factor

EM: expansion medium

EPC: endothelial progenitor cell

ESC: embryonic stem cell

ESLD: end-stage liver disease

FBS: fetal bovine serum

FGF-2: fibroblast growth factor-2

FRG: Fah-/-/Rag2-/-/Il2rg-/y

GDA: gastroduodenal artery

H&E: hematoxilin and eosin

HA: hepatic artery

HEK-293T: human embryonic kidney cells

HGF: hepatocyte growth factor

hMSC: human mesenchymal stem cell

hUVEC: human umbilical vein endothelial cell

IGF-1: insulin growth factor-1

i-Hep: Hepatocyte-like cell

IM: induction media

i-PSC: induced pluripotential stem cell

IVC: infrahepatic inferior vena cava

K19: keratin 19

LDH: lactate dehydrogenase

MEFs: mouse embryonic fibroblasts

MM: maturation media

NAFLD: nonalcoholic fatty liver disease

P/S: penicillin / streptomycin

PDGF-BB: platelet derived growth factor B

PHx: partial hepatectomy

pMSC: porcine mesenchymal stem cell

pUVEC: porcine umbilical vein endothelial cell

PV: portal vein

RT: room temperature

SEP: study end point

SFSS: small-for-size syndrome

Sh: shunt

SMC: smooth muscle cell

SVC: suprahepatic inferior vena cava

Tx: transplantation

UC: umbilical cord

VEGF: vascular endothelial growth factor

VEGFR3: vascular endothelial growth factor receptor 3

WL: waiting list

INTRODUCTION

Human liver anatomy and function

The liver is the biggest gland in the organism, with an approximate weight of 1.2-1.5 Kg in the adult.

Externally, the liver is divided by the falciform ligament, which forms a larger right lobe and a smaller left lobe. Current functional anatomy is based on Couinaud's classification of the liver[1] (Fig. 1). According to this, it is divided into eight functional segments (segments II, III, IV, V, VIII, VI and VII) based upon the distribution of portal venous branches and hepatic veins in the parenchyma. These segments are independent among them, and each one has its own portal pedicle, formed by a hepatic arterial branch, a portal venous branch, a bile duct and also a hepatic venous branch which carries outflow blood.

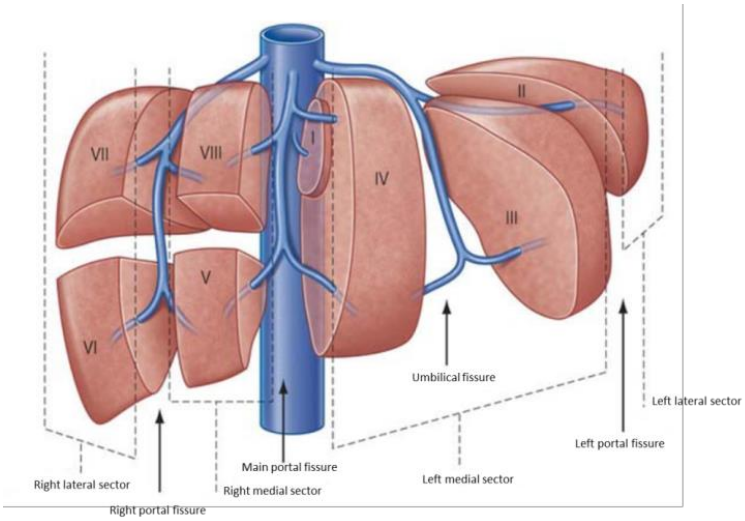

Figure 1. Sectors of the human liver. (Adapted from basicmedicalkey.com)

The liver plays a critical role in metabolic homeostasis. It is one of the most important organs due to functions like the regulation of the energetic metabolism that incorporates and processes the nutrients and distribute in a controlled way in the extra hepatic tissue. The liver also

synthetizes essential proteins, enzymes and cofactors needed in the digestion process and for the normal function of the organisms. It is also the main place for the detoxification and elimination of compounds, for the efficient incorporation of aminoacids, carbohydrates, lipids and vitamins and it storage, metabolic conversion and release to blood and bile.

Due to this metabolic role and secretion to blood stream, the liver is considered as a metabolic organ and exocrine gland. At the same time, due to its capacity for bile production and secretion, it is also considered as an exocrine gland.

This organ has the exclusive feature of receiving a double contribution of blood, reaching an approximately blood flow of 1,5L/min through the organ. The 80% of this blood comes from the portal vein, with a lower pressure and little oxygenation that provides the liver with all the nutrients from the gastrointestinal tract for its metabolism and elimination. The remaining 20% is arterial blood, coming through the hepatic artery, with a higher pressure and well oxygenated. The blood efflux is through the hepatic veins, which converge in the inferior vena cava, returning the blood to the heart. Both hepatic artery and portal vein bifurcate in branches into the hepatic tissue (like the portal venules and hepatic arterioles). Arterial and venous bloods finally converge at the sinusoid, which are capillaries surrounded by fenestrated endothelial cells (EC) that allow the transvascular interchange between blood and the parenchymal cells.

The functional morphologic unit is the hepatic lobule, with a hexagonal shape and organized around the central vein (CV). The inner part is

constituted by the hepatic cords, which are surrounding the CV. Hepatic sinusoids are between this cords and in the apexes of the hepatic lobule are located the portal trial (which is constituted by an hepatic artery, a portal vein and a bile duct). Repetitions if this functional unit constitutes the hepatic tissue (Fig. 2).

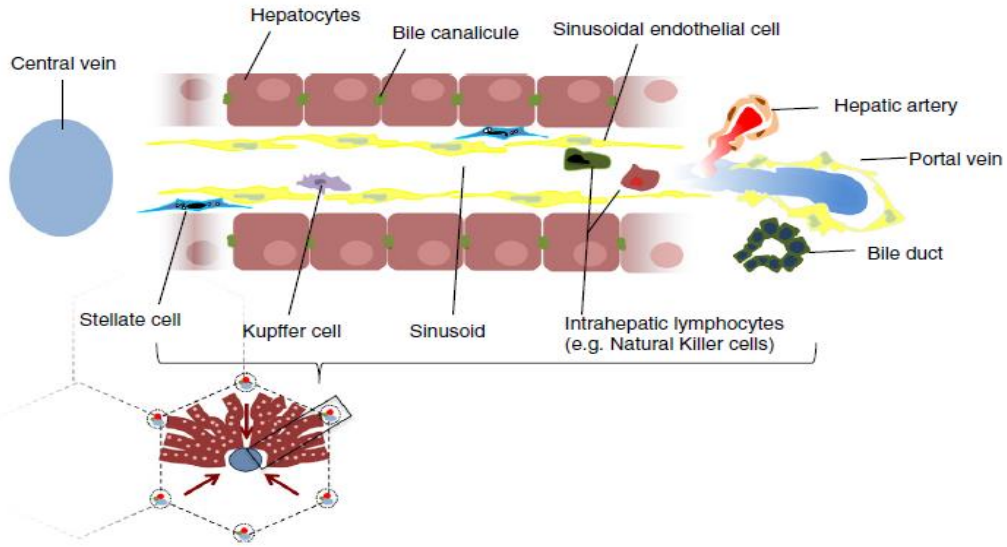

Figure 2. Hepatic acinus (extracted from Ebrahimkhani et al[2])

Liver is a very complex tissue, where there are different cells that coexist in the hepatic tissue: the parenchymal cells, which are the hepatocytes, comprising the 80% of the whole organ, and the non-parenchymal cells, comprising the remaining 20% that include the endothelial cells, ductular cells (cholangiocytes), kuppfer cells, stellate cells and Pit cells.

The biliary system is constituted by a complex of ramifications and channels (channels of Hering) that come together to the bile duct. Little is known about the route of these channels, but they are distributed close to portal tract, and they are partially surrounded by hepatocytes in one side and cholangiocytes in the other side. It has been postulated that

channels of Hering could be a stem cell niche in the liver[3] (Fig. 3). This is the place where, during the embryonic development, bipotential hepatoblasts form the primitive ductular plate, which have the same phenotype as progenitor cells in adults[4].

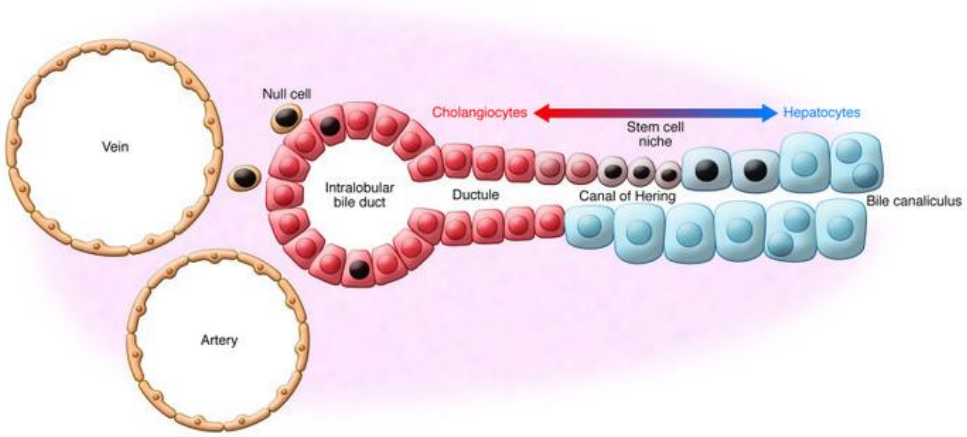

Figure 3. Model of hepatic stem cell niche in the channels of Hering (Extracted from Kordes and Häussinger[3]).

Liver disease

Liver disease means any condition that leads to liver inflammation and/or damage, affecting thus its normal function. It can be caused by many factors like infections, drugs or toxic compounds exposure, autoimmune processes or genetic malignances. The resulting effects include inflammation, scarring, blood clotting, bile duct obstructions and liver failure. The following table summarizes most liver diseases:

Table 1. Characteristics and causing agents of different hepatic diseases. Source adapted from AACC 2019[5].

Liver disease	Characteristics	Causing agents
Acute liver failure	Rapid decrease in liver function	Drugs, toxins, liver diseases
Alcoholic liver disease	Liver damage which can lead to fatty liver, alcoholic hepatitis or cirrhosis	Abusive alcohol intakes
Autoimmune liver disease	Body's immune system attacks liver cells	Primary biliary cirrhosis, autoimmune hepatitis
Biliary obstruction	Bile duct blocking	Trauma, tumors, inflammation
Cirrhosis	Liver scarring	Chronic hepatitis, alcoholism, chronic bile duct obstruction
Genetic diseases	Gene mutation	Hemochromatosis, Wilson disease
Hepatitis	Acute or chronic liver inflammation	Virus, alcohol, drugs, toxins
Infections	Can originate liver damage and/or bile duct blockage	Virus, parasites
Liver cancer	Abnormal growth of liver cells	Cirrhosis, chronic hepatitis, virus

Alcoholic liver disease (ALD) and non-alcoholic fatty liver disease (NAFLD) are chronic liver diseases with similar pathological responses, differing only in their etiology[6]. Patients with ALD abuse alcohol and NADFL patients are usually obese. Approximately one-third of the population in developed countries suffer from nonalcoholic fatty liver disease[7]. The first stage of these diseases is hepatic steatosis, where triglycerides begin to accumulate in unusual places, like hepatocytes, which can lead to

steatohepatitis, where hepatocytes dye because of ballooning. This stage presents also an inflammatory response and fibrosis. It can progress to cirrhosis, where hepatocytes present scar tissue due to the accumulation of collagen I, and end with the latest stage of cancer or hepatocellular carcinoma.

End-stage liver disease (ESLD) patients are those with cirrhosis presenting signs of irreversible liver decompensation, including hepatic encephalopathy, ascites, kidney impairment, lung issues and variceal bleed. In these cases, liver transplant means the only effective treatment. However, there is still a widening gap between available organs and patients waiting for liver transplant.

Liver disease causes approximately 2 million deaths per year worldwide: 1 million originated by cirrhosis complications and the remaining million because of viral hepatitis or hepatocellular carcinoma[8]. Cirrhosis is the 11th common cause of death worldwide with 1,16 million of global deaths per year. Liver cancer represents the 16th most common cause of death, with 788.000 global deaths[9].

Global data analyzed from 1990-2010 suggest that Latin America, Caribbean, Middle East and North Africa have the highest percentage of deaths due to liver disease. Egypt, Moldova and Mongolia have the highest cirrhosis mortality rate in the world. India represents a 18,3% of cirrhosis death in the world, followed by China with a 11%. Increasing mortality has been observed in Central Asia, the Russian Federation and Europe.

Almost any chronic liver disease leads to cirrhosis. Globally, the main causes are hepatitis B and C virus and alcohol. Other causes can be

immune liver diseases, drugs, cholestatic disease, among others. The causes vary among different countries: in Western and industrialized countries, alcohol and non-alcoholic fatty liver disease are the leading causes; whereas hepatitis B is the main cause in developing countries[9-11].

According to the Spanish Registry of Hepatic Transplant (RETH), during 2016 in Spain, the main base diseases in patients suitable for liver transplant were hepatocellular cirrhosis (52,2%), hepatocarcinoma (28,4%), cholestasis disease (8,1%), metabolic disease (3,2%) and acute/subacute liver failure (4,7%), among others. The waiting list evolution in Spain for the same year was as follows: from 2115 of total patients, 233 were excluded for different reasons (11%), 78 dead (3,7%) and 1159 received a donor liver (54,8%). A total of 645 patients (30,5%) were included in the waiting list of the following year 2017.

Globally speaking, the following tables recapitulate worldwide data from liver transplant in 2017 (data obtained from the Newsletter Transplant):

Table 2. Number of liver transplantations across the world

Country	Number of transplanted livers
Australia	282
Canada	585
European Union	7.984
Latin America	3.288
New Zealand	55
Russian Federation	438
Saudi Arabia	226
United States of America	8.082

The following table summarizes the number of global patients in the waiting list (WL) for a liver transplant and the number of patients who dead in 2017 (data obtained from the Newsletter Transplant):

Table 3. Number of patients waiting for a liver transplant and number of exitus.

Country	Nº of patients active on the WL	Nº of patients who dead on the WL
Australia	482	11
Canada	-	74
European Union	16.064	990
Latin America	8.112	1.087
New Zealand	-	-
Russian Federation	1.666	141
Saudi Arabia	658	-
United States of America	24.178	1306

Organ availability

Currently, liver transplantation is still the only effective treatment option for patients suffering from end-stage liver disease, acute hepatic failure and hepatocellular carcinoma. Despite the fact that short-term graft and recipient survival outcomes have improved thanks to advancements in the surgical technique, in the perioperative management and in the immunosuppressive therapy, there are still two main limitations in liver transplantation. The first one and the most important is organ shortage, as mentioned above. That is why big efforts are being developed to increase the existing scarce donor pool. This effort has derived in the use of liver allografts from donors after cardiac death in combination with extended criteria donors. The goal is to get a better selection of donors, selecting not only the most adequate ones, but has also helped in the

development of mechanical perfusion strategies[12]. The second limitation is long-term recipient's complications after liver transplantation. Infections, allograft failure, cardiovascular events or renal failure are the most common causes of later mortality after liver transplantation, which derive from long-term immunosuppression[13]. To maximize results, important efforts are being doing to improve recipient's long-term outcomes.

Due to organ shortage, it becomes necessary to find alternative therapies to treat liver failure. Extracorporeal liver support systems for patients suffering from liver failure consist on temporary systems developed to speed up liver recovery from injury or as a bridge to transplantation. There are two types of devices for temporal support: artificial livers (AL), which use non-living components to remove toxins accumulated in blood or plasma due to liver failure, using membrane separation associated with columns or suspension sorbents. On the other hand, bioartificial liver (BAL) provide not only liver detoxification but also synthetic functions, by combining chemical procedures and bioreactors containing cells to maintain the liver function[14].

Appropriate cell choice for BAL devices is still under investigation. Primary human hepatocytes represent the ideal source for replacing liver function, but they still are difficult to maintain *in vitro*. Primary porcine hepatocytes, on the contrary, suppose large quantities availability, with the immunologic and infectious problems they carry. This is why human or human-derived cells are more desirable.

Other cell types investigated are immortalized cells (like C8-B[15], HepZ[16], HH25[17]), which are easily cultivated *in vitro* and maintain liver-specific

functions. Their problem still resides in their potential transmission of oncogenic substances to the patient[14,18].

Up to date, BAL are still under investigation. Despite some of them have FDA clearance to perform clinical trials (like HepaMate, ELAD or Excorp Medical) there is still a lot to improve regarding their capacity to provide and replace liver functions. There are still important issues that have to be overcome, like cost, cell availability or maintenance of cell viability that have delayed their appearance on the clinic.

Split livers represent another choice. This technique means a way to increase the number of cadaveric donor organs for children and adults: it provides a left lateral (to be transplanted into a child) and a right extended liver graft (to be transplanted into one adult). Furthermore, the outcomes showed comparable results as those in whole organ liver transplantation[19]. Nevertheless, the main problem with split livers resides in that it is a complex variant of liver transplantation that requires a very high level of technical and logistical skills and an extensive knowledge of possible anatomic variations; it also needs a reliable judgment on graft quality and also an optimal graft-recipient size match (in order to avoid the small-for-size liver syndrome, SFSS).

However, in the latest years, new technologies like organ and tissue engineering have emerged not only to maintain liver function during injury, but for the creation of new organs *in vitro* able to be transplanted. Another potential alternative to liver transplantation is allogeneic hepatocyte transplantation[20,21] with the aim to restore the hepatic function once engrafted in the recipient's liver. Hepatocytes can be isolated from different sources: whole donor livers unsuitable for

transplant, from liver segments after split liver transplantation or from neonatal and fetal livers (which could provide very high hepatocyte quality). The advantages of this techniques include the fact that it is less invasive and less expensive than a surgery; it can be performed repeatedly if necessary; cryopreserved cells are available when necessary and like this procedure requires few cell quantities, different recipients could beneficiate from the same donor organ. On the contrary, the limitations reside in the difficult in isolating and *in vivo* maintaining of high-quality hepatocytes[22,23]. Liver cell engraftment is usually poor (approximately 0,1-0,3%)[24] and allogeneic rejection may be the main cause of failure in cell graft function.

Mesenchymal stem cells (MSC) cells are other important source to take into account. They are an attractive source due to their capacity to proliferate and differentiate *in vitro* and their anti-inflammatory and immune status[20]. Furthermore, there are several tissues containing hMSC: bone marrow, adipose tissue and umbilical cord. Some authors have recently isolated MSCs from liver too, called liver-derived human MSCs, which can be transdifferentiated towards hepatocyte-like cells[25]. However, they are still under investigation in the role of these cells in liver recipient repopulation and providing a satisfactory hepatic function.

Organ engineering is becoming a very promising new emerging technology. Combining engineering techniques and biology, the goal is to cope with organ shortage and organs for transplantation, creating autologous organs *in vitro* able to be transplanted. Eliminating thus the problems of organ donor, waiting list and rejection. Tissue engineering or regenerative medicine combines cells, engineering and materials for the creation of biological tissues viable for medical purposes. Advances in

whole organ decellularization techniques had allowed the obtaining of extracellular matrix (ECM) scaffolds suitable for organ engineering derived from many tissues like heart, lung, kidney, liver and pancreas[26]. The challenge is now in finding an adequately and efficiently recellularization method of these scaffolds, in order to create complete and functional organs.

Liver bioengineering

Recent studies demonstrate the need to replicate the liver structure and physiology observed *in vivo*, in order to get all its functions *in vitro,* trying to represent the cellular microenvironment *in vitro*. This microenvironment, or niche, plays a critical role in the stem cell regulation of survival, renewal and differentiation, as well as in the adult cell maintenance and function. The key components of this niche are the growth factors, cell-cell contacts and cell-ECM interactions.

Hepatic tissue engineering and cell-based therapies were considered as alternatives to liver transplantation, but there are no proven effective clinical success up to date[27,28]. With this necessity became the idea of whole organ engineering, with the main goal of the generation of biological substitutes to restore or maintain organ function in disease people. This could allow not only the generation of autologous organs ready for transplant, but also could remove organ rejection and help avoiding the big current problem of organ shortage, decreasing the number of patients in the waiting list and speeding up their health recovery, eliminating the need of immunosuppression. For this purpose of organ replacement, it is crucial to develop appropriate supporting

biomaterials that replicate the *in vivo* microarchitecture in an ex vivo setting. That is why the identification of the appropriate cells and scaffold are essential parameters to pursue.

Hence, there are two main components in whole-organ engineering: 1) a scaffold or support for cell attachment and growth and 2) tissue-specific cells, cultured with defined and specific culture medium.

1. Scaffold

Scaffolds can be defined as structures that guide or support cells for the growth of new tissue. They need to accomplish different requirements, which include: 1) biocompatibility: cells must adhere, function and migrate normally through the scaffold; 2) biodegradability: scaffolds or constructs are not permanent implants, they must degrade in tandem with tissue formation and by-products of this degradation should be non-toxic; 3) mechanical properties: scaffolds need to have enough mechanical properties consistent with the anatomical site of implantation; 4) scaffold architecture: scaffolds should have a highly porous structure to ensure cell penetration and diffusion of nutrients to the cells within and 5) manufacturing technology: scaffold generation should be cost effective, with the possibility of being scaled-up[29].

Scaffolds can have two different origins, artificial or natural, depending on the materials employed in their generation.

Artificial constructs include ceramics, such as hydroxyapatite and tri-calcium phosphate, mainly used in bone regeneration applications due to their chemical and structural similarities with the bone mineral phase.

Their limitations in clinical applications consist on their brittleness and difficulty of shaping for implantation. Synthetic polymers have also being studied, including polystyrene, poly-l-lactic acid (PLLA), polyglycolic acid (PGA) and poly-dl-lactic-co-glycolic acid (PLGA). In this case, the limitation is their high risk of rejection because of their poor bioactivity.

On the other hand, natural scaffolds employ biological materials like collagens, proteoglycans, alginate[30], chitosan[31] or hyaluronic acid for the scaffold generation. These materials present the advantages of low cytotoxicity and high biodegradability and biocompatibility properties. The main disadvantage is the difficulty in the creation of biological materials with homogeneous and reproducible structures.

Bioprinting is another novel technology consisting on printing programs that allow a very accurate detail positioning of living cells, layer by layer, within a 3D scaffold of biocompatible material like alginate or gelatin[32]. The advantage of this technique in the area of tissue engineering resides in its highly specific cell concentration and placing, making possible the generation of complex organs *in vitro*[33]. Other studies use bioactive organ-specific hydrogel bioinks to encapsulate primary cells. In this research, they used decellularized ECM-based solutions which were then incorporated into liver-specific bioink for the creation of *in vitro* liver constructs[34].

However, the role and importance of the ECM has considerably increased in the last two decades. It is not only an inert substrate where cells just grow, but it is considered today as a dynamic entity composed of many structural, chemical and functional components, conferring specific biophysical, biomechanical and biochemical properties[35]. Apart from

being structural support, the ECM also constitutes a reservoir of growth factors and other bioactive molecules, being implicated in the regulation of their availability[36]. It also plays an important role in cell attachment, growth and differentiation. And, the most important thing: it recapitulates the biochemical and architectural complexity of a fully assembled natural ECM microenvironment. With all these, it has been demonstrated that the ECM has a direct consequence with organ functions[37] , representing an excellent biomaterial for organ and tissue engineering.

That is why in recent years, natural ECM scaffolds are widely chosen for organ bioengineering, acting like delivery systems of growth factors, adhesion peptides and cytokines. This ECM is obtained from cadaveric organs (from human perished non-transplantable organs or from pigs, rats, ferrets…), after being decellularized and contain the essential bioactive signals (growth factors) that are vital for cell viability, attach and differentiation, difficult parameters to replicate *in vitro*. For this purpose os scaffold obtaining, organs are perfused with detergents in order to remove the entire cell content. The result is a non-immunogenetic 3D native ECM that preserves its micro and macro architecture, the vascular network and the biliary duct (in the case of the liver)[38,39].

The decellularization process is a technique that usually combines chemical (detergents, salts)[40], biological (enzymes)[41] and physical agents[42] (mechanical agitation, freezing/thawing cycles) to enhance the effectiveness of full cell removal from the native tissue[43,44]. This technique was first attempted in a solid organ by Ott et al[39] in 2008[26,32], with the decellularization of rat hearts. It is widely accepted that a good

decellularization process have <50 ng dsDNA/mg tissue (dry weight); the fragments length of DNA are <200bp and there is no nuclei presence in DAPI or hematoxilin and eosin (H&E) stainings[43,44]. Hence, ECM components like collagens, laminins, fibronectin, proteins and growth factors should be preserved too, in order to maintain the ultrastructure and provide spatial orientation for the cells during the recellularization process[26], as well as cell differentiation, proliferation and migration. The goal of obtaining a functional or effective ECM scaffold is to eliminate the maximum cell content while preserving the major ECM structure and composition. After decellularization, the vascular tree ultrastructure should be preserved too, a crucial aspect for further recellularization[38,45].

This is why it is very important to choose an appropriate decellularization protocol, depending on the tissue, in order not to affect matrix stiffness due to cell removal and damage the ECM components. Each decellularization technique alters the ECM components, so the use of inadequate detergents or decellularization techniques can damage the ECM 3D structure and components. There must be a balance in the decellularization process: poor detergent concentrations or low times lead to inefficient cell removal (maintaining thus the immunogenicity of the scaffold, driving to inflammatory responses during recellularization and/or after implantation). On the other hand, higher detergent concentrations and times of exposure drive to ECM disruption. Many researches coincide in doing freeze-thawing cycles prior to liver decellularization. The osmotic response and the ice crystals formation in the rapid thermal change accelerate cell lysis process[46] without affecting the ECM mechanical properties[47].

For liver decellularization, portal vein, hepatic artery, hepatic veins or combination of them are used to perfuse the detergent solutions. The following table cites some works performed by different groups for liver scaffold obtaining (Table 4).

Table 4. Liver decellularization techniques carried out by different authors

Reference	Decellularization technique	Animal model
Lang et al.[48]	Freeze-thaw; immersion and agitation 2% Triton X-100	Pig
Mattei et al.[49]	Freeze-thaw; immersion and agitation; 1% Triton X-100, 0,1% Triton X-100	Pig
Pla-Palacín et al.[50]	Freeze-thaw; Portal vein and hepatic artery perfusion (25mmHg) 1% Triton X-100 + 01% ammonium hydroxide	Pig
Mazza et al.[51]	Freeze-thaw; portal vein perfusion (0,2-0,3ml/min) 0,025%Trypsin-EDTA, 0,01-1% SDS, 3% Triton X-100, 1%SDS	Human
Geerts et al.[52]	Freeze-thaw; portal vein perfusion (1,2 ml/min) 0,01% SDS, 0,1% SDS, 0,2-0,5% SDS, 1% Triton X-100	Rat
Baptista et al.[38]	Freeze-thaw; portal vein perfusion (5ml/min) 1% Triton X-100 + 0,1% ammonium hydroxide	Mouse, rat, ferret, rabbit, pig.

Once the scaffold is ready, it must be sterilized prior to cell seeding. This sterilization process varies among authors, which include the use of peracetic acid, X-ray, gamma irradiation, ethylene oxide, glutaraldehyde or e-beam[27,53].

2. Cells

As mentioned before, for organ recellularization it is important to mimic the *in vivo* tissue niches. For this, appropriate cell sources are necessary, as well as optimal seeding methods and culture medium, in order to achieve complete organ regeneration able to be transplanted. A heterogeneous microenvironment *in vitro* allows mimicking a physiologically and anatomically healthy liver, providing the necessary stimuli for the generation of a developed organ *in vitro*, due to the synergy of the individual compartments like epithelia, mesoderm, parenchyma and vasculature[54,55]. However, complete organ recellularization is a very complex task, especially human or pig-sized livers. The process requires not only many cell types (parenchymal and non-parenchymal cells) but also requires a very large cell numbers. This is actually a current main limitation. It is estimated that a healthy 70kg-human contains about 100 billion hepatocytes[56]. Up to date, the production of such enormous numbers of cells is still difficult considering the our technical capabilities. Due to this process, the generation of a human-scale organ would still require a long time to be completed. Some authors limit this technique to those patients with chronic organ failure, because acute liver failure patient survival wouldn't have the necessary time to wait for the whole process of liver bioengineering[57].

The most sought cells are from autologous source, because patient-derived cells have lower risk of triggering the host immune response[43].

Allogenic cells are another source of cells, obtained from discarded cadaveric livers. However, the disadvantage of using them is their high capacity for triggering host immune responses. However, another limitation is the difficulty in growing primary hepatocytes *in vitro*, because they do not divide in culture. That is why many authors choose fetal liver cells or induced pluripotential stem cells (iPSCs) as the best candidates for their obtaining[58,59]. iPSCs can be differentiated into hepatocyte-like cells that express typical hepatocyte markers such as urea or albumin using viral vectors and activated cell mediators. That is why there are some concerns about their potential tumorigenic risk. Therefore, there is still much to research to do regarding this. Another way of hepatocyte obtaining is their production from fibroblasts (iHep cells). Xenogenic cells, like primary porcine hepatocytes, present the great advantage of being an unlimited source. The main issues regarding the use of these cells are severe immune rejection and potential zenozoonosis. However, some authors[60,61] are investigating the way to characterize the immune reaction caused, suggesting these cells as future option for human whole organ engineering[43].

Achieving a functional vascular tree is also critical for the communication of the organ with the rest of the body. It performs very important roles like oxygen and nutrient delivery, blood coagulation modulation, anastomosis promotion to the host vasculature and inflammatory cells transportation[62]. The ideal scenario would be to develop protocols for the development of endothelial layers, allowing the formation of different vessel sizes with vasomotility, perfusion and different endothelial patterns (normal or sinusoidal). However, it still represents a significant bottleneck nowadays[55]. Network of complex vessels are

composed of different interacting cell types: the endothelial cells, which line the vessel wall, and the perivascular cells (mainly pericytes and smooth muscle cells), which surround the endothelial cells. hUVECs (human vein endothelial cells) represent the most used cells for scaffold re-endothelialization, due to their easily isolation from umbilical cords and easy culture *in vitro*. However, it has been demonstrated that hUVECs alone are not able to form vessels, showing short long-term survival. That is why they are usually co-seeded with hMSC (human mesenchymal stem cells)[63], because they support endothelial cells and secret cytokines and chemokines that help in vascular maturation[26]. Endothelial progenitor cells (EPC) can also be easily isolated from peripheral blood, umbilical cord or bone marrow and represent another potential source of autologous cells in vasculogenesis[64,65]. iPSCs have also been studied as a source of endothelial cell. However, and as mentioned before, there are still concerns about their tumorigenic potential. To solve this, Ginsberg et al developed a method to direct convert somatic cells into a stable and expandable population of endothelial cells without the use of pluripotency factors[66].

Pericytes, like MSCs or smooth muscle cells, are important cells in the process of stabilize vessels formation during angiogenesis[67]. Vascular smooth muscle cells (SMCs) represent the main difference between microvasculature and larger vessels, delivering vasomotility and contributing to biomechanical blood flow response in veins and arteries. Neff et al demonstrated that co-seeding SMC and EC can provide advantages in arterial reconstruction when compared with vessels engineered with EC alone[68].

It is important to maintain and mimic the original tissue characteristics of the cultured cells, like viability and function preservation, without the induction of immunogenic responses, illnesses or tumor development[69].

3. Recellularization

Recellularization is the repopulation of the acellular ECM scaffold with specific cell types, which have been cultured and expanded *in vitro*, in order to reconstitute the organ microanatomy and restore its function.

As said before, it is important to mimic the liver physiological conditions to achieve a successful ECM recellularization. The ideal would be the scaffold seeding with all the cell types that comprise a native organ, however, up to date this is not yet completely feasible.

Once the cells are grown in desired numbers and the liver ECM is ready, bioreactor systems are assembled for ECM recellularization in a dynamic way, usually for long-term culture conditions (1-4weeks). With this, bioreactors try to mimic the complex mechanisms occurring *in vivo* during organ development. They allow monitoring real time parameters like temperature, pH, gases (O_2, CO_2), and glucose, lactate and electrolyte levels. As well as perfusion parameters like pressure or flow conditions[26]. Particularly in the liver tissue, it is important to monitor albumin or urea secretion as well.

Regarding recellularization, liver ECM can be seeded through multiple vascular routes: portal vein, hepatic artery, hepatic veins (supra hepatic inferior vena (SVC) cava and infra hepatic inferior vena cava (IVC)) and bile duct. Despite the fact that seeding methods depend on each organ,

more promising results were obtained when using different seeding routes, including different cell infusions and different cell types[26]. It is important to take into account that the more recapitulation of the intrahepatic organization observed *in vivo*, the best results will be obtained *in vitro*. That is why multi type cell seeding is desirable, due to cell capacity to interact with their same type of cells, with another cells present in their niches and with their surrounding ECM.

Uygun et al developed one of the first approaches of transplantation of whole bioengineered liver grafts[70]. In this research, they decellularized a whole rat liver and recellularized it with primary rat hepatocytes via portal vein, introducing $12{,}5x10^6$ cells in perfusion circulation. Afterwards, they added microvascular endothelial cells to the hepatocyte-repopulated graft, which was continuously perfused for 5 days. They observed that the endothelial cells lined the vasculature and encircled the hepatocytes, as well as hepatocytes remained viable. Finally, this bioengineered liver graft was auxiliary liver transplanted into a living rat, connecting the renal vein and artery to create blood flow and maintained for 8h *in vivo*. However, this work has some limitations: 1) hepatocytes were not able to spread within the scaffold due to the flow rate delivery, however, a higher flow rate would translate into hepatocyte aggregation and vessel clotting; 2) after graft transplantation into the living animal, it was rejected due to vascular thrombosis[32].

Soto-Gutiérrez et al tested three different ways, seeding the acellular scaffolds with murine hepatocytes[28]. The first one is direct cellular injection into the organ parenchyma. The second one is continuous perfusion, where the cells are suspended in the culture media and allowed to recirculate through a closed system which contains the ECM.

The third one is multistep infusion, were cells are directly infused into the ECM, in a closed circuit at different steps with 10-15 min intervals. They determined that the better engraftment efficiency was obtained in the multistep infusion protocol compared with direct injection or pump perfusion. However, this study failed in the adequate scaffold re-endothelialization before hepatocyte seeding. As a result, platelet activation is triggered after exposure to systemic circulation, because of the exposure of zones in the ECM which are still nude (without cell attachment)[32].

Afterwards, Baptista et al[38] determined the engraftment of fetal liver cells in co-culture with hUVECs in ferret liver scaffolds which were then seeded through two different sites: 1) through the portal vein, which allowed cell penetration to the capillary level; and 2) through the vena cava, allowing the cells to repopulate large and medium size vessels. With this, they determined the key importance of cell perfusion within the scaffold.

Currently, the creation of functional organs ready for transplant has not been achieved yet, but there are many research groups around the world working in other organs like heart[39], lung[71,72], pancreas[73,74] kidney[75] and intestine[76]. The main common problem is the lack of a functional and patent vascular tree for transplantation. However, up to date, a complete re-endothelialization covering the whole vascular tree from the main branches to the capillaries has not successfully been achieved. The main problem is *in vivo* clotting, due to the existence of areas of ECM which are not covered by cells.

This is the reason why there are several researchers that perfuse the ECM with antithrombotic and covering reagents (like heparin or gelatin) in order to decrease residual exposed ECM areas[77,78]. For example, Bao et al tested heparinized scaffolds prior to cell seeding, in order to reduce platelet activation and adhesion, and with this, thrombosis after bioengineered graft transplantation[79]. Other studies of Bao et al[80] and Hussein et al[78] made great advances in the creation of vascular trees *in vitro*, enhancing blood perfusion *in vivo* using heparin immobilized scaffolds. However, long-term perfusion was not successfully achieved, and vascular patency was lost 3 days after implantation into living animals[55].

Table 5 summarizes some of the protocols developed by different authors for whole-organ recellularization, using livers from different animal, types of cells used, time of *in vitro* culture and *in vivo* transplantation:

Table5. Different whole liver recellularization techniques developed by different authors in the last 10 years. Modified from Mazza et al[32].

Author	Liver specie	Cell source	*In vitro* culture	*In vivo* Transplan-tation
Uygun et al [70]	rat	Rat hepatocytes	1 week	8h
Baptista et al [38]	ferret	Human fetal liver cells + hMSC	1 week	-
Barrakat et al [81]	pig	Human fetal stellate cells + human fetal hepatocytes	2 weeks	-
Yagi et al [82]	pig	Porcine hepatocytes	1 week	-

Kadota et al [83]	rat	Rat hepatocytes + rMSC	1 week	1h
Ko et al [84]	pig	mUVECs	3 days	24h
Hussein et al [78]	pig	HepG2+hUVECs	10 days	1h

4. Culture media

Another key factor to consider when designing the bioreactor system for organ bioengineering is the appropriate definition of the culture media. This will contain nutritional supplements, minerals, growth factors, proteins, antibiotics and/or antimycotics in order to simulate the organ microenvironment. Due to the complexity of generating a new organ *in vitro*, which need different cell types, it is also important to define a "universal" culture media, able to sustain the growth of the different cell types that constitute the entire organ. Growth factors are important signaling molecules (mostly proteins) that direct cells during fetal development and in adult organisms. Their role is to control cell growth, migration and differentiation[36] and they are always required in the culture media.

Thesis aim

Despite the fact that considerable work has been done in the last decade related to liver bioengineering, there is still no whole bioengineered organs suitable for transplantation. As described above, most of the engineered tissues up to date still lack functional and patent vascular endothelialization, with the result of blood leaking and coagulation after graft anastomosis to the recipient model.

The work developed on this thesis sought to re-vascularize liver ECM, in order to achieve a functional and patent vascular tree for long term (1 month) after transplantation into a novel porcine model paving the way for further scaffold recellularization with all liver cell types, in order to get functional organs for transplantation (Fig. 3).

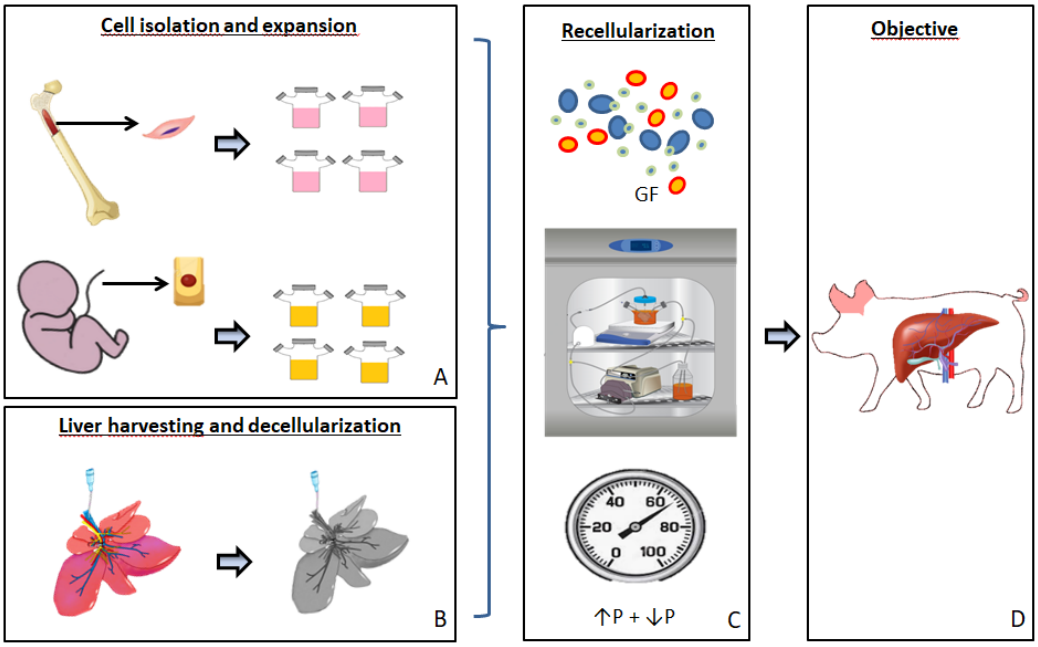

Figure 4. Schematic representation of the whole process of liver bioengineering developed in this thesis work. The process started with **A)** isolation, growth and long-scale cell production; and **B)** liver harvesting and decellularization to obtain the scaffold ECM. **C)** Once these components were ready, they were assembled in the bioreactor system for scaffold recellularization, where culture medium and pressure conditions were used in order to achieve a re-endothelialization of the vascular tree. **D)** Once this bioengineered liver was produced, it meant to be transplanted into our defined porcine model of liver regeneration.

Objectives

1. Scaffold and cell isolation

First, it was necessary to optimize a rat liver decellularization protocol. For this, different flow rates for detergent perfusion were tested in the

decellularization process, in order to determine the most appropriate that allowed better scaffold vascular preservation.

Parallel to scaffold preparation, different human cells were isolated and expanded *in vitro* at large scale, for further seeding in the scaffolds in the bioreactor system.

2. Scaffold seeding

Once we had established an optimal liver decellularization protocol and we had the necessary large number of cells, the second goal was to achieve complete cell penetration and homogenous distribution across the scaffold. For this, different pressure conditions were tested for cell seeding within the scaffold, always combining a lower pressure with a higher pressure. For this, short-term bioreactor systems of 3 days were performed, where GFP and RFP-labeled cells were seeded into the scaffolds. Indeed, different seeding methods were also tested.

Once all pressure conditions were performed, different analyses were carried out to determine the best pressure conditions for scaffold recellularization, allowing us to establish the most optimal seeding method.

3. Scaffold re-vascularization

Once the seeding method was optimized and we knew how to seed the cells within the scaffold, the next goal was to achieve their organization into vascular structures. For this, longer experiments in the bioreactor

systems were performed, moving from the previous 3d-bioreactors to 14d-bioreactors, where different culture media were tested and compared, in order to establish the most promising one in the revascularization process. These culture media contained specific growth factors which tried to mimic the angiogenesis and vasculogenesis environment.

4. Extrapolation of these results to decellularized porcine livers

Previous experiments were all done using rat livers, due to their smaller size and easy decellularization and recellularization. Once the techniques of scaffold seeding and scaffold revascularization were optimized in rats, results were meant to be extrapolated to 2kg piglet livers, where only the right lobe was employed (to minimize scaffold volume).

Furthermore, we were able to collaborate with the laboratories of Dr. Bart Spee and Dr. Hans Clever of the Hubrecht Institute (The Netherlands), which were able to generate hepatocyte-like cells generated by direct reprogramming from murine somatic cells which were then cultured in decellularized liver ECM[85]. Results from another collaboration with the same group revealed a novel strategy for large-scale *in vitro* expansion of Lgr5+ adult stem cells which preserve their capacity of differentiation both into hepatocyte- and cholangiocyte-like fates. This would represent an advantage for further seeding of these cells into our decellularized ECM in order to get more complex *in vitro* structures, mimicking even more the physiological liver structure and environment.

5. Development of a novel porcine model of auxiliary heterotopic liver transplantation and regeneration

A novel porcine animal model was created in order to induce liver regeneration after auxiliary heterotopic graft transplantation. For this, a portocaval shunt was performed in the recipient pig, which would then receive the graft transplantation in a manner that this graft received most of the recipient's portal blood, which carries all the hepatotrophic molecules and humoral factors involved in liver regeneration.

6. Bioengineered liver transplantation into our defined animal model

The final goal was to achieve a complete and functional vascular tree in the right-lobe of piglet livers, which were then transplanted into our novel porcine model. Once the bioengineered livers were successfully re-endothelialized, the goal was to test their functionality after transplantation in our porcine model.

As a result of this work, we isolated high quality primary cells and scaffolds for transplantation, efficient scaffold colonization and re-vascularization thanks to the bioreactor processes developed, achieving a bioengineered vascular network where large, intermediate and small vessels were created *in vitro*.

Furthermore, despite the need to optimize the anticoagulation protocol used in our pigs post-transplantatio, we believe that we have established a novel animal model for the adequate transplantation of bioengineered livers, enhancing their regeneration capacity *in vivo*.

BIBLIOGRAPHY

1. Couinaud, C. [Liver lobes and segments: notes on the anatomical architecture and surgery of the liver]. *Presse Med* **62**, 709-712 (1954).
2. Ebrahimkhani, M.R., Neiman, J.A., Raredon, M.S., Hughes, D.J. & Griffith, L.G. Bioreactor technologies to support liver function in vitro. *Adv Drug Deliv Rev* **69-70**, 132-157 (2014).
3. Kordes, C. & Haussinger, D. Hepatic stem cell niches. *J Clin Invest* **123**, 1874-1880 (2013).
4. Roskams, T. Different types of liver progenitor cells and their niches. *Journal of hepatology* **45**, 1-4 (2006).
5. AACC. (https://labtestsonline.org/conditions/liver-disease 2019).
6. Singh, S., Osna, N.A. & Kharbanda, K.K. Treatment options for alcoholic and non-alcoholic fatty liver disease: A review. *World J Gastroenterol* **23**, 6549-6570 (2017).
7. Cohen, J.C., Horton, J.D. & Hobbs, H.H. Human fatty liver disease: old questions and new insights. *Science* **332**, 1519-1523 (2011).
8. Mokdad, A.A*., et al.* Liver cirrhosis mortality in 187 countries between 1980 and 2010: a systematic analysis. *BMC Med* **12**, 145 (2014).
9. Asrani, S.K., Devarbhavi, H., Eaton, J. & Kamath, P.S. Burden of liver diseases in the world. *J Hepatol* **70**, 151-171 (2019).
10. Lozano, R*., et al.* Global and regional mortality from 235 causes of death for 20 age groups in 1990 and 2010: a systematic analysis for the Global Burden of Disease Study 2010. *Lancet* **380**, 2095-2128 (2012).
11. Lim, Y.S. & Kim, W.R. The global impact of hepatic fibrosis and end-stage liver disease. *Clin Liver Dis* **12**, 733-746, vii (2008).
12. Jadlowiec, C.C. & Taner, T. Liver transplantation: Current status and challenges. *World J Gastroenterol* **22**, 4438-4445 (2016).
13. Watt, K.D., Pedersen, R.A., Kremers, W.K., Heimbach, J.K. & Charlton, M.R. Evolution of causes and risk factors for mortality post-liver transplant: results of the NIDDK long-term follow-up study. *Am J Transplant* **10**, 1420-1427 (2010).
14. Carpentier, B., Gautier, A. & Legallais, C. Artificial and bioartificial liver devices: present and future. *Gut* **58**, 1690-1702 (2009).
15. Cai, J*., et al.* Construction of a non-tumorigenic rat hepatocyte cell line for transplantation: reversal of hepatocyte immortalization by site-specific excision of the SV40 T antigen. *J Hepatol* **33**, 701-708 (2000).

16. Werner, A.*, et al.* Cultivation of immortalized human hepatocytes HepZ on macroporous CultiSpher G microcarriers. *Biotechnol Bioeng* **68**, 59-70 (2000).
17. Kono, Y., Yang, S., Letarte, M. & Roberts, E.A. Establishment of a human hepatocyte line derived from primary culture in a collagen gel sandwich culture system. *Exp Cell Res* **221**, 478-485 (1995).
18. Allen, J.W., Hassanein, T. & Bhatia, S.N. Advances in bioartificial liver devices. *Hepatology* **34**, 447-455 (2001).
19. Broering, D.C., Schulte am Esch, J., Fischer, L. & Rogiers, X. Split liver transplantation. *HPB (Oxford)* **6**, 76-82 (2004).
20. Iansante, V., Mitry, R.R., Filippi, C., Fitzpatrick, E. & Dhawan, A. Human hepatocyte transplantation for liver disease: current status and future perspectives. *Pediatr Res* **83**, 232-240 (2018).
21. Laconi, E.*, et al.* Long-term, near-total liver replacement by transplantation of isolated hepatocytes in rats treated with retrorsine. *Am J Pathol* **153**, 319-329 (1998).
22. Ibars, E.P.*, et al.* Hepatocyte transplantation program: Lessons learned and future strategies. *World J Gastroenterol* **22**, 874-886 (2016).
23. Stephenne, X.*, et al.* Cryopreservation of human hepatocytes alters the mitochondrial respiratory chain complex 1. *Cell Transplant* **16**, 409-419 (2007).
24. Wang, L.J.*, et al.* Engraftment assessment in human and mouse liver tissue after sex-mismatched liver cell transplantation by real-time quantitative PCR for Y chromosome sequences. *Liver Transpl* **8**, 822-828 (2002).
25. Najimi, M.*, et al.* Adult-derived human liver mesenchymal-like cells as a potential progenitor reservoir of hepatocytes? *Cell Transplant* **16**, 717-728 (2007).
26. Scarritt, M.E., Pashos, N.C. & Bunnell, B.A. A review of cellularization strategies for tissue engineering of whole organs. *Frontiers in bioengineering and biotechnology* **3**, 43 (2015).
27. Faulk, D.M., Wildemann, J.D. & Badylak, S.F. Decellularization and cell seeding of whole liver biologic scaffolds composed of extracellular matrix. *J Clin Exp Hepatol* **5**, 69-80 (2015).
28. Soto-Gutierrez, A.*, et al.* A whole-organ regenerative medicine approach for liver replacement. *Tissue Eng Part C Methods* **17**, 677-686 (2011).
29. O'Brien, F.J. Biomaterials & scaffolds for tissue engineering. Vol. 14 (materials today, 2011).

30. Shteyer, E.*, et al.* Reduced liver cell death using an alginate scaffold bandage: a novel approach for liver reconstruction after extended partial hepatectomy. *Acta Biomater* **10**, 3209-3216 (2014).
31. Shang, Y.*, et al.* Hybrid sponge comprised of galactosylated chitosan and hyaluronic acid mediates the co-culture of hepatocytes and endothelial cells. *J Biosci Bioeng* **117**, 99-106 (2014).
32. Mazza, G., Al-Akkad, W., Rombouts, K. & Pinzani, M. Liver tissue engineering: From implantable tissue to whole organ engineering. *Hepatol Commun* **2**, 131-141 (2018).
33. Bhise, N.S.*, et al.* A liver-on-a-chip platform with bioprinted hepatic spheroids. *Biofabrication* **8**, 014101 (2016).
34. Skardal, A.*, et al.* A hydrogel bioink toolkit for mimicking native tissue biochemical and mechanical properties in bioprinted tissue constructs. *Acta Biomater* **25**, 24-34 (2015).
35. Akhmanova, M., Osidak, E., Domogatsky, S., Rodin, S. & Domogatskaya, A. Physical, Spatial, and Molecular Aspects of Extracellular Matrix of In Vivo Niches and Artificial Scaffolds Relevant to Stem Cells Research. *Stem Cells Int* **2015**, 167025 (2015).
36. Sanchez-Romero, N.*, et al.* The role of extracellular matrix on liver stem cell fate: A dynamic relationship in health and disease. *Differentiation* **106**, 49-56 (2019).
37. Bedossa, P. & Paradis, V. Liver extracellular matrix in health and disease. *J Pathol* **200**, 504-515 (2003).
38. Baptista, P.M.*, et al.* The use of whole organ decellularization for the generation of a vascularized liver organoid. *Hepatology* **53**, 604-617 (2011).
39. Ott, H.C.*, et al.* Perfusion-decellularized matrix: using nature's platform to engineer a bioartificial heart. *Nat Med* **14**, 213-221 (2008).
40. Xu, C.C., Chan, R.W. & Tirunagari, N. A biodegradable, acellular xenogeneic scaffold for regeneration of the vocal fold lamina propria. *Tissue Eng* **13**, 551-566 (2007).
41. Reddy, P.P.*, et al.* Regeneration of functional bladder substitutes using large segment acellular matrix allografts in a porcine model. *J Urol* **164**, 936-941 (2000).
42. Lee, R.C. & Kolodney, M.S. Electrical injury mechanisms: electrical breakdown of cell membranes. *Plast Reconstr Surg* **80**, 672-679 (1987).

43. Wang, Y., *et al.* Recent Advances in Decellularization and Recellularization for Tissue-Engineered Liver Grafts. *Cells Tissues Organs* **204**, 125-136 (2017).
44. Crapo, P.M., Gilbert, T.W. & Badylak, S.F. An overview of tissue and whole organ decellularization processes. *Biomaterials* **32**, 3233-3243 (2011).
45. Caralt, M., *et al.* Optimization and critical evaluation of decellularization strategies to develop renal extracellular matrix scaffolds as biological templates for organ engineering and transplantation. *Am J Transplant* **15**, 64-75 (2015).
46. Lu, H., Hoshiba, T., Kawazoe, N. & Chen, G. Autologous extracellular matrix scaffolds for tissue engineering. *Biomaterials* **32**, 2489-2499 (2011).
47. Nonaka, P.N., *et al.* Effects of freezing/thawing on the mechanical properties of decellularized lungs. *J Biomed Mater Res A* **102**, 413-419 (2014).
48. Lang, R., *et al.* Three-dimensional culture of hepatocytes on porcine liver tissue-derived extracellular matrix. *Biomaterials* **32**, 7042-7052 (2011).
49. Mattei, G., *et al.* Mechanostructure and composition of highly reproducible decellularized liver matrices. *Acta Biomater* **10**, 875-882 (2014).
50. Pla-Palacin, I., Sainz-Arnal, P., Morini, S., Almeida, M. & Baptista, P.M. Liver Bioengineering Using Decellularized Whole-Liver Scaffolds. *Methods Mol Biol* **1577**, 293-305 (2018).
51. Mazza, G., *et al.* Decellularized human liver as a natural 3D-scaffold for liver bioengineering and transplantation. *Sci Rep* **5**, 13079 (2015).
52. Geerts, S., Ozer, S., Jaramillo, M., Yarmush, M.L. & Uygun, B.E. Nondestructive Methods for Monitoring Cell Removal During Rat Liver Decellularization. *Tissue Eng Part C Methods* **22**, 671-678 (2016).
53. Ogiso, S., *et al.* Efficient recellularisation of decellularised whole-liver grafts using biliary tree and foetal hepatocytes. *Sci Rep* **6**, 35887 (2016).
54. Rossi, E.A., Quintanilha, L.F., Nonaka, C.K.V. & Souza, B.S.F. Advances in Hepatic Tissue Bioengineering with Decellularized Liver Bioscaffold. *Stem cells international* **2019**, 2693189 (2019).
55. Pellegata, A.F., Tedeschi, A.M. & De Coppi, P. Whole Organ Tissue Vascularization: Engineering the Tree to Develop the Fruits. *Frontiers in bioengineering and biotechnology* **6**, 56 (2018).

56. Stevens, K.R., *et al.* In situ expansion of engineered human liver tissue in a mouse model of chronic liver disease. *Sci Transl Med* **9**(2017).
57. Hillebrandt, K.H., *et al.* Strategies based on organ decellularization and recellularization. *Transpl Int* (2019).
58. Kanninen, L.K., *et al.* Hepatic differentiation of human pluripotent stem cells on human liver progenitor HepaRG-derived acellular matrix. *Exp Cell Res* **341**, 207-217 (2016).
59. Du, C., Narayanan, K., Leong, M.F. & Wan, A.C. Induced pluripotent stem cell-derived hepatocytes and endothelial cells in multi-component hydrogel fibers for liver tissue engineering. *Biomaterials* **35**, 6006-6014 (2014).
60. Nagata, H., *et al.* Prolonged survival of porcine hepatocytes in cynomolgus monkeys. *Gastroenterology* **132**, 321-329 (2007).
61. Glorioso, J.M., *et al.* Pivotal preclinical trial of the spheroid reservoir bioartificial liver. *J Hepatol* **63**, 388-398 (2015).
62. Carmeliet, P. & Jain, R.K. Molecular mechanisms and clinical applications of angiogenesis. *Nature* **473**, 298-307 (2011).
63. Koike, N., *et al.* Tissue engineering: creation of long-lasting blood vessels. *Nature* **428**, 138-139 (2004).
64. Asahara, T., *et al.* Isolation of putative progenitor endothelial cells for angiogenesis. *Science* **275**, 964-967 (1997).
65. Shirota, T., He, H., Yasui, H. & Matsuda, T. Human endothelial progenitor cell-seeded hybrid graft: proliferative and antithrombogenic potentials in vitro and fabrication processing. *Tissue engineering* **9**, 127-136 (2003).
66. Ginsberg, M., Schachterle, W., Shido, K. & Rafii, S. Direct conversion of human amniotic cells into endothelial cells without transitioning through a pluripotent state. *Nature protocols* **10**, 1975-1985 (2015).
67. Traore, M.A. & George, S.C. Tissue Engineering the Vascular Tree. *Tissue Eng Part B Rev* **23**, 505-514 (2017).
68. Neff, L.P., *et al.* Vascular smooth muscle enhances functionality of tissue-engineered blood vessels in vivo. *Journal of vascular surgery* **53**, 426-434 (2011).
69. Martin, M.J., Muotri, A., Gage, F. & Varki, A. Human embryonic stem cells express an immunogenic nonhuman sialic acid. *Nat Med* **11**, 228-232 (2005).
70. Uygun, B.E., *et al.* Organ reengineering through development of a transplantable recellularized liver graft using decellularized liver matrix. *Nature medicine* **16**, 814-820 (2010).

71. Ott, H.C., *et al.* Regeneration and orthotopic transplantation of a bioartificial lung. *Nature medicine* **16**, 927-933 (2010).
72. Petersen, T.H., *et al.* Tissue-engineered lungs for in vivo implantation. *Science* **329**, 538-541 (2010).
73. Salvatori, M., *et al.* Extracellular Matrix Scaffold Technology for Bioartificial Pancreas Engineering: State of the Art and Future Challenges. *Journal of diabetes science and technology* **8**, 159-169 (2014).
74. Goh, S.K., *et al.* Perfusion-decellularized pancreas as a natural 3D scaffold for pancreatic tissue and whole organ engineering. *Biomaterials* **34**, 6760-6772 (2013).
75. Song, J.J., *et al.* Regeneration and experimental orthotopic transplantation of a bioengineered kidney. *Nature medicine* **19**, 646-651 (2013).
76. Patil, P.B., *et al.* Recellularization of acellular human small intestine using bone marrow stem cells. *Stem cells translational medicine* **2**, 307-315 (2013).
77. Xu, L., *et al.* Constructing heparin-modified pancreatic decellularized scaffold to improve its re-endothelialization. *J Biomater Appl* **32**, 1063-1070 (2018).
78. Hussein, K.H., Park, K.M., Kang, K.S. & Woo, H.M. Heparin-gelatin mixture improves vascular reconstruction efficiency and hepatic function in bioengineered livers. *Acta Biomater* **38**, 82-93 (2016).
79. Bao, J., *et al.* Construction of a portal implantable functional tissue-engineered liver using perfusion-decellularized matrix and hepatocytes in rats. *Cell transplantation* **20**, 753-766 (2011).
80. Bao, J., *et al.* Hemocompatibility improvement of perfusion-decellularized clinical-scale liver scaffold through heparin immobilization. *Scientific reports* **5**, 10756 (2015).
81. Barakat, O., *et al.* Use of decellularized porcine liver for engineering humanized liver organ. *The Journal of surgical research* **173**, e11-25 (2012).
82. Yagi, H., *et al.* Human-scale whole-organ bioengineering for liver transplantation: a regenerative medicine approach. *Cell transplantation* **22**, 231-242 (2013).
83. Kadota, Y., *et al.* Mesenchymal stem cells support hepatocyte function in engineered liver grafts. *Organogenesis* **10**, 268-277 (2014).
84. Ko, I.K., *et al.* Bioengineered transplantable porcine livers with re-endothelialized vasculature. *Biomaterials* **40**, 72-79 (2015).

85. Chen, C.*, et al.* Hepatocyte-like cells generated by direct reprogramming from murine somatic cells can repopulate decellularized livers. *Biotechnol Bioeng* **115**, 2807-2816 (2018).

CHAPTER 1.

Liver vascular bioengineering

INTRODUCTION

During embryogenesis, the formation of a blood network occur through vasculogenesis (de novo formation of a primitive network due to mesoderm differentiation into endothelial cells) and angiogenesis (the growth of new vessels from pre-existing ones) for the generation of a hierarchical network including arteries, arterioles, capillaries, venules and veins[1].

Vasculogenesis starts with the formation of blood islands in the yolk sac which mature, differentiate and aggregate. This resultant fusion leads to the formation of a primitive network of primary capillary plexuses[2]. The inner cells of these aggregates become hematopoietic precursors while the outer ones become endothelial cells, which will anastomose, and constitute a primary capillary plexus.

During angiogenesis, interendothelial cell junctions are disrupted, destabilizing mature vessels. As a result of this disruption, perivascular stromal cells from the capillaries are removed, including matrix protein degradation. This allows the liberation of growth factors like VEGF (the angiogenic master regulator) and FGF, creating an environment that allow endothelial cells to migrate and proliferate, leading to vessel sprouting through chemotaxis following molecular gradients and mechanical stimuli. In these processes, the most relevant molecules involved are VEGF and FGF. Once this nascent vasculature was created during vasculogenesis and angiogenesis, it must mature to be capable to sustain the metabolic demand of the organism. In this step of the development, recruitment of perivascular stromal cells (pericytes and smooth muscle cells) and the generation of an ECM play critical roles[3,4]. Platelet-derived growth factor B (PDGF-BB) signaling pathways are

important molecules at this stage. They promote the recruitment, migration and growth of perivascular cells during vessel maturation and stabilization, allowing long-term function and stability. Angiopoietin-1 (Ang-1) is also involved, allowing the adhesion between endothelial cells and pericytes and affecting to vessel diameter and density[5].

The ECM is also crucial in the development of vascular maturation due to its capacity of regulating growth factor signaling and presentation. Furthermore, the ECM remodels its components (like laminins, collagen type IV, perlecan and other proteins) as the vasculature mature from the capillaries to higher structures like arteries[6,7]. Gianni-Barrera et al[8] and Banfi et al[9], have also reported long-term stability of angiogenesis inducing and maturating at the same time, by combining VEGF and PDGF-BB.

In this project, we sought to efficiently revascularize the liver decellularized ECM. For this, two types of cells were employed: human umbilical vein endothelial cells (hUVECs) and human mesenchymal stem cells (hMSC) were isolated and cultured *in vitro* at large scale for further seeding in rat liver ECM. The experiments for devising and optimizing an appropriate seeding technique for adequate ECM revascularization were performed with rat liver scaffolds due to their reduced size, with a decreased total number of cells necessary and cost of each recellularization experiment. In order to obtain efficient cell penetration and distribution across the whole volume of the ECM and to avoid cell aggregation in a specific area of the scaffold, different pressure conditions were tested. Starting from the base that the physiological blood pressure in the rat portal vein (PV) is 1-10mmHg, and in the hepatic artery is between 80-100mmHg[10], we tested different pressure

conditions, always combining a higher pressure followed with a lower pressure to determine cell distribution in each condition. The reason of this combination and our working hypothesis was to ensure heterogeneous cell distribution across the scaffold: higher pressures would allow cells to reach the inner parts of the scaffold, enabling small vessel recellularization. On the contrary, lower pressures would preferentially distribute cells in the inner parts of the scaffold, allowing recellularization of intermediate and larger vessels. With this, we would be able to revascularize all sizes of the vascular bed.

Finally, different seeding conditions and culture medium were tested in order to determine the optimal procedure not only to achieve homogeneous scaffold colonization, but also to induce cellular organization and *in vitro* blood vessel formation.

MATERIALS AND METHODS

1. Cells

1.1 Cell preparation

1.1.1 hUVECs isolation and culture

These cells were isolated from human umbilical cords. Samples and data from patients included in this study were provided by the Aragon's Tissue Bank under informed consent and were processed following standard operation procedures with the approval of the Ethical and Scientific Review Boards.

Umbilical vein of the umbilical cord (UC) was localized and cannulated with a 20G cannula (BD, BD393224) and washed with Dulbecco's

Phosphate Buffered Saline (DPBS) (Sigma, D8537). Then, one of the ends of the UC was clamped and warm Trypsin-EDTA (Gibco, 25200072) was injected through to the other end of the UC, which was afterwards clamped too. UC was incubated for 7min at 37°C. Trypsin was collected and neutralized with FBS and centrifuged 400g for 5min. The resultant pellet was then suspended in hUVEC media supplemented with 20% FBS and seeded in a well of a 6 multi-well dish, previously coated with 0,2% bovine gelatin.

The culture was allowed to grow for 3-4 days in normoxia conditions (37°C and 5% CO_2), and media was changed at day 4. Once the colonies of cells started to appear, the culture media was changed to hUVEC media supplemented with 5% FBS. Cultures were maintained and expanded *in vitro* in order to have a good cell stock, which was then frozen.

hUVEC media used: MCDB 131 (10372-019, Gibco), 5% FBS (10270106, Gibco), 2mM L-Glutamine (G7513, Sigma), 1% (v/v) P/S (15140122, Thermofisher), 5µg/mL Insulin (I9278, Sigma), 10µg/mL Transferrin (T0665, Sigma), 50ng/ml VEGF (100-20 Peprotech), 40ng/ml EGF (AF-100-15, Peprotech, 40ng/mL FGF-2 ((100-18B, Peprotech) and 40ng/mL IGF-1 (100-11R3, Peprotech).

1.1.2 hMSC isolation and culture

hMSCs, also called pericytes, were initially isolated from lipoaspirate samples transferred by the plastic surgery clinic Renobell in Zaragoza, with informed consent of the patients and the approval of the Ethics Committee and the Scientific Committee of Aragón.

First, a solution of 1X collagenase I was prepared in a 50ml falcon tube. The lipoaspirate samples were given in 50ml falcon tubes containing Advanced DMEM media supplemented with 1%P/S. These samples were centrifuged 1200g 10min. Afterwards, a clear phase separation was observed. The upper fraction containing the fat and the lower fraction containing the pellet were added to the collagenase I solution previously prepared, hand shacked vigorously at 300rpm and 37°C for 30 min and then centrifuged 1200 g for 10 min.

The fat from the top and the media in between were discarded, and the resultant pellet was suspended in hMSC medium and centrifuged at 400g for 5 min. Then, the supernatant was discarded and replaced by new media and centrifuged again. Then, the cell suspension was filtered through a 100µm cell strainer and seeded into a $10cm^2$ dish previously coated with 0,2% bovine gelatin. hMSC media used: DMEM F-12 (Sigma D8062), 10% FBS, 1% (v/v) P/S (15140122, Thermofisher) and 1% L-Glutamine (G7513, Sigma).

The culture was washed with PBS the following day to remove dead cells and red blood cells and kept in hypoxia conditions (37°C and 3% CO_2). Cultures were maintained and expanded *in vitro* in order to have a good cell stock, which was then frozen.

An alternative source of hMSCs was also generously donated by Dr. Álvaro Meana, from the Banco de Tejidos del Centro Comunitario de Sangre y Tejidos de Asturias.

1.2 Cell characterization

Once the cells where in culture, a nice and typical morphology was observed in all the cells. Immunostaining analyses were performed too: endothelial cells were stained with the endothelial cell marker anti-CD31 (MAD-0020-48, Master Diagnóstica), and hMSC were stained with the mesenchymal cell marker anti-vimentin (MAD-000326QD, Master Diagnóstica). The secondary antibodies employed were: goat anti-mouse 488 (A11029, Molecular Probes) and goat anti-rabbit 568 (A11036 Molecular Probes) respectively. Furthermore, hMSC where also cultured for three weeks with human adipocyte differentiation medium (811D-250, Sigma) in order to test their capability to differentiate towards adipocytes. Cells were then stained with Oil Red staining and quantified to determine the percentage of total adipocyte-positive cells.

1.3 Cell labeling and storage

Once an optimal cell source was achieved, cells with different fluorescent labeling were needed for further experimentation. Hence, some of the cells previously isolated were labeled with GFP (green label) and TdTomato (red label) using lentiviral vectors.

1.3.1 Lentiviral production

Lentiviral production was performed according to the Lipofectamine 3000 reagent protocol (L3000001, Thermofisher). Briefly, first (day 0), human embryonic kidney cells (HEK 293T) were plated in different 10 cm^2 dishes with culture media: DMEM high glucose (D6546, Sigma), 10% FBS, 1% P/S + 2mM L-Glutamine and allowed to grow until 95-99%

confluence. Once they have reached the desired confluence, expansion media was changed to Packaging medium: DMEM high glucose (D6546, Sigma), 5% FBS, 1% P/S, 2mM L-glutamine, 1mM sodium pyruvate, adding 12ml of this media to each dish.

The transfection was performed the following day (day 1). For this, lipid complex formation was carried out. Tube A, containing Lipofectamine 3000 reagent diluted in Opti-MEM medium reduced serum and tube B, containing the packaging mix, the expression vector (GPF or TdTomato) and P3000 enhancer reagent were mixed at a ratio of 1:1, then incubated at room temperature (RT) for 20 minutes. Afterwards, 6ml of media from each culture dish was removed. Then, the DNA-lipid complexes were added to each culture dish and incubated for 6 hours at 37°C At 6 hours post transfection, the media from the culture dishes were removed and replaced with 12 ml of Packaging medium and incubated overnight.

At day 2, the first viral batch was harvested. For this, supernatant was collected and stored at 4°C. Media from the dishes were replaced with 12 ml of fresh packaging medium and again incubated overnight.

At day 3, the second viral batch was harvested. For this, supernatant was collected and combined with the first batch, centrifuged at 2000 rpm for 10 min and filtered through a 45µm pore size filter. Finally, lentiviral particles were aliquoted and stored at -80ºC.

1.3.2 Titer of lentiviral vectors

In order to determine an optimal lentiviral concentration for cell infection, hUVECs were plated in a 6 multiwell plate, and allowed to grow until 85-90% confluency. They were then tested with different concentrations of GFP and TdTomato lentiviruses. The mentioned tested

concentrations were: 1, 1/2, 1/10; 1/100 and 1/1000. After 24-48h post infection, cells were observed with a fluorescence microscopy (Leyca) in order to determine the percentage of labeled cells per condition to calculate the optimal lentiviral concentration.

1.3.3 Cell labeling with resultant lentiviral vectors

Once the optimal concentration of lentiviral supernatant was established, the desired cells (hUVECs and hMSC) were infected with Lenti-GPF or Lenti-Tomato. Once the culture were 80-90% confluent, the cells where tripsinized and sorted via fluorescence-activated cell sorting (FACS Aria, BD) in order to separate labeled cells. Selected fluorescent cells where then re-seeded and expanded *in vitro* to build a working stock in liquid nitrogen.

2. Scaffold preparation

2.1 Rat liver harvesting and decellularization

The adopted procedure for rat liver harvesting is described by Baptista et al[11]. Briefly, livers where harvested from cadaveric rats, after one freezing/thawing cycle. First, a longitudinal abdominal incision was made, in order to visualize the liver. Then, the suprahepatic inferior vena cava was dissected and cut, followed by portal vein (PV) dissection, where lateral branches where ligated with 4-0 silk. Finally, the infrahepatic vena cava was dissected and cut. Diaphragm was carefully dissected from esophagus. All liver attachments were also removed and intact organ was separated from the body. PV was then cannulated with a 24G cannula (BD393224, BD) and then connected to a peristaltic pump (Masterflex

L/S, Cole Parmer) with silicon tubes L/S14 (96410-14, Cole Parmer) at 4°C.

Then, a first wash with hypotonic distilled water of 20-30 minutes was done in order to cause cell lysis by osmotic shock and to remove blood content. Then, between 2-5L of detergent were perfused, which consisted of 1% Triton X-100 (A1388, Panreac) to remove protein-lipid and lipid-lipid interactions, and 0,1% ammonium hydroxide (A1388, Panreac) for cell stripping. Once the liver was transparent and there were no visible cells remaining, livers where finally washed with double the volume of detergent with distilled water to remove the detergent from the liver ECM. Once washed, a partial hepatectomy was performed in order to reduce even further the total volume to be further recellularized. For this, left and medium hepatic veins were ligated and respective lobes were dissected. The remaining right lobe was then perfused with 50ml of sterilization solution (antibiotic/antimycotic solution 10X (A5955, Sigma), P/S 10% and $50 \cdot 10^{-3}$ mg/ml Gentamicin sulfate (345814, Merck)) and kept overnight at 4°C in this solution. Finally, scaffolds were washed the following day with sterile PBS (D8537, Sigma) and kept at 4°C until use.

Due to optimal decellularization process depends not only in the amount of cells removed, but also in the ECM and vascular tree preservation, different flows were tested, in order to determine an optimal one that allowed not only larger cell removal, but also good vascular preservation. The tested flows for whole organ liver decellularization were: 1ml/min, 3ml/min and 5ml/min. Once the scaffolds were decellularized, a corrosion cast was performed in order to determine the grade of vascular tree preservation, comparing decellularized and native liver rats. Briefly,

the technique of corrosion was performed with the Batson's No. 17 Plastic Replica and Corrosion Kit (07349, Polysciences Inc), which consisted on the perfusion of a mixture of a polymerized monomer and a promoter with a pigment (blue in this case) through the PV of native and decellularized livers. Once the whole organ was perfused with the polymer, it was rapidly moved to a recipient containing cold water and kept overnight to allow polymerization. Afterwards, the organ structure was macerated with 20% NaOH at 90°C overnight, getting with this only the plasticized vasculature.

The resultant vascular plastic cast were then analyzed under SEM microscopy, which has been conducted at the Laboratorio de Microscopías Avanzadas at Instituto de Nanociencia de Aragón - Universidad de Zaragoza. Samples were fractured and placed in supports which were previously coated with carbon tape. They were afterwards metalized with 14nm of palladium with a vacuum coater (Leica EM ACE200). Samples observation was performed with a FSEM FEI Inspect F50 at 10kV.

3. Rat liver bioengineering

Once the two components for liver bioengineering were ready (cells and liver ECM), the recellularization process followed. For this purpose, a bioreactor was assembled under sterile conditions, using sterile material, gloves and face mask in the laminar flow hood (Fig. 1).

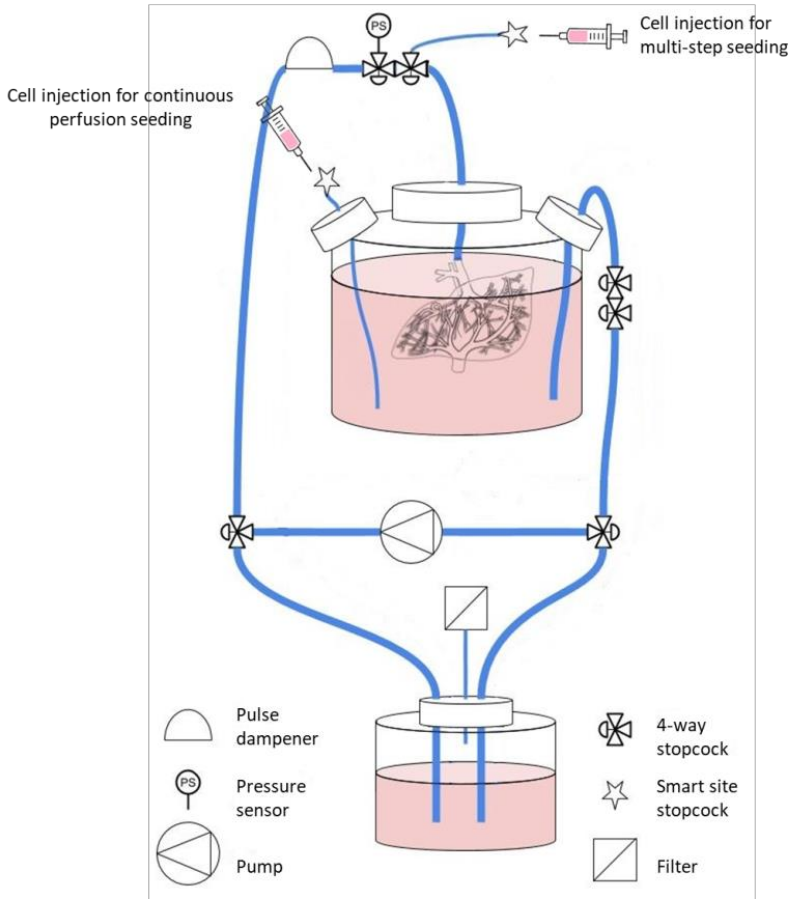

Figure 1. Scheme of the bioreactor setup for rat scaffold recellularization. (Figure modified from Morini et al[12]). Syringes represent the two methods tested for scaffold seeding: continuous perfusion, where cells were delivered in the culture medium contained in the spinner flask; and multistep infusion, where cells were directly injected in the scaffold's portal vein.

The components used in our bioreactor system are listed below:

1. Spinner flask, which contained the scaffold resuspended in culture media.
2. Pulse dampener, used for air bubbles retention and for the signal modulation (continuous PV flow).
3. Peristaltic pump, for culture media perfusion.
4. TAM-A for pressure control and modulation (not represented).
5. Pressure sensor, which is connected to TAM-A.

6. Reservoir, for media changing during the experiment.
7. 4-way stop-cocks, male and female fittings and smart site stop-cocks for circuit assembly.
8. L/S 14 tubing

The process for liver recellularization was described before[13]. Briefly, it was necessary to assemble the setup described in Fig. 1. The first day of the bioreactor experiment was for priming, where all the components were assembled under sterile conditions. Once the circuit was closed, it was primed with culture medium using a 20mL luer-lock syringe (8SS+20L1, Terumo) to eliminate the air form the system. Afterwards, liver ECM was connected through the PV and stayed suspended on the culture medium within the spinner flask. Finally, the bioreactor setup was transferred to an incubator with normoxia conditions and attached to the peristaltic pump and TAM-A. Liver ECM was then perfused at low flow conditions (1ml/min) overnight.

The culture media employed in the bioreactor system was the "Bioreactor Media", a culture media that had been previously tested in tissue culture dishes to ensure growth of both cell types and then translated to the bioreactor system. It was a combination of 50% of the standard culture media used for hMSC *in vitro* expansion, with 50% of the culture media used for the hUVECs *in vitro* expansion.

3.1 Determination of the optimal pressure conditions for rat scaffold recellularization

3.1.1 Seeding conditions

Different combinations of pressure conditions and seeding methods were tested to determine the best option to achieve cellular distribution across the scaffold. The combinations of pressures are listed in Table 1.

Table 1. Different combinations of pressure conditions tested for cell penetration and colonization through the scaffold. Higher seeding pressures were used with GFP-labeled cells and lower seeding pressures for RFP-labeled cells.

Condition	↑P (mmHg)	↓P (mmHg)
1)	14	7
2)	25	14
3)	50	25
4)	100	50

For the determination of the optimal pressure conditions for scaffold recellularization, short experiments of 3 days in the bioreactor system were performed. With this, the process started with the priming, where the circuit was assembled under sterile conditions; the first day was for cell seeding at higher pressure, where a mix of GFP-hUVEC and GFP-hMSC were seeded; the second day was for cell seeding at the lower pressure, where a mix of Tomato-hUVEC and Tomato-hMSC were seeded, and finally, the recellularized scaffold was fixed at day 3 (Fig.2).

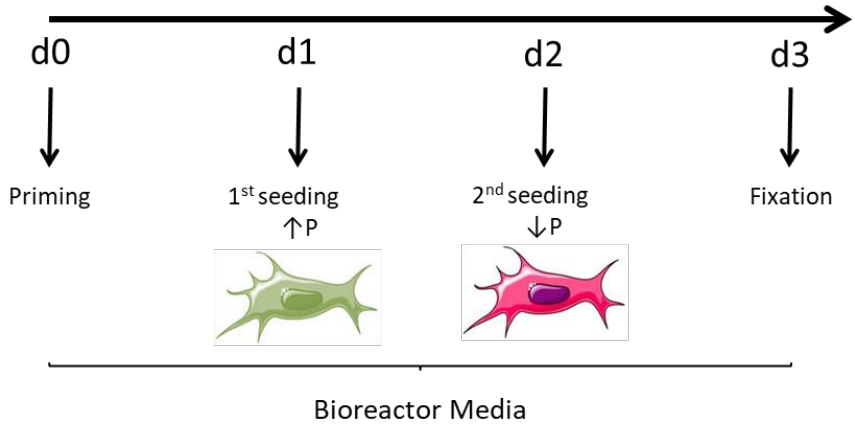

Figure 2. Schematic representation of a 3d-bioreactor using combination of higher and lower pressures. GFP-labelled cells were seeded the first day, at a higher pressure, and red cells were seeded the second day, at a lower pressure. Afterwards, the recellularized scaffold was fixed with formol for histological analysis.

For scaffold recellularization, an average number of $150x10^6$ cells were seeded (hUVECs were seeded at a maximum passage of p6-7; and p7-8 for hMSC). Two cell seeding methods were tested: 1) continuous perfusion, where cells were injected directly in the media contained in the spinner flask and entered to the PV of the liver scaffold thanks to the peristaltic pump; and 2) multi-step infusion, where cells were directly injected in the scaffold PV in two seedings separated by 15 minutes, based on Soto-Gutierrez et al work[14].

After 3 days in the bioreactor system, culture media was extracted for further analysis, and the recellularized scaffolds were removed from the spinner flask and fixed. For this, recellularized scaffolds were perfused at 1ml/min with formaldehyde 3,7-4,0% pH=7 stabilized with MeOH (252931.1214, Panreac) for 20 minutes. Finally, samples were embedded in paraffin blocks for tissue processing. This procedure of paraffin block preparation was made in collaboration with the Department of

Pathology at the Hospital Clínico Universitario Lozano Blesa. Each paraffin block was afterwards cut with a microtome (Microm HM 355S, Thermofisher) at 7 µm thick. 50 serial slides were done in total for each bioreactor, cutting the first 10 slides, trimming the following 100 µm, then cutting another 10 slides at 7 µm and so on, until getting a total number of 50 slides of each recellularized scaffold. With this, we were sure that we were sectioning almost the whole thickness of the recellularized scaffold.

H&E stainings (Hematoxilin: 253949.1612, Panreac; Eosin: 251299.1608, Panreac; Ethanol absolute pure: 141086.1214, Panreac; Ethanol 96% pure, pharma grade: 141085.1214 Panreac; Etahanol 70%, Montplet) were performed in slides 1, 10, 20, 30, 40 and 50 of each bioreactor, following standard protocols to have an overview of cell distribution through the whole thickness of the sample. Afterwards, samples were covered with mounting media and observed with an inverted microscope. In order to have an overview of the whole recellularized scaffold, multiple image alignment (MIA) pictures were taken at 4x and combined afterwards, to have the panoramic view and determine the grade of scaffold colonization, determining nude areas, where only eosin staining from the ECM was observed, and colonized areas, where hematoxilin nuclei were observed.

After testing different bioreactor systems with the different pressure conditions and different seeding methods, different parameters were analyzed.

3.1.2 LDH Test

Culture media of the bioreactor systems were tested with Pierce LDH citotoxicity assay kit (Thermofisher; 88953), in order to determine whether high pressures affected cell viability; Lactate dehydrogenase (LDH) is a protein present in cell cytoplasm. Presence of high levels of LDL measurement would indicate cell lysis, indicating cell stress in the conditions of the bioreactor system. Absorbance of the culture media was measured at 490 and 680nm with a plate reader (SynergyHT, Biotek Instruments).

3.1.3 Scaffold total recellularization (DAPI staining)

DAPI staining of slides number 19 and 39 were performed to determine the total scaffold area covered by cells, for having also an overview of cell distribution through the whole thickness of the sample.

A total of n=2 of each pressure condition bioreactor were analyzed with the purpose of determining the best option for complete scaffold recellularization. For this, slides number 19 and 39 of each bioreactor were stained with DAPI, in order to have sections from the external part of the recellularized scaffold (slide number 19) and sections from the inner part of the recellularized scaffold (slide number 39). Five random pictures at 10x were taken of each slide, and analyzed with Image J to count the number of pixels present in the total scaffold area. Number of pixels would correspond with DAPI signal, representing the areas covered by cells.

3.1.4 Quantification of the labeled cells present in vascular structures with different diameter. Anti-GFP and anti-RFP immunofluorescence analysis.

Immunostaining with anti-GFP (sc-9996, SantaCruz Biotech) and anti-RFP (600-401-379, Rockland) were performed in order to determine cell migration through the scaffold according to their seeding pressure. The secondary antibodies employed were goat anti-mouse 488 (A11029, Molecular Probes) and goat anti-rabbit 568 (A11036, Molecular Probes) respectively. Immunostaining pictures were analyzed with an inverted microscope (Olympus YX81).

Once scaffold recellularization was completed, a protocol was defined in order to characterize the process of revascularization achieved with the four different pressure combinations used in the seeding.

The first goal was to quantify and characterize our engineered vasculature. For this, Traore et al[15] mentioned that capillaries (small vessels) have a diameter of 10-50 µm, arterioles and venules (intermediate vessels) have a diameter of 30-300µm, and arteries and veins (large vessels) have a diameter ranging from 0,4-8mm. Taking this into account, we defined the following sizes to characterize our bioengineered vascular tree: sizes <40µm would represent small vessels, sizes ranging from 40-100µm would represent intermediate vessels and sizes >100µm would represent large vessels.

Then, one of the slides previously cut of each bioreactor was stained with anti-GFP and anti-RFP. Afterwards, six random pictures at 10x were taken with an inverted microscope across the whole area of the recellularized scaffold, in order to have representative results. Four pictures of each selected area were taken: 1) with DAPI channel, to see nuclear staining

(in blue); 2) with FIT-C channel, for GFP staining (in green) and 3) with RFP channel, for Td-Tomato staining (in red) and 4) a merge, which is the combination of the three mentioned channels. Taking these four pictures of each area into account, vessels were localized and measured with the Cell-D Software. A total of 24 pictures of each recellularized scaffold were analyzed. The aim of this was to determine not only vessel size but also categorize the label of the cells lining them, which ranged from: 1) Nude, meaning that the vessel was not covered by any cell; 2) GFP, meaning that the vessel was predominantly covered by green cells (both endothelial and mesenchymal), which were seeded at high pressure; 3) RFP, meaning that the vessel was covered mainly by red cells (both endothelial and mesenchymal cells), which were seeded at low pressure; and 4) Both, meaning that the vessel was covered by GFP and RFP cells.

3.2 Quantification of vessel formation in vitro with growth factor supplementation.

Two new culture media were formulated for our bioreactor system, with specific growth factors that mimicked the biochemical environment present during vasculogenesis and angiogenesis. We also increased the time in the bioreactor system from 3 to 14 days.

For these experiments, co-seeding of hUVEC and hMSC were performed, but in this case, they were not GFP or Tomato-labeled. Priming, first and second seedings were done with the Bioreactor Media (BM), and then, interchange of Induction Media (IM) and Maturation Media (MM) was performed the following days. At day 14, the recellularized scaffold was fixed with formol.

The goal with this bioreactor setup was the promotion of cell growth and proliferation with the IM, once the cells have been seeded within the scaffold, and then, changed to MM to induce cell maturation and organization into a vascular vessel configuration. This cycle was repeated twice. Furthermore, each change to MM was accompanied by an extra seeding of hMSC ($1x10^6$ cells) to promote vessel stabilization.

Induction media: designed for cell proliferation once seeded in the scaffold, contained: 50% DMEM F12 (D8062, Sigma) combined with 50% MCDB 131 (10372019, Thermofisher) and supplemented with 1% FBS, 2mM L-glut, 1% P/S, 5 µg/ml Insulin (I9278, Sigma), 10µg/ml transferrin (T0665, Sigma), 25µg/ml VEGF (100-20, Peprotech), 40µg/ml FGF-2 (100-18B, Peprotech), 40ng/ml IGF-1 (100-11R3, Peprotech) and 100ng/ml Ang-2 (130-07, Peprotech).

Maturation Media: defined for vascular maturation, contained: 50% DMEM F12 (D8062, Sigma) combined with 50% MCDB 131 (10372019, Thermofisher) and supplemented with 1% FBS, 2mM L-glut, 1% P/S, 5 µg/ml Insulin (I9278, Sigma), 10µg/ml transferrin (T0665, Sigma), 50ng/ml Ang-1 (130-06, Peprotech); 0,1ng/ml TGFβ1 (100-21, Peprotech) and 10ng/ml PDGF-BB (100-14B, Peprotech).

Once the bioreactor has been seeded, BM was changed to IM to perform the first cycle which lasted 3d. Then, media was changed to MM, for another 3 days. This change was accompanied by an extra seeding of hMSC. This cycle of induction/maturation was repeated twice, and then fixed for further analysis (Fig. 3).

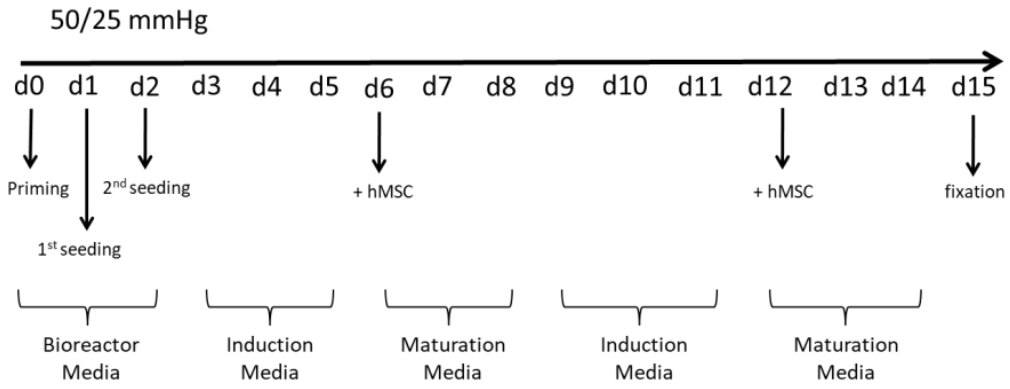

Figure 3. Bioreactor system designed for scaffold revascularization using interchanges of induction and maturation medium. Seeding pressure condition were 50 and 25mmHg.

A total of three bioreactors were performed with this interchange of Induction and Maturation media.

Then, three other bioreactors were performed with a "Combined Media" formulation, which was the combination of our previously defined IM and MM in a unique culture media. The bioreactor system procedure was similar to the previous one, but using a unique culture media which was changed every 3 days (Fig. 4).

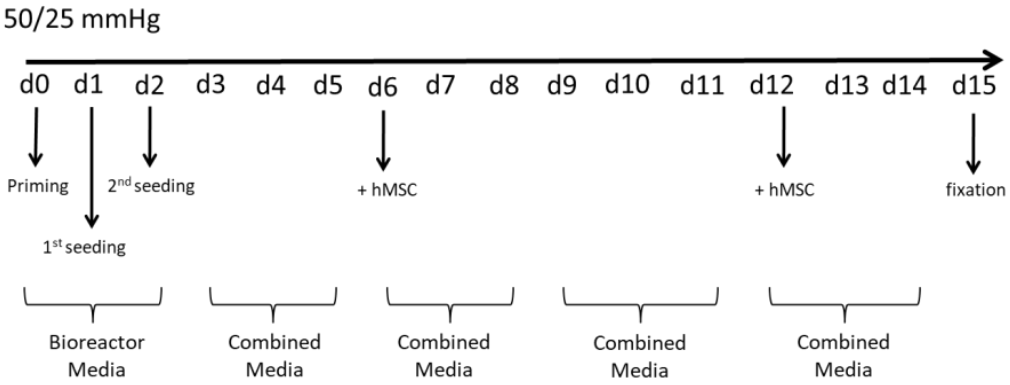

Figure 4. Bioreactor system designed for scaffold revascularization using the combined media. Seeding pressure condition were 50 and 25mmHg.

After the 14d experiments finished, recellularized scaffolds were fixed with formol, embedded in paraffin blocks and cut like mentioned before. H&E stainings and immunostaining with the nuclear staining DAPI, anti-CD31 (MAD-002048-QD, Master Diagnóstica) and anti-vimentin (MAD-000326-QD, Master Diagnóstica) followed. Finally, both experimental conditions were compared to determine if there were differences in the generation of a new vasculature *in vitro*.

Furthermore, in order to have a visual perspective of the recellularized vascular tree, immunostaining with anti-CD31 and anti-vimentin were also performed in 50µm thick paraffin sections. The secondary antibodies employed were: goat anti-mouse 488 (A11029, Molecular Probes) and goat anti-rabbit 568 (A11036 Molecular Probes), respectively. A 3d bioreactor, a 14d bioreactor performed with the alternate media, and another 14d bioreactor performed with the combined media were stained and compared. Z-stack images of each sample were taken using a confocal microscope Zeiss LSM 880.

Once acquired the bioengineered vasculature with both medias (Induction + Maturation medium and the combined media), it was characterized as before, attending to our previously defined vessel sizes.

For this, six random pictures at 20X were taken with the inverted microscope across the whole area of the recellularized scaffold, in order to have representative and random images. Afterwards, four pictures of each selected area were taken: 1) with DAPI channel, to see nuclear staining (in blue); 2) with FIT-C channel, for CD31 staining (in green) and 3) with RFP channel, for vimentin staining (in red) and 4) a merge, which is the combination of the three mentioned channels.

Taking these four pictures of each area into account, vessels were localized and measured with the Cell-D Software. A total of 24 pictures of each recellularized scaffold were analyzed. The aim of this was to determine not only vessel size but also categorize the type of cell coating they had, which ranged from: 1) Nude, meaning that the vessel was not covered by any cell; 2) CD31, meaning that the vessel was predominantly covered by endothelial cells; 3) Vimentin, meaning that the vessel was covered mainly by mesenchymal cells; and 4) Both, meaning that the vessel had both endothelial and mesenchymal covering.

The following picture summarizes the whole process of each bioreactor run, taking into account the preparation of cells, scaffolds, setting up of each bioreactor experiment, and the final data analysis (Fig.5).

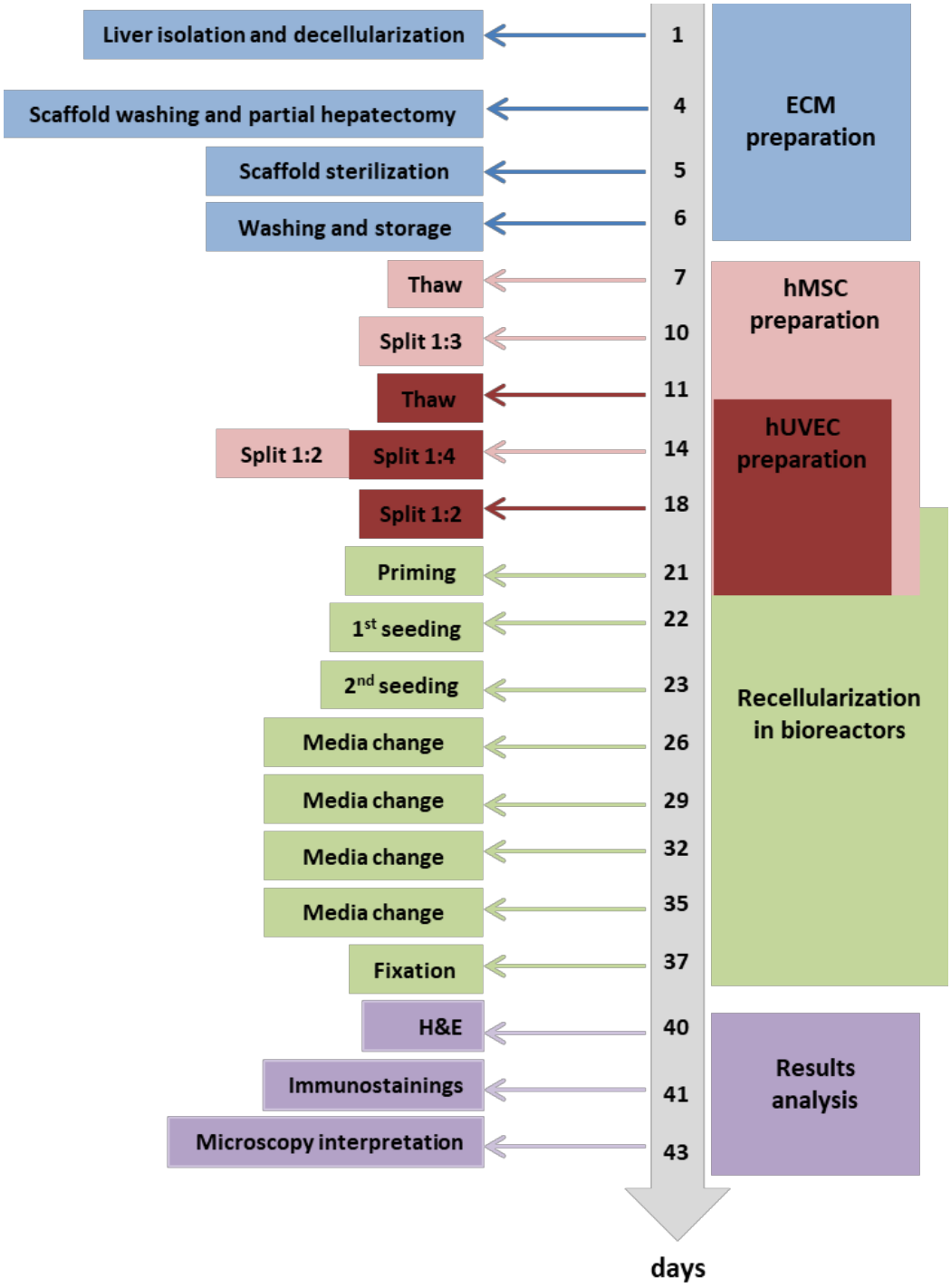

Figure 5. Schematic representation of each bioreactor experiment time consuming.

RESULTS

1. Cells

1.1 Cell isolation, culture and characterization

After cell isolation and expansion, the cells were appropriately characterized (Fig. 6)

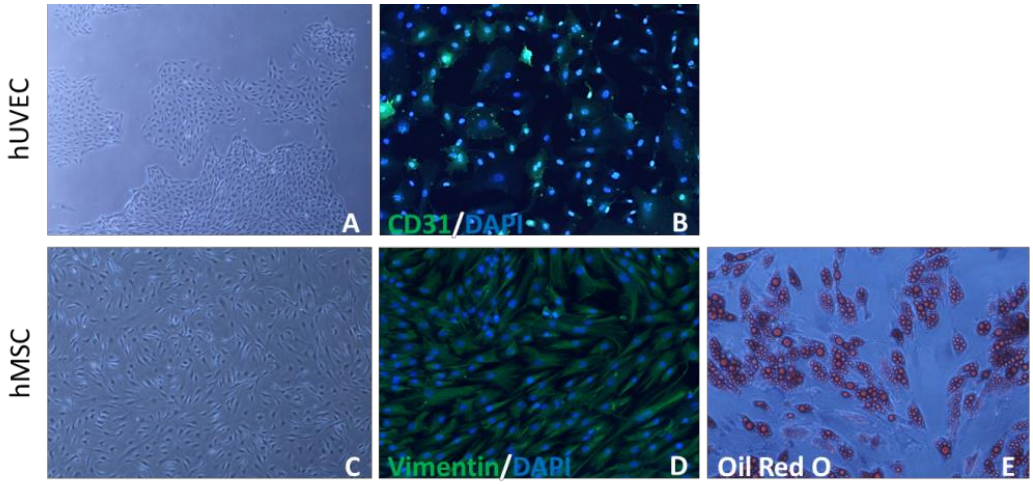

Figure 6. Cell characterization. A) hUVECs in culture; **B)** CD31 positive cells in hUVECs culture; **C)** hMSC in culture; **D)** vimentin positive cells in the hMSC culture; **E)** Oil Red staining for the determination of hMSC differentiation into adipocyte fate. Pictures at 10x.

hUVEC were small, rounded cells growing in colonies, CD31 positive cells and hMSC were larger cells, Vimentin positive and able to differentiate towards adipocytes after 3 weeks of differentiation.

1.2 Cell labeling with lentiviral vectors

After careful quantification of the number of cells labeled with the different dilutions, the results obtained suggested that the optimal concentration for GFP labelling was 1/10 and 1 for TdTomato.

2. Scaffold preparation

2.1 Determination of an optimal detergent flow for organ decellularization

As at first sight, it can be observed in Fig.7 that the native liver presents a rougher texture, due to all the vascularization present. Lower flows of 1ml/min preserves the vascular architecture better than when compared with higher flows of 3 and 5ml/min. In the case of flows of 3ml/min, it can be observed that the vascular tree is more damaged, causing vessel breakage and polimer exit, resulting in the formation of polymer bubbles in certain areas. In the last case of 5ml/min it can be observed that the aspect is completely smooth when compared with the other conditions. In this case, the liver vasculature is completeley damaged and the resultant scaffold's cast seems a ballon filled with polymer.

.

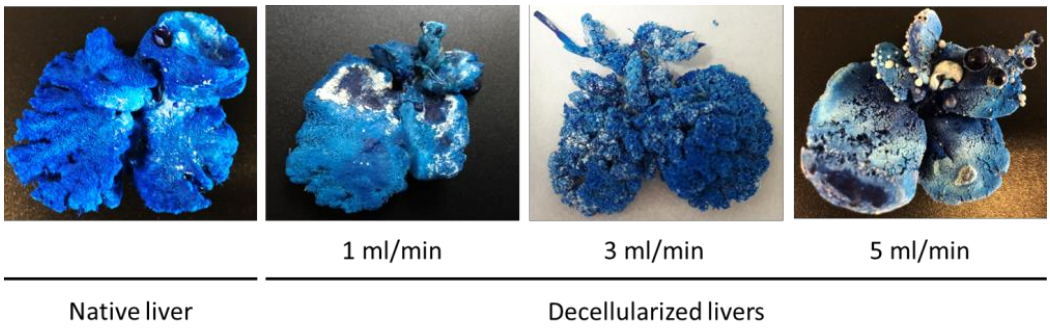

Figure 7. Macroscopic comparison of resultant corrosion casts of native and decellularized livers at different flows perfusion.

These results are contrasted when comparing the SEM pictures. Large, intermediate and small vesseld can be observed in the native liver (Fig. 8 A).

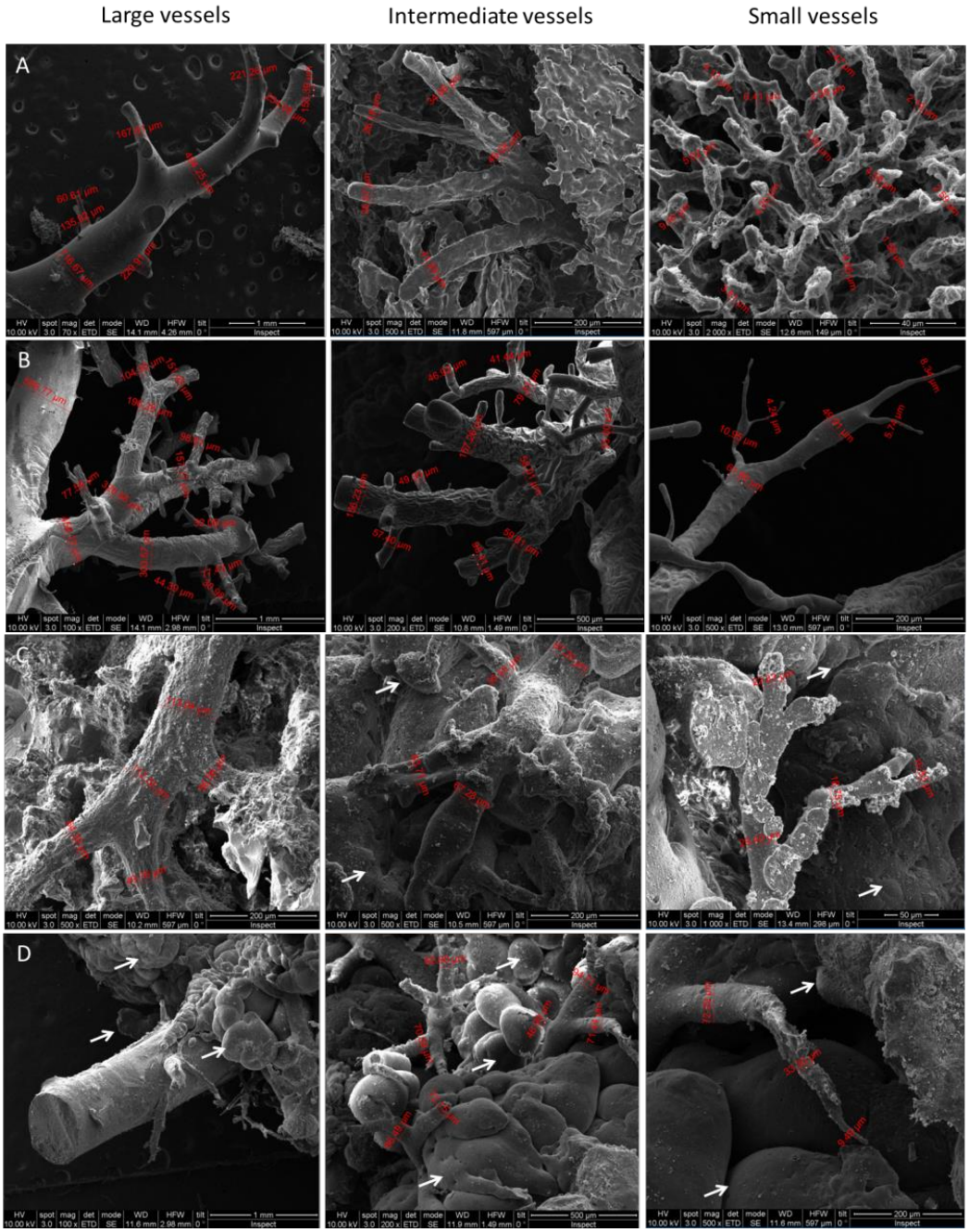

Figure 8. Microscopic comparison of resultant corrosion casts observed with SEM microscopy. A) native liver**; B)** decellularized liver at 1ml/min; **C)** decellularized liver at 3 ml/min and **D)** decellularized liver at 5ml/min. From all of them, large, intermediate and small vessel preservation was compared. Arrows point plastic bubbles, determining vascular breaking.

From the decellularized scaffolds, the ones decellularized at 1ml/min presented structures that closely reminded the native organ (Fig. 8 B). However, this preservation was lost in higher decellularization conditions of 3ml/min (Fig. 8 C), which still preserves some vessels of the different sizes, but also show polymer agglomerations, indicating vessel breakage. This case of vessel damage is very well seen in the case of livers decellularized at 5ml/min, where all it can be seen in the SEM pictures is polymer aggregations (Fig. 8 D).

2.2 *Organ decellularization characterization*

After the decellularization protocol, we were able to eliminate all the cellular content, preserving only the liver ECM (Fig. 9). Furthermore, the resultant ECM preserved all the structural proteins like collagens I, III, IV and laminins as native livers (Fig. 10).

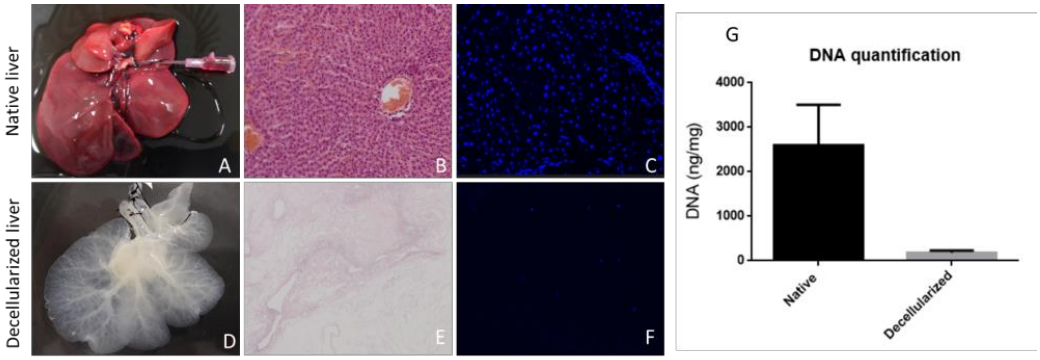

Figure 9. Rat liver comparison before and after decellularization. A) Macroscopic view of a native liver after harvesting; **B)** H&E staining and **C)** DAPi staining of the native liver; D) macroscopic view of a rat liver after decellularization (scaffold); **E)** H&E staining; **C)** DAPI staining of the scaffold, where no nuclei were visible. (Pictures at 10x); **G)** Comparative of DNA quantification in native and decellularized livers.

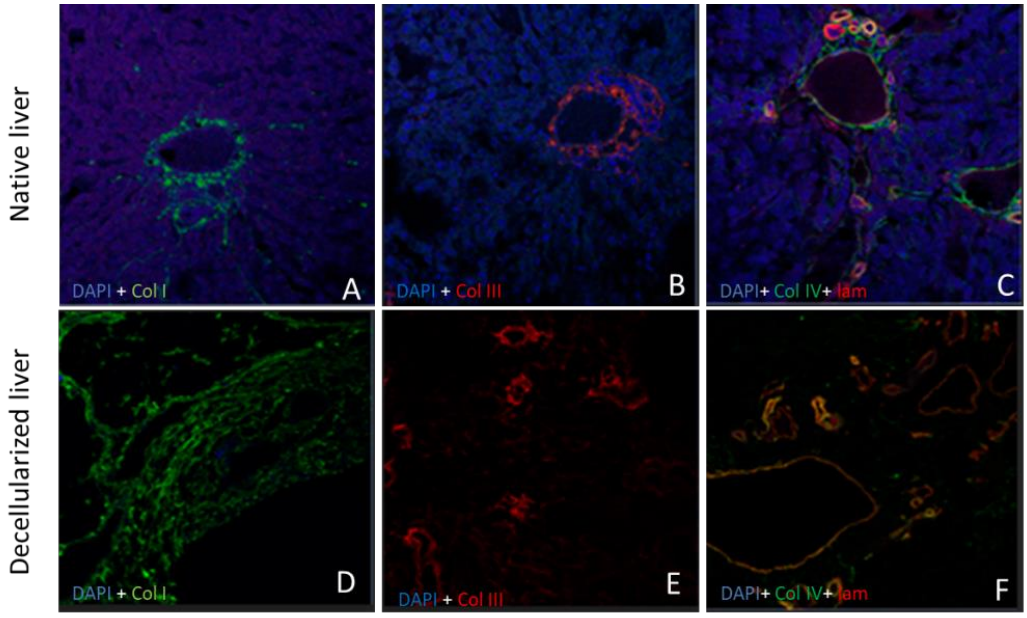

Figure 10. ECM characterization of native and decellularized rat livers. Immunostaining of different structural ECM proteins in native and decellularized livers, showing the preservation of Col I, Col III, Col IV and laminins after decellularization. Pictures at 10x.

3. Rat liver bioengineering

3.1 Determination of the optimal pressure conditions for rat scaffold recellularization

3.1.1 Seeding conditions

The first combination of 14/7 mmHg with continuous perfusion determined so poor cell engraftment that immunostainings with anti-GFP and anti-RFP were not performed. This pressure condition was also discarded when testing the multistep infusion (Fig. 11).

It could be observed that in both cases of seeding methods, the higher pressure conditions used yielded the best scaffold colonization. However, better cell engraftment could be determined with the multistep method.

Taking into account the whole area of the ECMs, more cell distribution across the scaffold was observed in H&E and DAPI stainings of multistep infusion. GFP stainings showed similar results according to cell distribution as H&E and DAPI stainings. On the contrary, RFP staining outcomes from continuous perfusion were almost imperceptible: there were very low numbers of cells when seeded at lower pressures. However, larger amount of red cells could be observed with the multistep infusion. This clearly indicated that, in order to appropriately seed cells at lower pressures, direct cell injection with the multistep infusion was much more effective rather than with the continuous perfusion.

Conditions of 50/25 mmHg and 100/50 mmHg in multistep infusions showed similar results with homogenous cell distribution across the whole area of the scaffold. On the contrary, the lower condition of 25/14 showed relevant areas of the scaffold which were not recellularized. For these reasons, further experiments were performed with the multi-step infusion method.

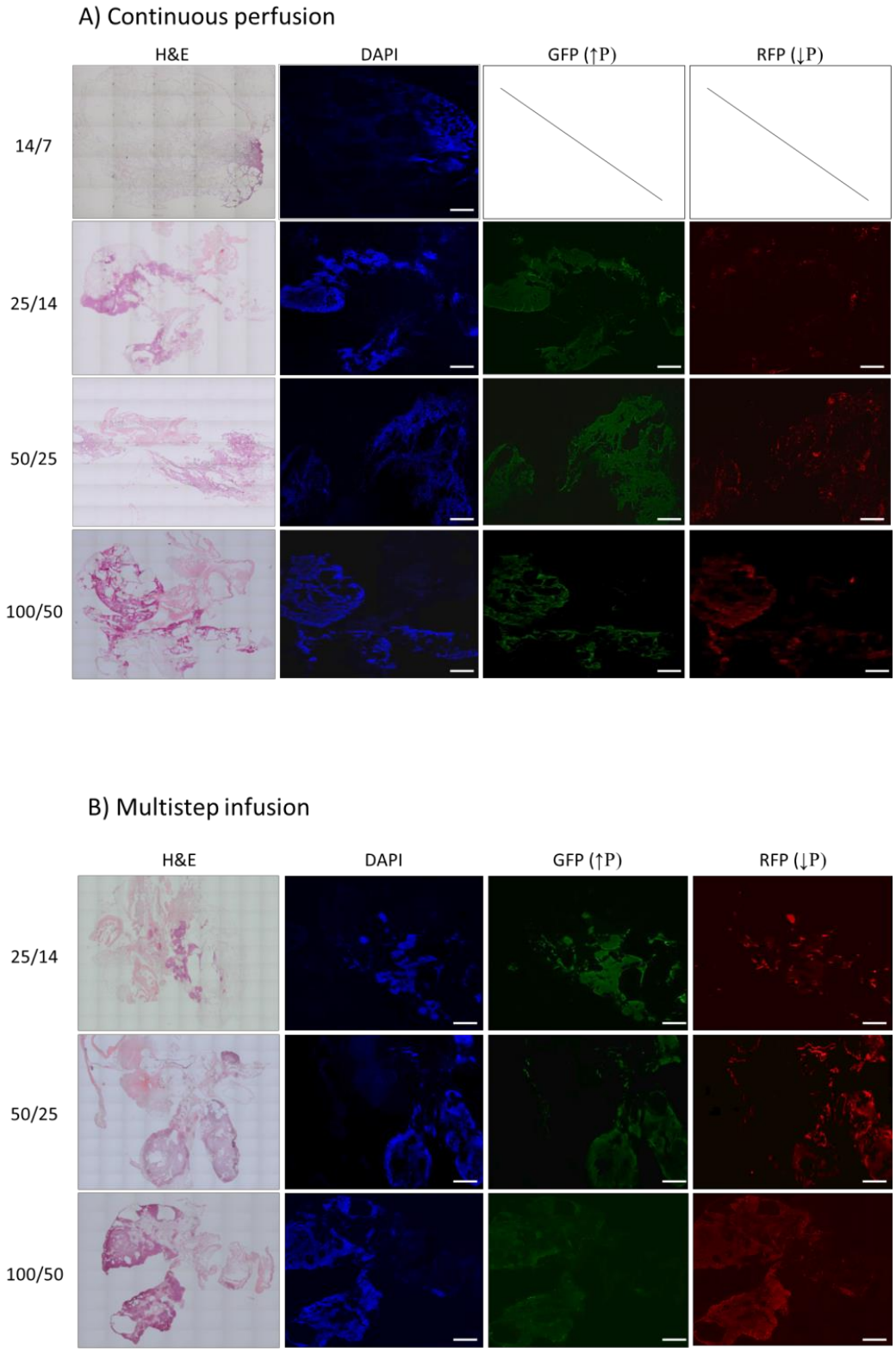

Figure 11. Comparison between different seeding methods at different pressure conditions. H&E, and immunofluorescent staining comparing results from **A)** Continuous perfusion seeding system, where cells were delivered in the culture medium form the spinner flask at different pressure conditions**. B)** Multi-step seeding system, where cells were directly injected in the scaffold through the portal vein at different pressure conditions. Scale bars 1mm.

3.1.2 LDH test

Statistical analyses determined that there were no significant differences between the four groups of pressure (P value > 0,05). This ensured that even the highest pressures used did not affect cell viability in the bioreactor system. Once determined that the four pressure combinations chosen did not affect cell viability during the experiment in the bioreactor system, the next goal was to determine an optimal seeding condition (Fig. 12).

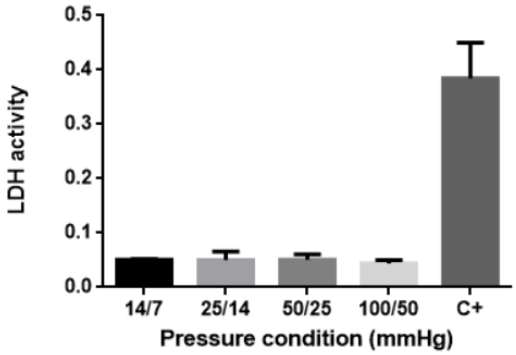

Figure 12. LDH values for each bioreactor pressure condition. C+ represents the kit positive control.

3.1.3 Scaffold total recellularization (DAPI staining)

Our integration of all the data collected from the different scaffolds seeded at different pressure combinations revealed that the higher pressure combination condition used for cell delivery produced the highest cell engraftment within the scaffold. This was statistically significant when compared with the other conditions (p<0,05) (Fig, 13)

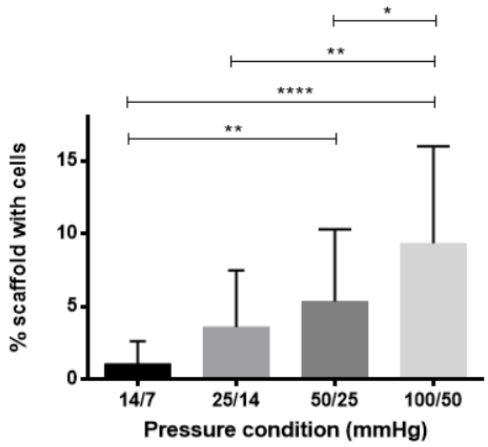

Figure 13. Percentage of scaffold colonization using different pressure combinations. Statistical analyses determined that there were statistical differences between the combinations of 50/25 and 14/7 (P=0,0047); 100/50 and 14/7 (P<0,0001); 100/50 and 25/14 (P=0,002) and 100/50 and 50/25 (P=0,0427). No statistical differences were found between 25/14 and 14/7 and between 50/25 and 25/14 (P<0,05).

3.1.4 Quantification of the labeled cells present in vascular structures with different diameter. Anti-GFP and anti-RFP immunofluorescence analysis.

Data analysis of scaffolds recellularized with GFP (determining the location of cells seeded at higher pressures) and RFP (determining the location of cells seeded at lower pressures) stainings determined also that higher pressure combinations allowed better scaffold recellularization, as seen in Fig. 13. Then, we represented vessel diameter (small, intermediate and large) and the type of cell lining the vessels identified by immunofluorescence (GFP: cells seeded at higher pressure; RFP: cells seeded at lower pressure; Both: cells seeded at higher and lower pressure and Nude: the vessel was not coated by any cell). These data are represented in a graph, accompanied by their respective representation (Fig.14).

When cells were seeded at 14/7 mmHg (Fig. 14A), we observed that the majority of vessels were devoid of any cells (cells were not able to reach them with this pressure condition). Hence, the graphic representation attached to the bar graph is completely blue, meaning that the majority of the vessels found in these bioreactors were mostly nude.

At 25/14mmHg pressure combination, it can be observed that large (>100 µm) and small vessels (<40 µm) are still predominantly nude, however, the majority of the intermediate diameter vessels (40-100 µm) are lined with GFP-labeled cells (Fig. 14B).

Finally, seeding conditions at 50/25 (Fig. 14 C) and 100/50 mmHg (Fig. 14 D) showed very similar patterns of cell distribution, where large and intermediate vessels were surrounded by both RFP- and GFP-labeled cells, while smaller vessels were predominantly lined with GFP-labeled cells.

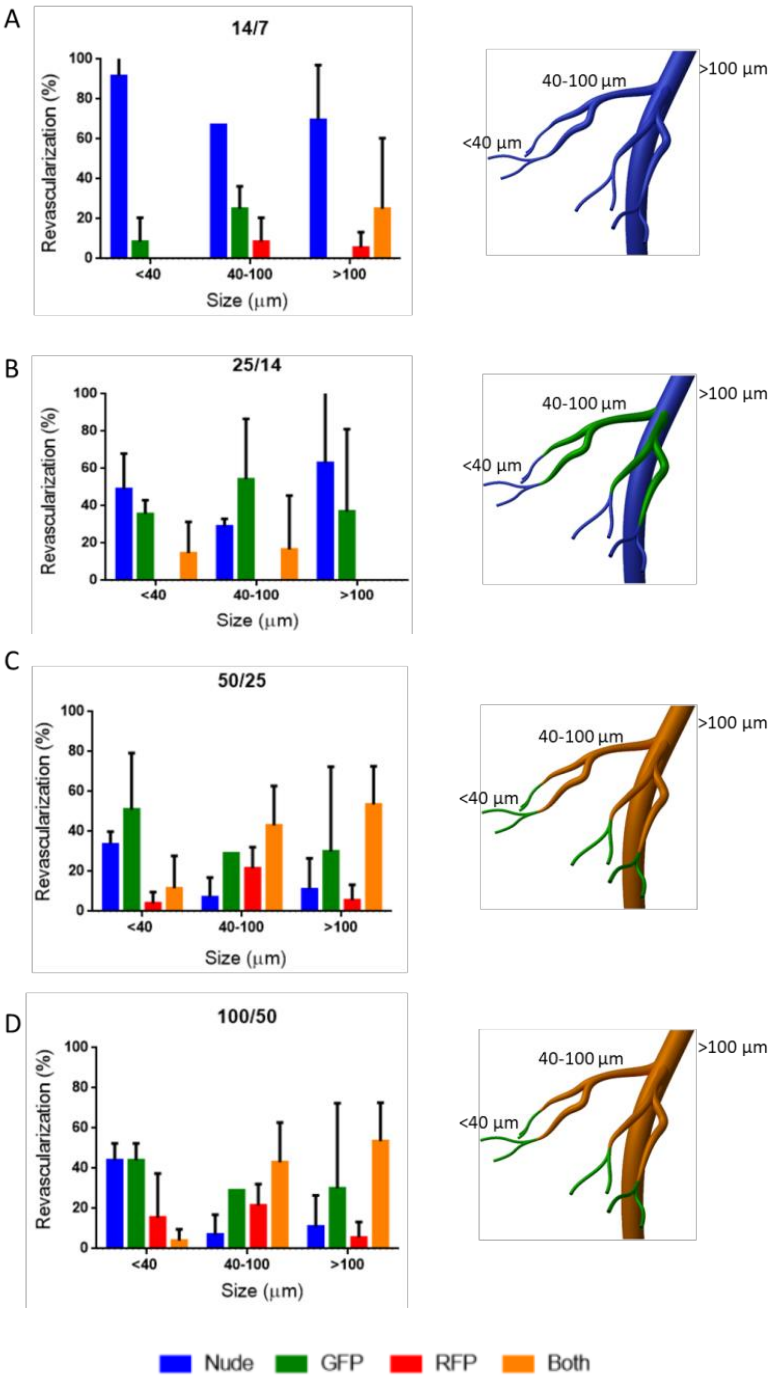

Figure 104. Vascular structure colonization (sorted by vessel diameter) according to different combinations of pressure conditions in the seeding. A) seeding conditions of 14/7mmHg were not enough to achieve vessel revascularization, so the majority of vessels from this bioreactors remained nude; **B)** with the pressure condition of 25/14mmHg, the majority of the vessels still remained nude, but intermediate vessels were reached with cells seeded at the highest pressure of 25mmHg; **C)** 50/25 mmHg and D) 100/50mmHg pressure conditions displayed similar results, where cells were able to reach all vessel sizes, meaning that these pressure combinations were able to sustain vessel revascularization, where both cells seeded at high and low pressures reached any vessel structure.

3.2 Quantification of vessel formation in vitro with growth factor supplementation.

Immunofluorescence staining with anti-CD31 (for endothelial cell labeling) and anti-vimentin (for hMSC labeling) revealed the first large difference when comparing 3d-bioreactors and 14d-bioreactors with alternate configuration (Fig. 15 A and B). In short-term bioreactors, only a mixed cell distribution with no apparent organization was observed, while in long-term bioreactors with induction and maturation medium showed cell aggregation and organization in vascular structures with different diameter. This cell reorganization seemed progressive and in many vessels endothelial cells were surrounded by hMSCs or pericytes, as naturally occurring during vasculogenesis and angiogenesis. Furthermore, different vessel sizes could be observed, ranging from larger to smaller vessels (Fig. 15 C).

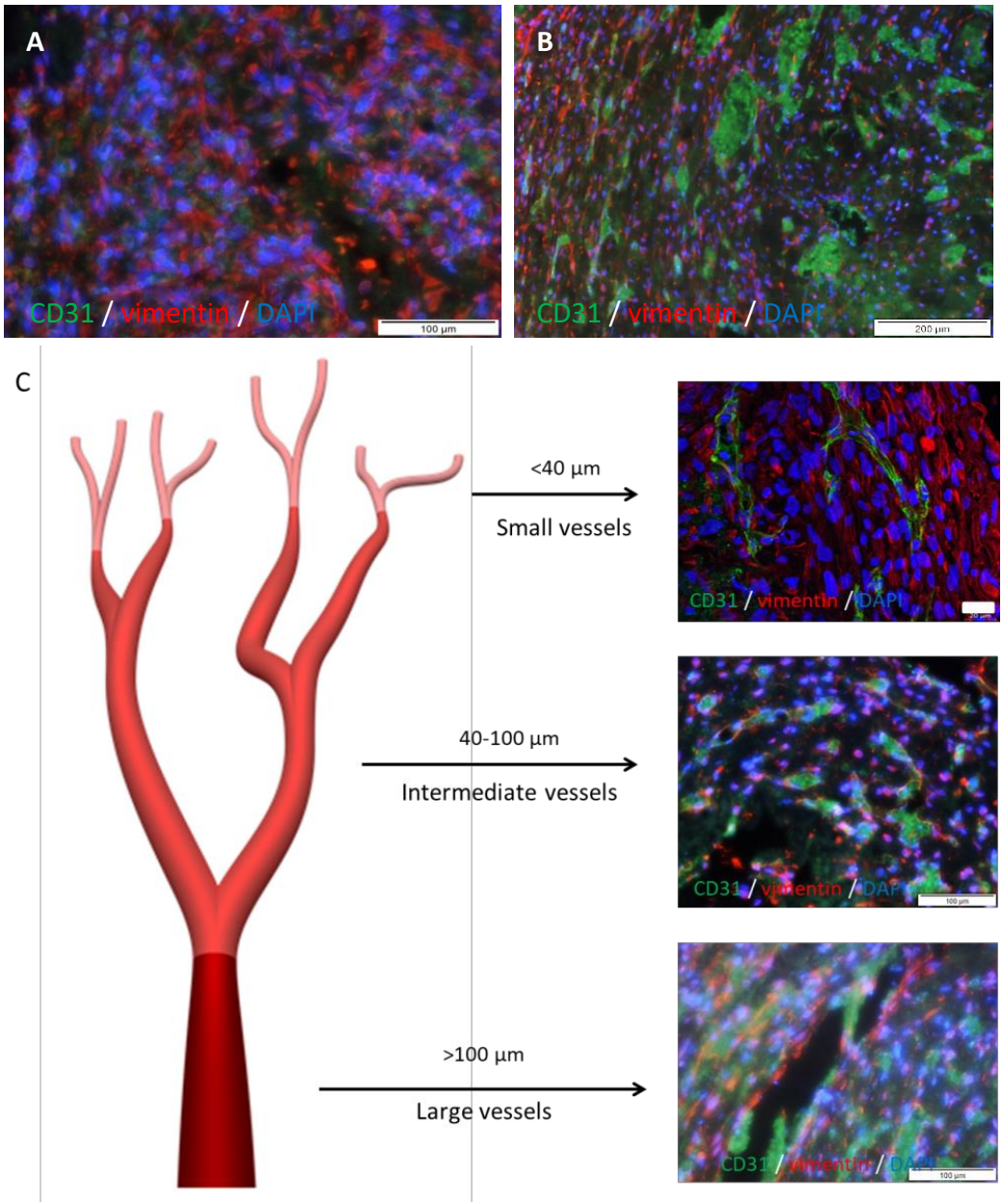

Figure 15. Immunostaining to determine cell distribution in the recellularized scaffolds. **A)** Mixed and homogeneous distribution of endothelial (green) and mesenchymal cells (red) after 3d in the bioreactor system; scale bar 100µm; **B)** Cell reorganization in clusters and lining vascular structures, where endothelial cells are surrounded by mesenchymal cells; scale bar 200 µm; **C)** Different vessel diameter lined with endothelial and pericytes could be obtained after 14d in the bioreactor system with induction and maturation media; scale bar 20 µm in small vessels, 100 µm in intermediate and large vessels.

Afterwards, we compared long-term bioreactors performed with alternate and combined media. To do this, we performed the same analysis devised before, the quantification of vessel diameter (small,

intermediate and large) and the cells lining these vessels (determining now the number of vessels with CD31-positive cells - endothelial cells, vimentin-positive cells - mesenchymal cells, both or nude). These data are represented in a graph, accompanied by their respective representation and immunostaining, where both mediums are compared (Fig. 16).

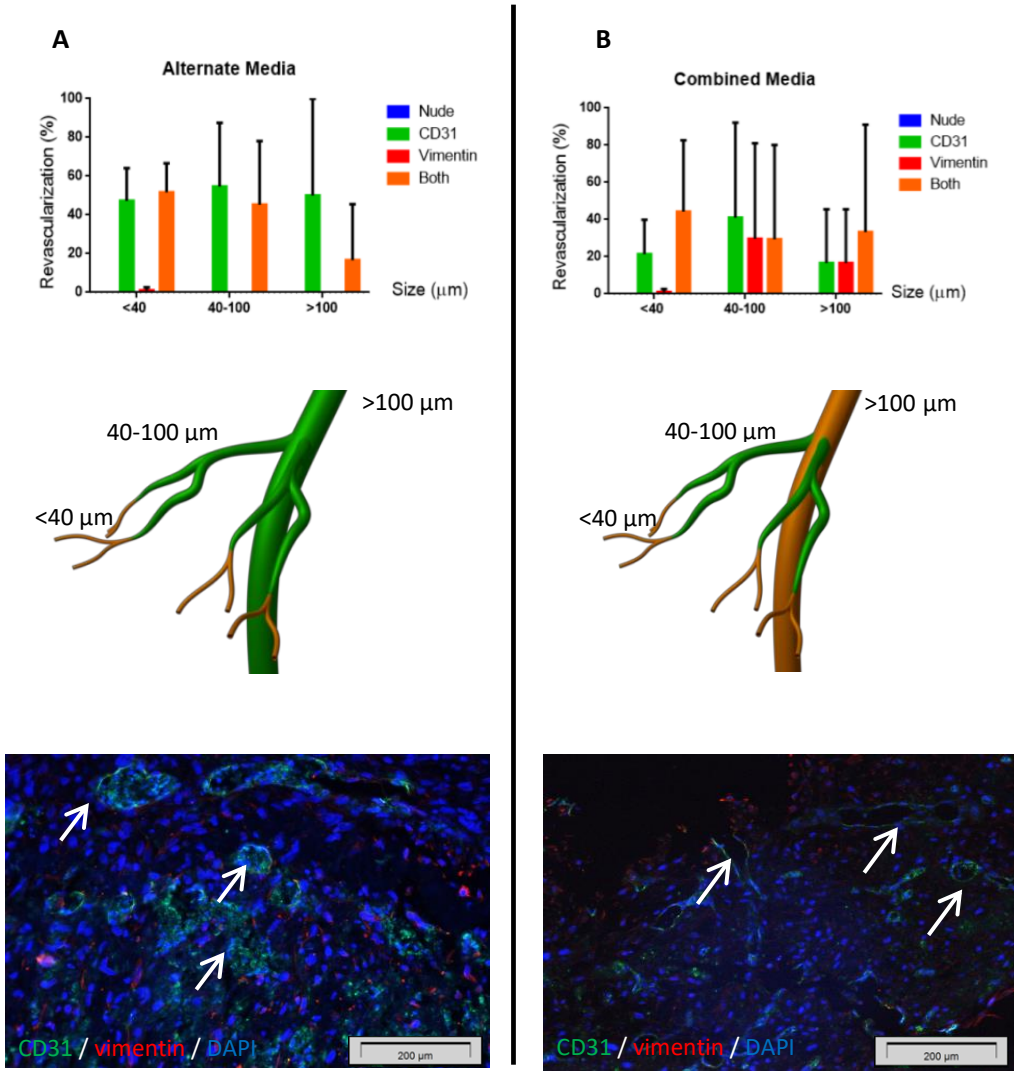

Figure 16. Vasculature characterization with both media formulations: A) Alternate and **B)** Combined. For each condition, a graphic is represented, where vessel sizes and the cell type lining the vascular structures were characterized. Representation of this vascular characterization and immunostaining with anti-CD31, showing the resultant vessel structures (arrows). Scale bar 200µm.

When alternate media was employed in the bioreactor system, we observed that large (>100µm) and intermediate (40-100 µm) vessels are predominantly lined with CD31 cells; small vessels (<40 µm) were coated by both type of cells (Fig. 16A). When combined media was employed in the bioreactor system, large and small vessels were lined with both types of cells and intermediate vessels are predominantly coated with endothelial cells (Fig. 16B).

Focusing in the immunostaining with CD31, revascularized scaffolds with combined media resulted in a more defined revascularization pattern of the ECM, because the large majority of vessels observed have a clear luminal structure. On the other hand, bioreactors performed with alternate media presented vessels with less defined lumens and an apparent accumulation of endothelial cells on them. It could be determined that a cluster-like structure derived in a more mature vessel structure, with the endothelial cells delimiting a lumen.

Immunostaining and confocal microscopy of thick sections (50µm) of bioreactor samples confirmed our theory that 3d in the bioreactor system allows for cell engraftment, but it is not enough to allow for effective cell reorganization. When changing to longer bioreactor timepoints of 14d, it could be observed more defined vascular structures at this stage, when using the alternate media and the combined media. Furthermore, a larger number of mature vessel structures with tubular shapes (and lined with hUVECs and hMSC) were found in the combined media (Fig. 17).

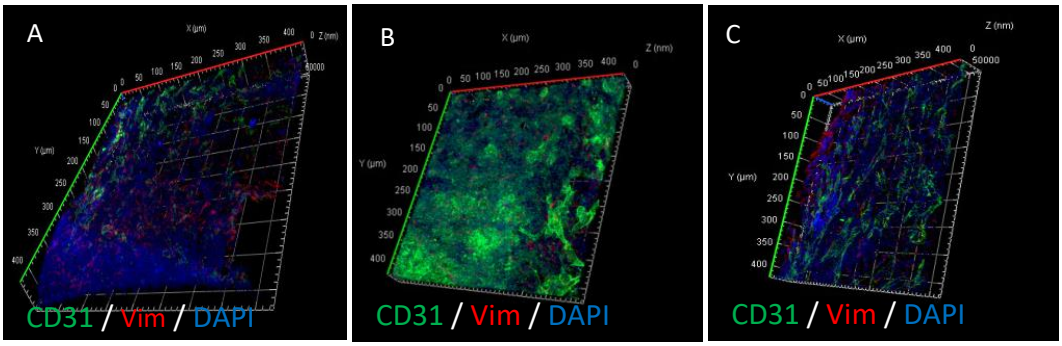

Figure 117. Immunofluorescence analysis of 50µm thick sections. A) a 3d bioreactor, **B)** a 14d bioreactor with the alternate medium, and **C)** 14d bioreactor with the combined medium. Pictures at 200x.

Finally, in order to fully determine which media formulation was better to achieve a complete revascularization, we performed different statistical analyses, considering vessel size, cell type and the cell type in each vessel diameter. The chi-square test was used to assess the relationship between qualitative variables and was replaced by Fisher's exact test when application criteria were not met.

1) Vessel size: there were no statistically significant differences between the vessel size that each media was able to revascularize (p=0,233) (Table 2).

Table 2. Comparison between recellularized vessel sizes with each culture medium configuration. No statistically differences are observed between the vessel size and the type of cells covering them.

			CULTURE MEDIUM		Total
			COMBINED	ALTERNATE	
VESSEL SIZE	<40	Count	146	146	292
		% inside of MEDIUM	72.3%	70.2%	71.2%
	40-100	Count	53	53	106
		% inside of MEDIUM	26.2%	25.5%	25.9%
	>100	Count	3	9	12
		% inside of MEDIUM	1.5%	4.3%	2.9%
Total		Count	202	208	410
		% inside of MEDIUM	100.0%	100.0%	100.0%

2) Type of cell: there were statistically significant differences (p<0,001) among the two different cell types found in each scaffold's vessel with the two different culture media (Table 3).

Table 3. Comparison between type of cell and culture media. There was a statistically significant difference between the type of cells found in each vessel. There was a 66,8% of vessels lined with both cell types with combined media, versus 52,4% of I+M media. Data labelled in red is statistically different.

			CULTURE MEDIUM		
			COMBINED	ALTERNATE	Total
CELL TYPE	CD31	Count	56	97	153
		% inside of MEDIUM	27.7%	46.6%	37.3%
	VIM	Count	11	2	13
		% inside of MEDIUM	5.4%	1.0%	3.2%
	BOTH	Count	135	109	244
		% inside of MEDIUM	66.8%	52.4%	59.5%
Total		Count	202	208	410
		% inside of MEDIUM	100.0%	100.0%	100.0%

3) Vessel size and type of cell: there were no significant differences for a vessel size <40µm or >100µm between both culture medias in terms of cell type lining (P=0,190; p=0,151, respectively). However, there were significant differences for the vessel size 40-100µm (p<0,001). (Table 4).

Table 4. Resulting tables from the integration of data from the immunostaining, showing the type of cell that revascularized each vessel size in each culture medium configuration. Red data are statistically different.

<40µm			CULTURE MEDIUM		
			COMBINATED	ALTERNATE	Total
CELL TYPE	CD31	Count	47	62	109
		% inside of MEDIUM	32.2%	42.5%	37.3%
	VIM	Count	2	2	4
		% inside of MEDIUM	1.4%	1.4%	1.4%
	BOTH	Count	97	82	179
		% inside of MEDIUM	66.4%	56.2%	61.3%
Total		Count	146	146	292
		% inside of MEDIUM	100.0%	100.0%	100.0%

40-100 µm			CULTURE MEDIUM		
			COMBINED	ALTERNATE	Total
CELL TYPE	CD31	Count	8	28	36
		% inside of MEDIUM	15.1%	52.8%	34.0%
	VIM	Count	8	0	8
		% inside of MEDIUM	15.1%	0.0%	7.5%
	BOTH	Count	37	25	62
		% inside of MEDIUM	69.8%	47.2%	58.5%
Total		Count	53	53	106
		% inside of MEDIUM	100.0%	100.0%	100.0%

>100 µm			CULTURE MEDIUM		
			COMBINED	ALTERNATE	Total
CELL TYPE	CD31	Count	1	7	8
		% inside of MEDIUM	33.3%	77.8%	66.7%
	VIM	Count	1	0	1
		% inside of MEDIUM	33.3%	0.0%	8.3%
	BOTH	Count	1	2	3
		% inside of MEDIUM	33.3%	22.2%	25.0%
Total		Count	3	9	12
		% inside of MEDIUM	100.0%	100.0%	100.0%

It can be summarized from these statistical analyses that both culture mediums (combined and alternate) were able to induce revascularization of acellular scaffolds, however combined media was significantly better recellularizing intermediate vessels (40-100µm).

DISCUSSION

As in many cellular systems, the quality of cells obtained from the different isolations was critical. This allowed for their long *in vitro* expansion without losing their capacity of self-organization once recellularized in the liver decellularized ECM.

Furthermore, the decellularization process is a technique that allows for the complete cell removal from the organ or tissue, preserving its ECM microarchitecture. Here, we first sought to develop an efficient protocol for rat liver decellularization that could preserve the vascular network. Hence, several flows of the decellularization solution were tested (1, 3 and 5ml/min) to choose the most efficient one, without compromising the vascular tree integrity. A corrosion cast was generated with the resultant scaffolds, where it could be observed that higher perfusion flow at 5ml/min of the decellularization solution was too high and the vascular tree was significantly damaged, resulting in intermediate and small vessel fracture (Fig. 8). On the contrary, flows at 1 and 3ml/min allowed for better vascular architecture preservation, being the most conservative the flow of 1ml/min, when compared with native livers. According to these results, we chose a flow rate of 2ml/min for organ decellularization, because it was low enough to ensure ECM preservation at a relatively higher speed than 1ml/min.

Furthermore, ECM-protein staining results demonstrated that typical ECM structural proteins like collagens I, III and IV, laminin and fibronectin were present in the decellularized livers at their putative locations, indicating a suitable ECM preservation, when comparing with the native tissue.

Then, our first goal was to introduce the cells in the scaffold, avoiding cell aggregation and enabling the cells to spread homogeneously throughout the scaffold. For this reason, we decided to seed the cells always combining two perfusion pressures. Higher pressures would allow cells to penetrate and distribute further into deeper places of the ECM (reaching the small vessels); meanwhile lower pressures would distribute the cells into shallower areas of the vascular tree of the scaffold (reaching intermediate and large vessels).

The different tests performed, allowed us to choose an appropriate pressure combination for scaffold seeding. Results from H&E stainings (Fig. 11) determined on the one hand that continuous perfusion was not enough to distribute the cells in the whole area of the scaffolds. On the other hand, these results determined that lower pressures combinations like 14/7 and 25/14mmHg offered very poor scaffold colonization. On the contrary, higher pressure combinations of 50/25 and 100/50mmHg allowed very similar results of efficient scaffold recellularization, distributing the cells in a homogeneous fashion throughout the whole ECM.

Results of LDH determined that cell viability and survival in the bioreactor systems (Fig. 12) were not affected when using higher pressures combinations. Furthermore, DAPI staining analyses (Fig. 13) determined

that lower pressure combinations of 14/7 and 25/14mmHg presented the lowest recellularization rate, confirming the suggestions from the H&E stainings, and pressure combinations of 50/25 and 100/50mmHg presented higher scaffold colonization rate, being 100/50 mmHg the best condition. However, low significant statistical differences between pressure conditions of 50/25 and 100/50mmHg were observed. Finally, immunostainings with GFP (representing green cells seeded at higher pressure) and Tomato (representing red cells seeded at a lower pressure) demonstrated that, once more, pressure combinations of 50/25 and 100/50mmHg displayed similar results. Both pressure combinations allowed the cells to reach not only large and intermediate vessels, but also the capillary level.

Considering all these results, it could be determined that there was no significant difference between using the pressure conditions of 50/25 or 100/50mmHg for the scaffold recellularization. Homogeneous cell penetration and distribution, and high cell viability were achieved with both of them. However, the perfusion pressure of 50/25mmHg was chosen because it was lower than 100/50mmHg, and could benefit scaffold integrity during the recellularization process. That said, this condition of 50/25mmHg was chosen for further experiments.

The second goal was to achieve cell reorganization into vascular structures within the liver ECM. Once we knew how to introduce the cells into the scaffold, we sought them to organize and mature into a vascular configuration. For this, it was crucial to determine an appropriate vessel size, in order to characterize the type of vessels that could be revascularized, and also define an appropriate culture medium which allowed cell maturation and organization into vascular structures.

Due to this, several experiments were performed combining an induction media with a maturation media (alternate media) with the idea of first inducing growth of the seeded cells and then alternate to a maturation media, which allowed cell organization and distribution. This cycle of maturation was accompanied by an extra seeding of hMSC, which have an essential role in vascular maturation during embryogenesis[4].

Our results from immunostaining analysis with anti-CD31 and anti-vimentin revealed that there was a significant difference between a 3d-bioreactor and a 14d bioreactor system: in 3d-bioreactors, only cell distribution was observed within the scaffold. However, 14d-bioreactors displayed a nice cell organization, where clusters of endothelial cells were surrounded by MSC or pericytes. This cell organization observed *in vitro* is particularly important, because this is what naturally occurs during embryogenesis. Besides, we were able to identify different vessel sizes, ranging from larger, intermediate and small ones, revealing that longer times in the bioreactor system and in our defined induction and maturation medium were able to generate an organized vascular tree.

Afterwards, we decided to compare the resultant vascular tree formation when comparing the interchange of induction and maturation medium with a unique media (the combined media), in order to determine if there were differences between the two regimens. When analyzing the immunofluorescence staining obtained with anti-CD31 immunostaining, we could observe that more mature vessel structures were completed when using the combined configuration, because they presented a lumen-like structure, whereas vessels observed with the alternate configuration were mostly clusters of cells with smaller lumens that had not matured into a tubular structure yet (Fig. 15 A and B). These results

were also confirmed when comparing the Z-stack of both experimental conditions in the immunostainings performed in 50µm sample sections (Fig. 17). Statistical analysis determined that both culture mediums were able to induce revascularization of the liver ECM, however combined media presented statistical differences in the recellularization of intermediate vessels when vessel size and type of cell were compared. This is why we believe that combined media would be the most appropriate culture medium to achieve a complete scaffold revascularization.

Relevant publications up to date regarding vascular engineering include Nyberg et al work[16] , which have recently published a method of porcine whole organ engineering, were hUVECs were used for the seeding of the acellular scaffold. They demonstrated that hUVECs had a particular phenotypic plasticity, with the capacity to differentiate into sinusoidal cells, which showed specific sinusoidal markers and also de presence of plasma membrane fenestrations. Another recent publication from Nichols et al[17] was also concentrated in the generation of microvascular structures in lung bioengineering. Despite both have achieved some degree of microvasculature regeneration, they did not characterized in extent the rest of the vasculature, focusing their work in the characterization of only small vessels.

Indeed, after bioengineered grafts were transplanted into living recipients, the in vivo perfusion did not reach day 7 after transplantation, due to graft thrombosis, which still represents a current common phenomenon in bioengineered organs.

Hence, we have established a novel and more efficient strategy for liver scaffold revascularization, defining specific bioreactor conditions that allow the *in vitro* revascularization of small, intermediate and large vessels, which showed endothelial and mesenchymal cell organization and association as naturally occurs *in vivo.* However, we could not perform any test to validate the functionality and permeability of our engineered vasculature.

Future studies should concentrate on procedures to allow the formation of more mature/complex vascular structures, in order to be functional and stable once anastomosed to the recipient's vasculature. This would include the seeding of additional cell types that constitute blood vessel niches such as smooth muscle cells, macrophages or monocytes, together with hUVECs and hMSCs, in order to fully recreate a vascular niche as close as possible to the *in vivo* environment.

Indeed, we believe this multiple cell types could be more effectively organized within the scaffold if they are seeded through different blood vessels. The use of hepatic arteries, inferior vena cava and/or bile duct for cell seeding would more effectively distribute them within the scaffold, reaching different zones of the vascular architecture. After further characterization *in vitro* research could allow future extrapolation into porcine or human liver scaffolds.

CONCLUSIONS

1. We were able to generate a functional and preserved rat liver ECM after the decellularization process.

2. We were able to establish an efficient bioreactor system for liver ECM revascularization:
    a. We could determine suitable pressure conditions for scaffold seeding, achieving high cell viability, penetration and homogeneous distribution across the liver ECM.
    b. We could formulate appropriate culture media that enhanced not only cell survival, but also allowed the endothelial–pericyte association, mimicking what occurs during embryogenesis *in vivo*.
    c. Both culture media tested were able to effectively enhance scaffold revascularization, allowing the revascularization of small, intermediate and large vessels. However, the combined medium showed a superior capacity to revascularize intermediate vessels of 40-100µm.

BIBLIOGRAPHY

1. Carmeliet, P. Mechanisms of angiogenesis and arteriogenesis. *Nat Med* **6**, 389-395 (2000).
2. Eichmann, A.*, et al.* Vascular development: from precursor cells to branched arterial and venous networks. *Int J Dev Biol* **49**, 259-267 (2005).
3. Hallmann, R.*, et al.* Expression and function of laminins in the embryonic and mature vasculature. *Physiol Rev* **85**, 979-1000 (2005).
4. Armulik, A., Abramsson, A. & Betsholtz, C. Endothelial/pericyte interactions. *Circ Res* **97**, 512-523 (2005).
5. Thurston, G.*, et al.* Angiopoietin 1 causes vessel enlargement, without angiogenic sprouting, during a critical developmental period. *Development* **132**, 3317-3326 (2005).
6. Davis, G.E. & Senger, D.R. Endothelial extracellular matrix: biosynthesis, remodeling, and functions during vascular

morphogenesis and neovessel stabilization. *Circ Res* **97**, 1093-1107 (2005).
7. Davis, G.E. The development of the vasculature and its extracellular matrix: a gradual process defined by sequential cellular and matrix remodeling events. *Am J Physiol Heart Circ Physiol* **299**, H245-247 (2010).
8. Gianni-Barrera, R*., et al.* Long-term safety and stability of angiogenesis induced by balanced single-vector co-expression of PDGF-BB and VEGF164 in skeletal muscle. *Sci Rep* **6**, 21546 (2016).
9. Banfi, A*., et al.* Therapeutic angiogenesis due to balanced single-vector delivery of VEGF and PDGF-BB. *FASEB J* **26**, 2486-2497 (2012).
10. Wang, Y*., et al.* Comparison of invasive blood pressure measurements from the caudal ventral artery and the femoral artery in male adult SD and Wistar rats. *PLoS One* **8**, e60625 (2013).
11. Baptista, P.M*., et al.* The use of whole organ decellularization for the generation of a vascularized liver organoid. *Hepatology* **53**, 604-617 (2011).
12. Sara Morini, N.S.-R., Iris Plá Palacín, Pilar Sainz Arnal, Manuel Almeida, Laurens Verscheijden, Joana I. Almeida, Alberto Lue, Sara Llorente, Helen Almeida, Pablo Royo Dachary, Agustín García Gil, Trinidad Serrano-Aulló, Pedro M. Baptista. Liver Tissue Engineering. in *Bioreactors for Stem Cell Expansion and Differentiation* (ed. Joaquim M.S. Cabral, C.L.d.S.) 27 (2018).
13. Pla-Palacin, I., Sainz-Arnal, P., Morini, S., Almeida, M. & Baptista, P.M. Liver Bioengineering Using Decellularized Whole-Liver Scaffolds. *Methods Mol Biol* **1577**, 293-305 (2018).
14. Soto-Gutierrez, A*., et al.* A whole-organ regenerative medicine approach for liver replacement. *Tissue Eng Part C Methods* **17**, 677-686 (2011).
15. Traore, M.A. & George, S.C. Tissue Engineering the Vascular Tree. *Tissue engineering. Part B, Reviews* **23**, 505-514 (2017).
16. Shaheen, M.F*., et al.* Sustained perfusion of revascularized bioengineered livers heterotopically transplanted into immunosuppressed pigs. *Nat Biomed Eng* (2019).
17. Nichols, J.E*., et al.* Production and transplantation of bioengineered lung into a large-animal model. *Sci Transl Med* **10**(2018).

CHAPTER 2.

Effect of liver ECM in the differentiation/function of liver stem cells and directly reprogrammed hepatocytes

INTRODUCTION

The quest to bioengineer a whole-liver for transplantation has many challenges. When focusing on the different cell types necessary, there are many cell populations that need to be isolated, characterized and expanded from hepatic tissue or others, to ultimately use them to seed the decellularized liver scaffolds in bioreactors. Choosing the most appropriate hepatic cells to use, amenable to large-scale cell expansion, is one of the hardest tasks, since many different cells are available nowadays[1,2]). Primary hepatocytes have shown promise before, but are difficult to obtain in large quantities for human liver bioengineering[3,4]. Hence, several researchers have been focusing on primary hepatic stem/progenitor cells, or a myriad of hPSC- or hMSC-derived hepatic progenitors or hepatocytes[5-7].

In this regard, human organoids derived from Leucine-rich repeat-containing G-protein coupled receptor 5 (LGR5)-positive adult tissue stem cells offer exciting new possibilities as an autologous cell source for tissue engineering or cell therapy[8,9], since they can be easily obtained from a liver biopsy and expanded in culture for years while remaining genetically stable[5,10]. Unfortunately, reproducibility and upscaling of current organoid systems remain major bottlenecks in their clinical application[11]. Establishing large numbers of organoids with current protocols is tedious, since organoids are cultured in droplets of Matrigel™ [5,10], which hampers clinically-relevant production times of organoids for tissue engineering and transplantations.

One other promising alternative for generating hepatocytes is the direct reprogramming technique. As from the first direct reprogramming

experiments inducing myoblasts over 30 years ago, more and more types of tissue have been generated with this technique[12]. Transcription factors together with other epigenetic modifiers coordinately play an important role in maintaining cellular identities by regulating cell-type specific gene expression programs. Based on this theory, direct reprogramming was aimed at the forced expression of these key transcription factors to activate the regulatory network supporting a specific cell fate. During direct reprogramming, one somatic cell (*e.g.* fibroblast) is transdifferentiated into another somatic cell (*e.g.* hepatocyte) without intermediate stages of pluripotency. Due to this feature, direct reprogramming represents a more reproducible and time-efficient technique compared to pluripotent stem cell-based differentiation. Direct reprogramming has been shown to allow the generation of induced hepatocytes (iHeps) from many types of somatic cells[13-16] . These iHeps acquired hepatocyte function to some extent and could extend the survival of mouse models with lethal liver disease after cell transplantation. However, full maturation of these cells *in vitro* has thus far not been achieved.

Finally, in the liver, hepatocytes are surrounded by extracellular matrix (ECM), of which the dominant ECM-components are collagens (type I, III, IV and V). Natural-based ECM, especially type IV collagen, has been routinely used for maintaining hepatocytes and iHeps[14,17]. Apart from serving as the scaffold for hepatocytes, ECM also performs signaling function by storage and release of numerous growth factors, hormones, enzymes, and cytokines. Considering the complexity of natural ECM, a single or combination of several types of collagens may not be able to mimic the genuine *in vivo* microenvironment for hepatocytes. Therefore,

the decellularized liver tissue may be a better alternative. Previously we and others have reported that decellularized liver tissue could provide an excellent environment for the in vitro differentiation of hepatic stem cells[1,18], as well as maintenance of primary hepatocytes[19] . However, it is still unknown whether iHeps or Lgr5+ liver stem cells can repopulate decellularized liver tissue and whether the maturation of these cells can be enhanced by this more natural environment.

Previously, we and others have reported that hepatic stem cells and primary hepatocytes could repopulate decellularized liver tissue[1,4,19]. Hence, in this study we tested the effect of liver decellularized matrix in the differentiation and maturation of two promising and novel hepatic cell sources: organoid-derived liver stem cells expanded in a novel large-scale method in spinner-flasks/bioreactors[20] and iHeps produced with a novel tandem lentiviral vector[21]. We then examined the differentiation potential of these two cell populations towards functional hepatocytes, and assessed their use for tissue engineering approaches and liver transplantation.

MATERIALS AND METHODS

1. Rat liver scaffold generation and disc preparation

Briefly, livers from 4-8 months old cadaveric rats were harvested with intact vessels. The livers were then cannulated through the portal vein and successively perfused at the rate of 2 ml/min with 0.5 L distilled water 5 L detergent comprising 1% v/v Triton-X 100 (Sigma-Aldrich) and 0.1% v/v ammonium hydroxide (Sigma-Aldrich), and 10 L distilled water to wash out the decellularization detergent.

To obtain liver discs, decellularized livers were cut into wedges and embedded in plastic molds (Sakura Finetek) with OCT and frozen at -80°C. These cryopreserved liver wedges were mounted onto a cryomicrotome (Leica CM 1950) to obtain liver ECM sections of 250 µm thickness. A 4-mm diameter biopsy punch was used to generate a disc from the liver sections and the discs were placed in 96-well plates. After multiple washes with PBS, the discs were sterilized by UV irradiation for 2h and stored in sterile PBS at 4°C until use.

2. Organoid culture and differentiation in spinner flasks

For the large-scale production of human adult stem cell-derived liver organoids, disposable 125 ml spinner flasks (Corning) were inoculated with $2.5x10^6$ cells in 25 ml of expansion medium (EM) including 10% v/v Matrigel™. Due to single cell seeding, 10 mM Y-27632 (Rho kinase-inhibitor, Selleckchem) was added to the medium during the first week of culture. Rotation speed was set to 85 rpm. Every 2-3 days, new medium was added to the spinner flasks.

For hepatic organoid differentiation in spinner flasks[20], organoids were primed for 2 days with addition of BMP-7 (25 ng/ml) to the EM. Subsequently, to separate organoids from the EM, the organoid suspension was filtered through a 70 µm cell strainer. The organoids were transferred to a new spinner flask and differentiated for 12 days in human organoid differentiation medium (DM) supplemented with 10% Matrigel™.

As a positive control, LiverPool™ Cryoplateable Hepatocytes (10-donor, mixed gender) were purchased from BioreclamationIVT (Brussels, Belgium).

3. Generation of induced hepatocyte-like cells (i-Heps)

The procedure is as described before. Briefly, on the one hand, the polycistronic lentiviral hepatocyte-generating vector was designed, constructed and produced[21]. On the other hand, mouse embryonic fibroblasts (MEFs) were cultured. Afterwards, MEFs were transduced with the lentiviral particles for the generation of i-Heps.

As a positive control , primary hepatocytes were isolated from C57BL/6 mice[22] by Percoll medium according to the manufacturer's instructions (GE Healthcare). Afterwards, hepatocyte functional tests were performed in the iHeps, MEFs and primary hepatocytes.

4. Cell seeding on discs

4.1 Recellularization of liver discs with organoids

The seeding procedure was performed as previously described[23]. Briefly, organoids were mechanically disrupted, and for each disc, organoid fragments corresponding to 2.5 × 105 cells were suspended in 10µl EM supplemented with 25ng/ml BMP-7 (Bone Morphogenetic Protein 7). The organoid suspension was slowly pipetted on top of each disc (Fig.1) and incubated for one hour at 37°C to allow the cells to attach. Subsequently, 250µl additional EM with 25ng/ml BMP-7 was added to each well. Medium was changed twice per day. After 2 days of culture, the discs

were carefully transferred to a 24-well plate and cultured in DM for 5 days. DM was refreshed after 2 days.

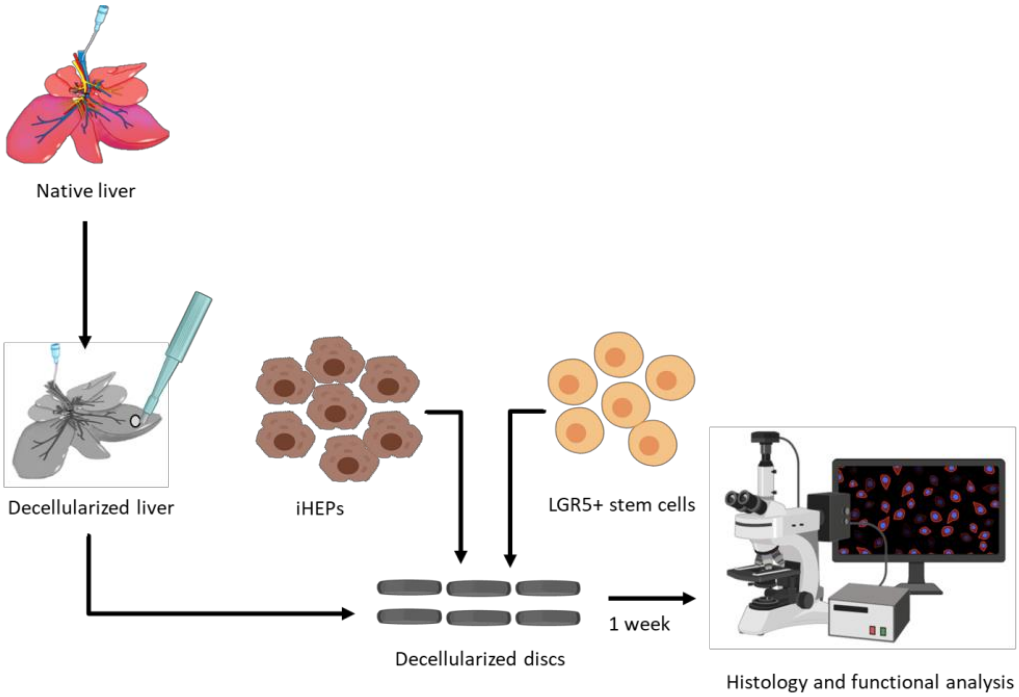

Figure 1. Schematic representation of the work performed. The process started with the decellularization of a rat liver, which was then cut into smaller pieces and embedded in OCT. Afterwards, this small pieces were cut with a cryomicrotome and decellularized discs wre obtained with a biopsy punch. These discs were then seeded with different cell types: i-Heps and LGR5-positive stem cells. Finally, results were processed and analyzed.

4.2 Recellularization of liver discs with i-Heps

Seeding procedure was performed as previously described[1]. Briefly, $2.5x10^5$ of iHeps were suspended in 10µl iHep medium for each disc. Discs were placed in 96-well round bottom microwell plates (Nunc). The cell suspension was slowly pipetted on top of each disc (Fig.1) and incubated for about an hour at 37°C to allow the cells to attach. Afterwards 200µl additional iHep medium was added to each well and was maintained for 7 days. As a 2-dimensional control, same number of iHeps were seeded on collagen (type I) coated 96-well tissue culture plates.

RESULTS

1. Spinner flask organoids repopulate decellularized liver discs

Since mRNA sequencing analysis revealed that a group of genes related to cell adhesion was significantly downregulated in the spinner flask organoids compared to the Matrigel™ controls (data not shown), we investigated whether the spinner flask organoids were able to engraft, a crucial requirement for clinical application of organoids. We therefore seeded the spinner flask organoids on decellularized rat liver discs. We and others had previously shown that primary hepatocytes[19], human liver stem/progenitor cells[4,18,23] and induced hepatocyte-like cells (iHEPs)[24] can repopulate decellularized liver tissue. We harvested organoids after 14 days of expansion in spinner flasks, mechanically dissociated them and seeded organoid fragments onto decellularized rat liver discs. After one week of culture in differentiation medium (DM), the organoid cells had repopulated the discs, were viable and had adapted a columnar shape, with the nuclei on the extracellular matrix (ECM) side (Fig. 2A). Analysis of the discs by immunofluorescent stainings revealed that we had different cell populations on the discs, which we quantified: The majority of the cells (56%) showed a $K19^+/K18^-$ cholangiocyte-like phenotype (Fig. 2B) and 28% were K19/SOX9 double positive (Fig. 2C), 22% of cells had an intermediate $K19^+/K18^+$ phenotype (Fig. 2B), and only a minority of the cells (10%) were $K18^+/HNF4a^+$ hepatocyte-like cells (Fig. 2D). This indicates that organoids seeded on decellularized discs clearly interact with the ECM, adapt a columnar shape and can obtain either a cholangiocyte or a hepatocyte-like fate, as such proving the true

bipotential nature of these organoids and their great potential for tissue engineering approaches.

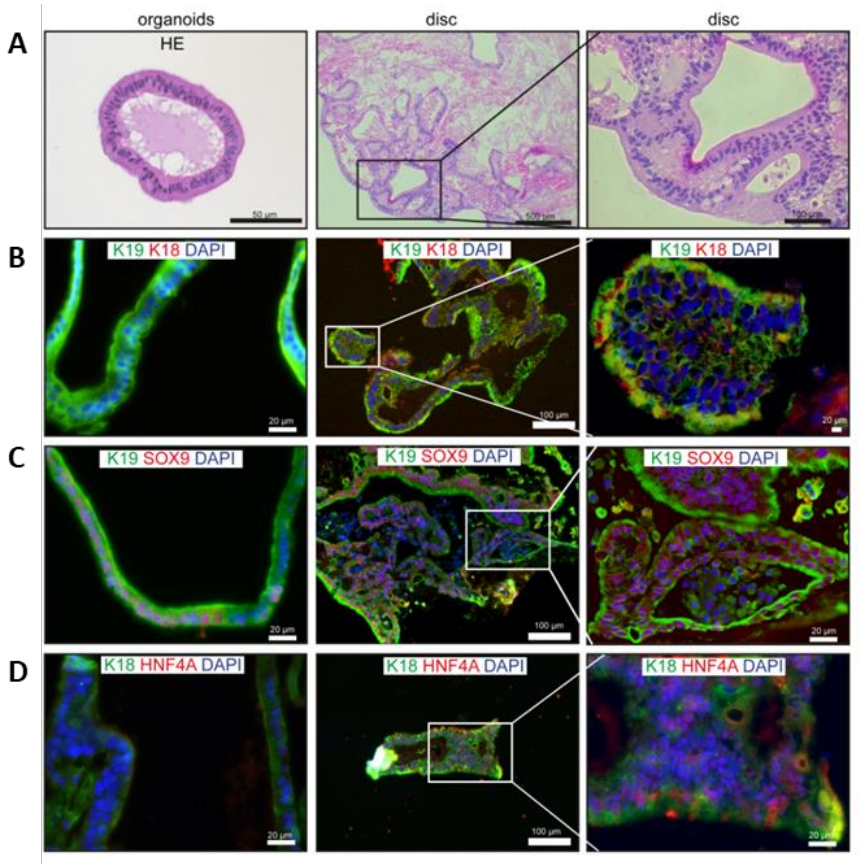

E

	single positive cells [%]	single positive cells [%]	double positive cells [%]
K19/K18 staining	55.9	2.5	21.9
K19/SOX9 staining	45.5	3.5	28.0
K18/HNF4A staining	30.2	12.9	10.4

Figure 2. Tissue formation of spinner flask organoids on liver ECM. A-D) Organoids were expanded in spinner flasks for 14 days and then seeded on decellularized rat liver discs. Re-seeded discs were cultured for 2 days in EM supplemented with BMP-7, and then differentiated for 5 days in human organoid differentiation medium (DM). 4 different donors (2-3 discs per donor) were analyzed in independent experiments. **A)** H&E stainings and **B-D**) immunofluorescent analysis of paraffin-embedded organoids and liver discs. Note that $K18^+$ and $HNF4a^+$ cells were not present in the organoids at the time of seeding on decellularized discs. **E)** Quantification of the different cell populations.

2. Repopulation of decellularized liver discs with iHeps

Then, we questioned whether iHeps also possessed the same repopulation capacity of the liver ECM discs. When iHeps were seeded on

rat decellularized liver discs (DLD), we found they survived and could repopulate DLD within one week (Figure 3A). In contrast non-reprogrammed MEFs seeded on DLD did not survive (data not shown).

Since the ECM in DLD represents a natural habitat for hepatocytes, we determined whether DLD could further enhance the maturation of iHeps. Gene expression analysis demonstrated that cytochromes P450 including *Cyp1a1*, *Cyp1a2*, *Cyp2c40*, *Cyp3a11* and *Cyp3a13*, and epithelial marker *Cdh1*, were dramatically upregulated, while early hepatocyte marker *Afp*, was downregulated (Figure 3B). Interestingly, we observed that *Alb* and exogenous FHG were significantly downregulated (Figure 3 B,D). Immunofluorescence analysis demonstrated the expression of CYP1A2 and tight junction protein 1 (TJP1) (Figure 3C). Finally, iHeps cultured with DLD exhibited increased enzyme activity of LDH, GLDH, CYP3A and CYP1A2 (Figure 3D), while GGT and ALP activity were undetectable (data not shown). Together, these results indicate that iHeps reached a high level of maturation. Although albumin expression was downregulated, the iHep-on-decellularized-liver-tissue system still represents an excellent model for phase I drug metabolism studies.

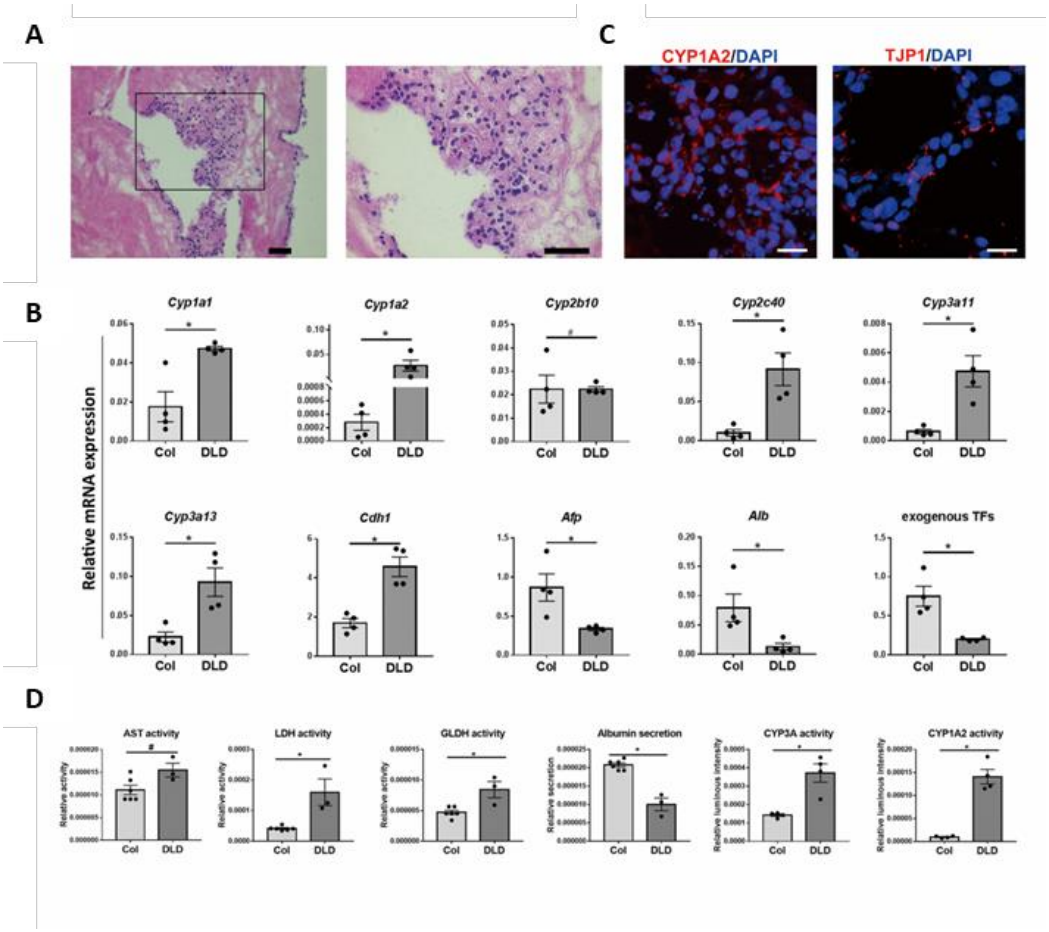

Figure 3. Repopulation of decellularized liver discs by iHeps. A) H&E staining showing the repopulation of decellularized liver discs by iHeps after one week. Scale bar = 50 µm. **B**) Immunofluorescence analysis for iHeps cultured on decellularized liver discs (DLD). Scale bar = 20 µm. **C)** Gene expression analysis for iHeps cultured on collagen (type I) coated plates (Col) and DLD. **D)** Relative activity of hepatocyte-specific enzymes (AST, LDH, GLDH), CYP3A and CYP1A2 activity and albumin secretion in iHeps cultured on Col and DLD. All results were normalized with cell input with Alamar blue. Data are shown as mean ± SEM of six independent experiments for collagen 2D cultured iHeps for AST, LDH, GLDH and albumin tests, three for DLD cultured iHeps for AST, LDH, GLDH and albumin tests, four for both 2D and DLD cultured iHeps for CYP3A and CYP1A2 tests. Asterisk represents statistical significance. *p< 0.05. Hash represents non-significance (two-tailed Mann–Whitney U test).

DISCUSSION

It is widely known that ECM comprises not only a structural support, but also a dynamic entity with biophysical, biomechanical and biochemical properties. This natural-based ECM, mainly containing collagens, laminin and fibronectin, does not only provide mechanical and structural support for cells, but also serves as the reservoir for growth factors like HGF and bFGF[19]. Hence the importance in achieving a functional ECM after the decellularization process, in order to preserve all its properties to be able to interact with the cells which will be further seeded.

In this study, we observed that expansion of organoids in spinner flasks led to a significant downregulation of adhesion-related genes in the organoids (Fig. 1E), raising doubts about their capacity for engraftment *in vivo*, which is mediated by integrin-ECM interactions[25]. We therefore seeded the spinner flask organoids on decellularized liver discs[23], and observed clear interaction with the ECM, as well as a columnar cell shape and selective differentiation towards both a cholangiocyte and a hepatocyte-like fate, indicating their bipotential nature and great potential for tissue engineering approaches. Of note, only a minority of the cells obtained a $K19^-/K18^+$ hepatocyte phenotype, whereas the vast majority had a $K19^+/Sox9^+$ cholangiocyte phenotype or a $K19^+/K18^+$ intermediate phenotype (Fig.1). This inefficient hepatocyte differentiation may partly be explained by the origin of the decellularized liver discs used in this study, which were derived from rats and not from humans.

On the other hand, in order to improve the maturation of iHeps, we introduced them into decellularized liver tissue. After seeding on

decellularized liver discs, we observed that the exogenous expression of *Foxa3*, *Hnf1α* and *Gata4* was downregulated (data not shown). This explains that *Alb*, a direct downstream target of these three transcription factors[26-28], also showed lower expression. Although the precise mechanism behind the quenching of exogenous gene expression is unknown, it is a relatively common phenomenon during cell fate reprogramming[14,29] and indicates the dominance of the microenvironment. Having said this, the drug metabolism potential of iHeps were greatly enhanced and reached levels that were close to primary hepatocytes.

The combined robust differentiation capability together with the ECM discs resulted in a liver model that is more representative of the native liver tissue and has comparable hepatic features. These results indicate that the decellularized-liver-tissue may represent an excellent tool for phase I drug metabolism studies.

CONCLUSIONS

1) We have effectively tested the cells generated by a novel method for highly efficient and safe expansion of LGR5-positive liver stem cells able to differentiate towards highly mature and functional hepatocyte-like cells when seeded in liver decellularized ECM.

2) Culture of directly reprogrammed hepatocytes in decellularized liver tissue can induce important hepatic functions in these cells derived from somatic fibroblasts, resulting in enhanced hepatic features.

BIBLIOGRAPHY

1. Vyas, D.*, et al.* Self-assembled liver organoids recapitulate hepatobiliary organogenesis in vitro. *Hepatology* **67**, 750-761 (2018).
2. Sanchez-Romero, N.*, et al.* The role of extracellular matrix on liver stem cell fate: A dynamic relationship in health and disease. *Differentiation* **106**, 49-56 (2019).
3. Uygun BE, S.-G.A., Yagi H, Izamis ML, Guzzardi MA, Shulman C, Milwid J, Kobayashi N, Tilles A, Berthiaume F, Hertl M, Nahmias Y, Yarmush ML, Uygun K. Organ reengineering through development of a transplantable recellularized liver graft using decellularized liver matrix. *Nat Med* (2010).
4. Baptista, P.M.*, et al.* The use of whole organ decellularization for the generation of a vascularized liver organoid. *Hepatology* **53**, 604-617 (2011).
5. Huch, M.*, et al.* Long-term culture of genome-stable bipotent stem cells from adult human liver. *Cell* **160**, 299-312 (2015).
6. Si-Tayeb, K.*, et al.* Highly efficient generation of human hepatocyte-like cells from induced pluripotent stem cells. *Hepatology* **51**, 297-305 (2010).
7. Wu, X.B. & Tao, R. Hepatocyte differentiation of mesenchymal stem cells. *Hepatobiliary Pancreat Dis Int* **11**, 360-371 (2012).
8. Huch, M. Regenerative biology: The versatile and plastic liver. *Nature* **517**, 155-156 (2015).
9. Forbes, S.J. Organoid cultures boost human liver cell expansion. *Hepatology* **62**, 1635-1637 (2015).
10. Huch, M.*, et al.* In vitro expansion of single Lgr5+ liver stem cells induced by Wnt-driven regeneration. *Nature* **494**, 247-250 (2013).
11. Huch, M., Knoblich, J.A., Lutolf, M.P. & Martinez-Arias, A. The hope and the hype of organoid research. *Development (Cambridge, England)* **144**, 938-941 (2017).
12. Kelaini, S., Cochrane, A. & Margariti, A. Direct reprogramming of adult cells: avoiding the pluripotent state. *Stem Cells Cloning* **7**, 19-29 (2014).
13. Du, C., Narayanan, K., Leong, M.F. & Wan, A.C. Induced pluripotent stem cell-derived hepatocytes and endothelial cells in multi-component hydrogel fibers for liver tissue engineering. *Biomaterials* **35**, 6006-6014 (2014).

14. Huang, P.*, et al.* Induction of functional hepatocyte-like cells from mouse fibroblasts by defined factors. *Nature* **475**, 386-389 (2011).
15. Huang, P.*, et al.* Direct reprogramming of human fibroblasts to functional and expandable hepatocytes. *Cell Stem Cell* **14**, 370-384 (2014).
16. Sekiya, S. & Suzuki, A. Direct conversion of mouse fibroblasts to hepatocyte-like cells by defined factors. *Nature* **475**, 390-393 (2011).
17. LeCluyse, E.L., Bullock, P.L., Parkinson, A. & Hochman, J.H. Cultured rat hepatocytes. *Pharm Biotechnol* **8**, 121-159 (1996).
18. Wang, Y.*, et al.* Lineage restriction of human hepatic stem cells to mature fates is made efficient by tissue-specific biomatrix scaffolds. *Hepatology* **53**, 293-305 (2011).
19. Soto-Gutierrez, A.*, et al.* A whole-organ regenerative medicine approach for liver replacement. *Tissue Eng Part C Methods* **17**, 677-686 (2011).
20. Schneeberger, K.*, et al.* Large-scale Production of LGR5-positive Bipotential Human Liver Stem Cells. *Hepatology* (2019).
21. Chen, C.*, et al.* Hepatocyte-like cells generated by direct reprogramming from murine somatic cells can repopulate decellularized livers. *Biotechnol Bioeng* **115**, 2807-2816 (2018).
22. Severgnini, M.*, et al.* A rapid two-step method for isolation of functional primary mouse hepatocytes: cell characterization and asialoglycoprotein receptor based assay development. *Cytotechnology* **64**, 187-195 (2012).
23. Vyas, D.*, et al.* Self-assembled liver organoids recapitulate hepatobiliary organogenesis in vitro. *Hepatology* (2017).
24. Chen, C.*, et al.* Hepatocyte-like cells generated by direct reprogramming from murine Somatic cells can repopulate decellularized livers. *Biotechnology and bioengineering* (2018).
25. Kumaran, V., Joseph, B., Benten, D. & Gupta, S. Integrin and extracellular matrix interactions regulate engraftment of transplanted hepatocytes in the rat liver. *Gastroenterology* **129**, 1643-1653 (2005).
26. Cirillo, L.A.*, et al.* Opening of compacted chromatin by early developmental transcription factors HNF3 (FoxA) and GATA-4. *Mol Cell* **9**, 279-289 (2002).
27. Kajiyama, Y., Tian, J. & Locker, J. Characterization of distant enhancers and promoters in the albumin-alpha-fetoprotein locus during active and silenced expression. *J Biol Chem* **281**, 30122-30131 (2006).

28. Lichtsteiner, S. & Schibler, U. A glycosylated liver-specific transcription factor stimulates transcription of the albumin gene. *Cell* **57**, 1179-1187 (1989).
29. Takahashi, K. & Yamanaka, S. Induction of pluripotent stem cells from mouse embryonic and adult fibroblast cultures by defined factors. *Cell* **126**, 663-676 (2006).

CHAPTER 3.

Novel porcine model of liver transplantation to induce liver regeneration

INTRODUCTION

Mechanisms for triggering liver regeneration

Liver regeneration is a highly complex and organized phenomenon tissue regrowth process carried out by the participation of all mature hepatic cell types, growth factors and cytokines[1]. This process is particularly remarkable, since hepatocytes are quiescent cells that rarely divide in the normal state and includes three phases: the initial step, which is the priming stage, where cytokines, tumor necrosis factor-α (TNFα) and Interleukin-6 (IL-6) are responsible molecules to stimulate hepatocytes to enter the cell cycle. It is followed by the second or proliferative phase, where molecules like hepatic growth factor (HGF), epidermal growth factor (EGF), vascular endothelial growth factor (VEGF), insulin and bile acids (among others) induce hepatocytes to re-enter G1 and mitosis. The last step is the termination stage, where transforming growth factor beta (TGF-β) and activin induce hepatocytes to stop proliferating and maintain normal hepatic mass and function[2]. During the process of regeneration, the liver not only recovers the entire loss mass, adjusting its size to the normal situation, but at the same time, it keeps providing full support for body homeostasis[3].

There are two types of regenerative models: partial hepatectomy (PHx), which is a process consisting in the resection of up to 90% of the liver mass, where the remaining hepatocytes start to divide to compensate for the loss of hepatic tissue. The other type can be triggered by toxins or viral infections. In this case, many hepatocytes are injured and oval cells (which are putative progenitor cells) differentiate towards both hepatic and cholangiocyte fate[2]. In situations in which hepatocytes or biliary cells

are blocked from regeneration, they can themselves function as facultative stem cells for each other[1,4-6].

Despite that liver regeneration after partial hepatectomy is one of the most studied models in rodents, there are still questions regarding its induction and termination that are under investigation. Such investigations have also been performed in dogs[7,8] and pigs[9,10].

Rapid liver regeneration observed in rodents after two-thirds PHx had brought two important features that highlight the major reason for its usefulness and acceptance by many investigators: in one hand, massive necrosis is not associated with the removal of the resected tissue, suggesting that the regeneration of the residual lobes is developed by processes related only to liver tissue, and not to necrosis or inflammation. On the other hand, because PHx stimulates immediate response to regeneration and can be performed in a few minutes in rodents, it can be precisely timed, with a reference (time 0) and an end point[11]. The process of liver regeneration concludes when the remnant lobes increase up to the size of the original liver. This takes around five to seven days in rats and mice, and it is a process driven my multiple signals. For example, portal circulation, which increases threefold, is one of the first mechanisms triggering liver regeneration. It is due to the simple fact that after PHx, portal and hepatic supplies remain the same, but the liver mass is reduced to one third from its original size. This originates that the total portal blood circulates through a reduced liver, increasing with this total blood per liver mass.

Whereas the amount of arterial blood remains essentially the same through the lobes, the relative proportion of portal blood entering each lobe increases threefold.

The first changes observed 5 minutes after PHx in rats include the increase of urokinase activity and β-catenin migration to hepatocyte nuclei. These rapid signaling induction changes suggest two possibilities: 1) portal blood flow increase is a sufficient stimulus for the initiation of further signaling cascades; and 2) portal blood may contain signaling molecules (like insulin from pancreas and EGF from duodenum) driving to the regenerative process[12-14].

This second point can be contrasted with an older experiment developed by Moolten and Bucher in 1965, in which two rats were joined by parabiotic circulation. In this experiment, carotid-to-jugular cross circulation was performed between a couple of rats: one had a PHx and the other remained normal. The results reported that the PHx of one subject stimulated DNA synthesis in the control partner[15]. This supports the idea that humoral hepatotrophic molecules are secreted during liver regeneration.

Other reports point that these changes in blood perfusion lead to the alteration in the mechanotransduction of endothelial cells, regulating the secretion of angiocrine signals derived from endothelial cells, like the vascular endothelial growth factor receptor 3 (VEGFR3) and integrin β-1[16]. In this study, Lorenz et al used fetal rats developing livers as a model to study these angiocrine signals, showing that the liver growth rate correlates with blood perfusion through the organ. They induced changes in heart beat demonstrating that this can modify the expression of

angiocrine signals, by increasing the activation of VEGFR3 and HGF with the increase in the heart beat, and by decreasing their activation when they halted heartbeat.

This mechanical stretching of endothelial cells during vasodilation induced the activation of angiocrine signals, leading to liver growth and survival. The triggering reason is that after PHx, the remaining parts of the liver dilate to allow the same amount of blood which flows through a smaller liver mass. This vasodilation provokes circumferential stretching in the endothelial cells, inducing with this the release of hepatocyte growth-promoting signals.

It has been reported that the use of small grafts in partial-liver transplantation result in graft failure, due to portal hypertension after transplantation[17]. An appropriate size graft for successful liver Tx is 30-40% of the expected liver volume for the recipient or 0.8-1% of the body weight. Liver grafts with lower values are considered small-for-size (SFS) grafts[18]. Also, even grafts with greater values can fail in recipients with severe portal hypertension[19,20]. The term of SFSS applies in both situations. After liver transplant, recipients can develop a specific syndrome called “small-for-size syndrome” (SFSS), which causes prolonged cholestasis, ascites, coagulopathy and encephalopathy[18,21].

A higher portal flow per gram of liver tissue is provoked by the reduction of the hepatic vascular bed, causing the rising of portal pressure and stress in the hepatic sinusoid, which lead to sinusoidal endothelial injury, hepatocellular damage and death[22,23]. Subsequently to the loss of endothelial cells integrity, leukocytes initiate the coagulation and inflammatory cascade, causing impaired blood flow. With this,

vasoconstrictive genes are upregulated and local tissue macrophages initiate portal tract infiltration.

Due to the fact that portal hypertension seems to be central to the pathogenesis of SFSS, modulation and decreasing of blood inflow to the liver is a popular strategy[17]. This includes splenic artery modulation, shunts (portacaval or mesocaval) and less commonly, splenectomy[24]. There are still no studies directly comparing outcome from these techniques, however portacaval shunts are the most used because of their easier performance, potential reversibility and to avoid possible splenic infarction[25].

Porcine models to study liver transplantation and regeneration

Porcine animal models present the advantage of having similarities with the human in terms of gastrointestinal anatomy, metabolism and physiology[9]. Human functional anatomy can be applied to porcine livers, showing small differences: porcine lobular hepatic veins are entirely intrahepatic in contrast to humans, and the supra-hepatic inferior vena cava (IVC) is encircled by hepatic parenchyma in pigs.

According to Couinaud, human liver hepatobiliary anatomy and physiology is comparable with the pig[26,27]. Porcine livers are divided into 3 different lobes: right, median and left, which are independent of each other. The median lobe is larger than the lateral ones, and it is incompletely divided into right and left paramedian lobes along the umbilical fissure. The gallbladder is located in the right paramedian lobe (Fig 1).

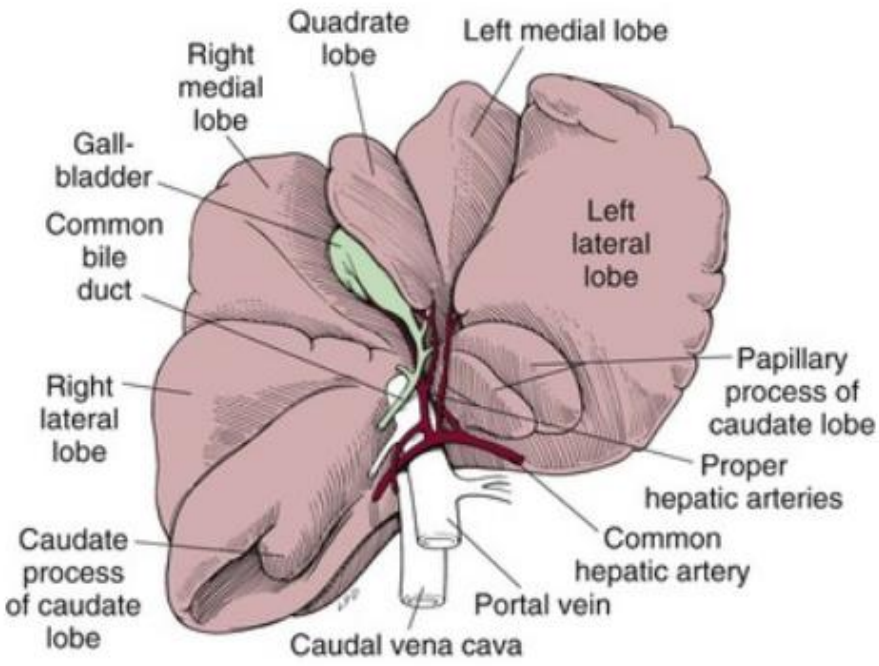

Figure 1. Pig liver anatomy. (Extracted from https://veteriankey.com/surgery-of-the-liver/)

Due to this anatomical and physiological similarities, and also the size – young pigs have a similar size and mass of a human adult, it makes the pig a widely used animal model in liver transplantation and regeneration studies[28-32].

Taking this into consideration, this makes the pig the animal model of choice to test the *in vivo* vascular patency of bioengineered livers. To do this, several models are available, but the need to provide adequate portal and arterial flow without risking dangerously high blood pressure in the transplanted bioengineered graft which could induce small for size syndrome is critical. Furthermore, to induce liver regeneration, it will be necessary to provide the liver graft with hepatotrophic factors coming

from the portal vein and bypass the native liver all along to put the bioengineered graft in the center stage. Hence, a novel model of auxiliary heterotopic liver transplantation with porta-cava shunt is needed.

In this study, we decided to define a liver regeneration porcine model which included: 1) partial hepatectomy (where 20-40kg recipient's right lobe was resected, removing 40% of the hepatic tissue)[32]; 2) transplantation of a donor graft (which was the right lobe from a 7-10 kg donor pig)[33,34] and 3) a portocaval shunt (in order to reduce the volume of portal blood perfusing the graft, to avoid SFSS, and to increment the shear stress in a controlled way to induce with this the liberation of angiocrine factors needed for graft regeneration)[35,36].

Due to the lack of literature on some of these models, different experimental groups were performed according to the acquired results and knowledge. The generation of our porcine model was a procedure of constant learning and changing techniques, always trying to improve the model.

MATERIALS AND METHODS

Animal acclimatization period

Animals arrived to CIBA installations at least 10 days before the surgical procedure was scheduled, according with regulation. They were kept in pens complying with measures established in the RD 53/2013, of February 8th, which establishes the specific basic rules for the protection of animals used in experimentation and other scientific purposes, including teaching.

Animals had water and food *ad libitum*, and they were treated with a single intramuscular dose of Anthelmin (1ml/10Kg) as anti-parasitic treatment.

Preoperative treatment

48h prior to the surgery, animals were administered via intramuscular with antibiotic (Alsir®,Enrofloxacino, 2,5 mg/Kg/day). They were also food restricted with plenty access to water.

Operative learning

Our main goal was to establish an optimal animal model that supported liver graft regeneration 30 days post implantation. For this, three main groups were initially established: 1) a positive control, where recipient pigs would receive a liver graft from 7-10 kg donor piglets to check that our defined animal model worked properly with a native liver; 2) a negative control, where a decellularized porcine liver scaffold would be transplanted to the recipient animal, to check that, as expected, thrombosis of the scaffold graft would happen, and 3) our control of the bioengineered liver graft, which would be transplanted to check if its behavior was compared to the positive control, working properly after anastomosis to the recipient, or if by the contrary, it would produce a thrombotic response after implantation like our negative control.

Female industrial crossing pigs from 7-10kg were used as donors and 20-30kg pigs were used as recipients in group 1; 2kg piglet decellularized livers were used as donors and 20-30 kg pigs were used as recipients in group 2. Animals were generously donated by Mercazaragoza, S.A. All

surgeries were performed by expert digestive surgeons, under processed following standard operation procedures with the approval of the Ethical and Scientific Review Boards.

For timing reasons, only surgeries of the first and second groups could be performed. The first group was divided into different subgroups, which reflect our learning process. Development of the surgical procedure model, the pharmacological protocol and the criteria to determine the viability of the graft, have been changing throughout the study. These changes are reflected in the progression of our learning.

The following table summarizes the abbreviations used in the text to refer to the surgical techniques developed in the dirretent experimental groups (Table 1).

Table 1. List of abbreviatures and respective meaning

Abbreviation	Surgical process
PHx	Partial hepatectomy
Sh	Portocaval shunt
Tx	Transplant

A) GROUP 1 (POSITIVE CONTROL)

As mentioned before, different subgroups were performed within the first group, where recipient pigs would receive a native liver right lobe from donor pigs.

1. PHx + Sh + Tx

A total of 7 surgeries were performed in this group, where recipient animals were performed with a partial hepatectomy (removing left

lateral hepatic lobe), the portocaval shunt and the graft transplantation (donor's hepatic right lobe).

2. PHx + Sh

A total of 2 animals were done in this group, where only portocaval shunt and graft transplantation were performed.

3. Sh

A total of 5 animals were in this group, which was established to study biochemical survival modifications and modifications on the native liver by performing only the portocaval shunt.

4. Sh + Tx

A total of 12 animals were in this group, which was in turn subdivided into two groups, according to our on-going technical modifications.

Pig surgeries (biologic model procedure)

1. Donor operation

First, through a right subcostal laparotomy, the hepatic hilum was dissected. Then, the piglet was heparinized and portal vein and abdominal aorta were dissected and cannulated. Cold Ringer heparinized solution at 4°C was infused through both the aorta and the portal vein. Renal vessels and superior mesenteric artery were ligated too. The inferior vena cava was sectioned and sutured. The suprahepatic vena cava was then cut and the liver graft was harvested and preserved in Ringer solution at 4°C during the back table preparation, where partial

hepatectomy (PHx) took place, to obtain the final graft (right hepatic lobe). For the PHx, left and middle hepatic veins were ligated and their respective liver lobes were dissected. Finally, vascular integrity of the graft was insured.

Prior to transplantation, both complete liver, and final graft were weighed.

2. Recipient operation

A central venous line was placed in the jugular for fluid administration and blood extraction during the surgical procedure and through the postoperative follow-up. A midline laparotomy was used to access the abdominal cavity and find the hepatic hillium. First the porta-caval shunt was performed by sectioning the portal vein just before the pancreatico-duodenal branch and making an end-to-side anastomosis of the proximal end to the infrahepatic vena cava, just where it begins to become intrahepatic. Later on, in order to calibrate the amount of portal blood the graft would receive from the recipient's portal vein, a silk ligature was placed around the native portal vein (as a constriction ribbon) distal to the grafts venous anastomosis. This shunt would divert the portal flow (avoiding SFSS), but would allow the reception of the necessary blood flow required for graft regeneration.

With the shunt in place, grafts were transplanted orthotopically with vascular anastomosis performed as follows: graft's suprahepatic vena cava (SVC), was anastomosed to the recipient's distal portal vein; graft's portal vein, was anastomosed to the recipient's proximal portal vein, right before the shunt; and graft's hepatic artery (prolonged with the

mesenteric axis and the donor's aorta), was anastomosed to the recipient's abdominal aorta. (Fig.2). Flow probes (which were specifically designed to adapt to the vessel sizes we handled) were located on the graft's SVC (MC10PSB, Transonic) and hepatic artery (MC6PSB, Transonic), to measure incoming blood flow. Finally, a catheter was inserted in the common bile duct for bile drainage, and a pezzer probe was inserted in the stomach for decompressive gastrostomy.

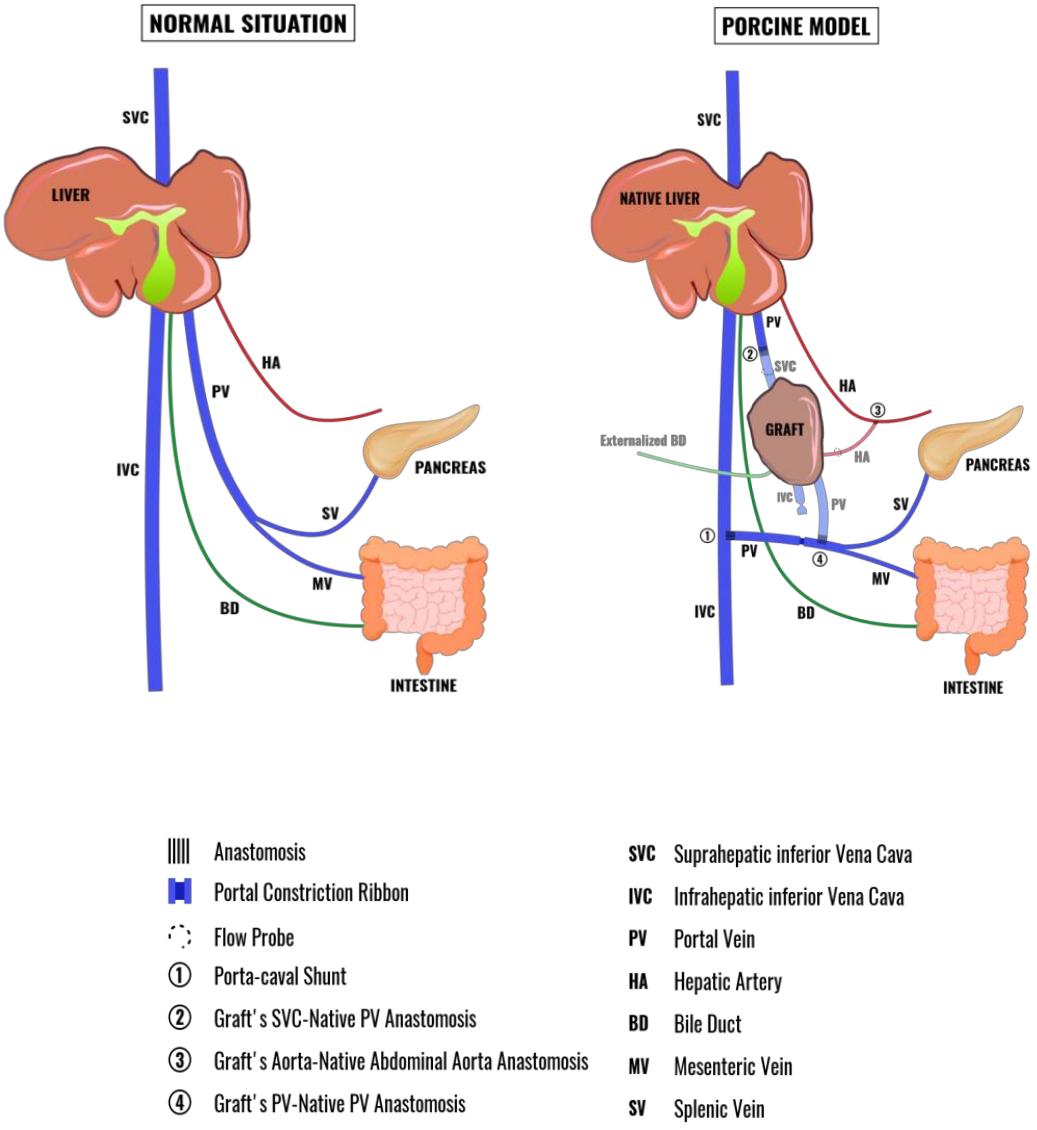

Figure 2. Schematic representation of our latest surgical model of graft transplantation.

B) GROUP 2 (NEGATIVE CONTROL)

Only one surgery from this group could be performed. Due to this, porcine liver scaffolds from 2kg piglets were harvested, decellularized and sterilized as mentioned in Chapter 3. Graft Tx was performed with a portocaval shunt as well.

It was mainly performed to determine if our scaffolds had an optimal consistency to be anastomosed to a native vessel, due to scaffold texture varies significantly from a native tissue.

Anesthetic treatment

Pre-anesthesia was induced by intramuscular injection of Zoletil® + Dexmedetomidine (5mg/Kg + 0,0075mg/Kg). Anesthesia was then induced by intravenous injection of Propofol (max. 6mg/Kg) and maintained with inhalation anesthesia (Sevoflurane, Et: 1.9%). Intraoperative analgesia was maintained with intravenous injection of Remifentanil (5mg), in continuous infusion (0,3µg/Kg/min). During the intervention, Ringer-Lactato solution was administered (8-10 mg/Kg/h). Sodium heparin was also administered intravenously (3mg/Kg). Eye protection was performed with ophthalmic lubricant.

Postoperative treatment

Recipients were maintained with gluco-saline Ringer solution until they started to eat by themselves, with Ringer Lactate support. The analgesic and anti-inflammatory treatment was performed with fentanyl patches (25µg/h) or with intravenous injection of Buprenorphine (0.05mg/kg/12h) for 72h, combined with intravenous injection of

Meloxicam (0,4 mg/Kg/day) for 72h. Antibiotheraphy was performed with intravenous injection of Alsir® (Enrofloxacin 2,5 mg/Kg/day) for 2-4 days, depending on the animal progress. Immunosuppresor treatment consisted on the injection of Prograf® (Tacrolimus) 0,2 mg/Kg, orally taken until the end of the experiment. Corticosteroid treatment was performed with Urbasón® (Metilprednisolone) (2 mg/Kg, administered by intravenous injection or orally taken). The anticoagulant treatment consisted of 1) the administration of Clexane® (Sodium Enoxaparin, 2mg/kg/24h) given in 2 doses and simultaneously administered with Sintrom (acenocumarol, 2mg/animal). Subsequently, the treatment with Clexane was suspended and Sintrom doses were adjusted according to coagulation analysis and 2) Adiro® (Acetylsalicylic acid, 325 mg/day) administered orally or intramuscular injection of Inyesprin® (0,5 g) at doses of 325mg.

Euthanasia or study end point (SEP)

Euthanasia was perfomed in donor piglets right after liver harvesting, and recipient pigs at day 30 of the study (or earlier when required). For this, animals were anesthetized with Zoletil® + intramuscular injection of Dexmedetomidine (5mg/Kg + 0.0075 mg/kg) and intravenous injection of potassium chloride at doses> 1 mEq/Kg. Once death was confirmed in recipient pigs, graft was harvested and weighted to determine whether it had grown or not. Liver samples (native liver and graft) were taken for pathological anatomy interpretation, which was performed by our collaborator Dr. Lourdes Bengochea, from the Patology Department of Hospital Clínico Universitario Lozano Blesa.

Parameters examined

1. During the post-surgery days

1.1 Blood analyses

Blood samples were taken from recipient animals at day 0 (the surgery day, before the surgical procedure), 1, 3, 5, 7, 15, 23 and 30 for blood testing. This consisted of a biochemistry panel, which included parameters of albumin, GPT, GOT, bilirubin, glucose and creatinine and also for hemogram blood test?. The hemogram panel included hematocrit, red blood cells, hemoglobin, mean corpuscular volume (MCV), mean corpuscular hemoglobin (MCH), mean corpuscular hemoglobin concentration (MCHC), leucocytes, neutrophils, basophils, lymphocytes, monocytes, platelets, mean platelet volume (MPV), platelet distribution width (PDW) and procalcitonin (PCT) (Data not shown). Blood analyses were performed by the veterinary clinic Albeitar.

1.2 Bile secretion

In case the transplanted graft produced bile, its secretion was collected and measured as a proof of graft's functional performance.

1.3 Blood coagulation analysis

In the latest surgeries, we performed also a blood coagulation analyses performed to adjust blood coagulation and aggregation drugs to avoid graft thrombosis. This coagulation panel included partial thromboplastin time (PTT), prothrombin time (PT) and fibrinogen.

1.4 Blood flow monitoring

In the latest surgeries, we included live SVC and HA blood flow monitoring, as a test of blood perfusion in the graft.

2. After recipient humanitarian death

2.1 Graft size

Grafts were measured to determine if there has been liver growth since the surgery day or not.

2.2 Pathologic anatomy analysis

Two samples of different parts of the native liver and another two samples from different parts of the graft were taken and fixed in formol for tissue processing. Afterwards, H&E stainings were performed and analyzed by an expert pathologist.

RESULTS

A) GROUP 1 (POSITIVE CONTROL)

1. PHx + Sh +Tx

From the 10 animals included in this group, 6 of them did not wake up after the surgery; 1 died at day 1, and 3 died at day 3.

Due to our poor outcomes in the first three surgeries, we decided to change the portocaval shunt, which was firstly latero-lateral, to a

termino-lateral, due to easier handling. Furthermore, we established two surgery teams in order to reduce surgery time and animal surgical stress.

2. PHx + Sh

Results showed the same poor outcomes as in the previous group. From the 2 animals of this group, 1 did not wake up, and the other died at day 2.

From here on, we decided to discard the PHx. We believed that partial hepatectomy did not contribute to our model and, on the contrary, it allowed the improvement of technical aspects like decreasing surgical times and aggression and improving anesthetic-metabolic aspects. Furthermore, we decided to respect the pancreato-duodenal branch of the portal vein in next surgeries.

3. Sh

A total of 5 animals were in this group, which had implemented the monitoring techniques learned from the previous groups.

We observed an increase in animal survival, with 3 of them reaching day 30 of the study, and 2 of them sacrificed due to other complications not related with the liver graft (intestinal fistula and sepsis).

We observed dilated stomachs in pigs in the necropsies, so we decided to perform gastrostomies in following surgeries to avoid this problem.

4. Sh + Tx

This group was subdivided into two groups, according to our technical learning:

4.1) Initial Surgeries (n=3)

In the first three surgeries, animals reached days 17, 21 (sacrificed for other complications, independent from the liver graft) and 30 of the study. However, autopsy results revealed advanced necrosis in all the grafts.

According to this, we decided to perform sonographies and angiographies at earlier days post-surgery, in order to determine at which point of the post-operative time the graft perfusion ceased. From here on, we stopped considering animal survival up to 30d as endpoint, and started considering graft's vascular status as our endpoint.

4.2) Current Surgeries (n=10)

Animals of this group were sacrificed around day 8 post-surgery because results obtained from sonographies, arteriographies or blood flow probes did not showed blood perfusion within the grafts. Autopsy results revealed graft thrombosis and different grades of necrosis.

One of the changes performed in this group of Sh+Tx included the reduction of mesentery manipulation in the recipient animal, which we have observed from previous surgeries that high mesenteric manipulation leaded to a poorer recipient recovering after surgical proceeding. For this, we first used the recipient's gastro duodenal artery (GDA) to anastomose graft's hepatic artery (HA). With this, we observed prolonged survival rates, until we began to establish as a final point

criterion the demonstration that there was no blood perfusion in the graft and not the day 30 of the study. Animal survival was subjected to the verification of graft's suprahepatic and arterial flow.

Observation of graft's perfusion with the echo doppler was not easy, due to the location of the pig liver, which are deeper than in humans, and the ultrasound was often not enough to determine whereas there was blood flow. As an alternative option, angiography can show better and significant outcomes related to vascular graft perfusion, however, it presents the disadvantage of animal re-intervention. Given these reasons, we decided to use two blood flow sensors, adapted to the diameters of the vessels we were working with: recipient's hepatic artery and suprahepatic vena cava. Flow probes were sterilized and placed in recipients mentioned blood vessels after graft implantation, allowing the monitoring of blood perfusion continuously throughout the time of the experiment.

Another change performed included the arterial anastomosis, which changed from recipient's gastro duodenal to abdominal aorta (AA). This process required more mesentery manipulation and abdominal aorta clamping. However, it offered the advantage of ensuring greater blood flow from the donor artery.

All data collected with results from echo Doppler (when possible), angiographies and blood flow monitoring revealed a common problem: graft thrombosis. Our goal then was to avoid this thrombosis. For this, antiplatelet and anticoagulant treatment was derived according to the blood flows registered and results from blood coagulation analysis.

The solution we managed to implement to decrease blood coagulation and graft thrombosis after implantation, was to treat recipients with antiplatelet (acetylsalicylic acid, 325mg) and anticoagulation drugs (acenocoumarol, 2mg) before the surgery. We made a first attempt, administering acenocoumarol 3d prior to surgery (performed in Tx29). However, it was not possible to achieve a successful intervention due to blood loss during the surgery and the animal perished during the surgery. With this, our latest subject (Tx30) was administered with acenocoumarol only 1d prior to the surgery day. In this case, it was much easier during the intervention and we were able to maintain hemostasis and graft perfusion up to 8 days post-surgery with a suitable outcome: continuous blood flow in both suprahepatic vena cava and hepatic artery. There was also an average of bile production of 100ml/day, which was daily produced. This meant another relevant outcome, as such quantities and continuous bile production was not observed in previous cases, where only small amounts of bile (5-10ml) were recollected, and it was not continuously produced. Unfortunatly, it died at day 9 due to massive hemorrhage due to the difficult management of acenocoumarol.

A summary of our technical learning is explained in Fig.3.

SURGERIES PERFORMED IN GROUP 1

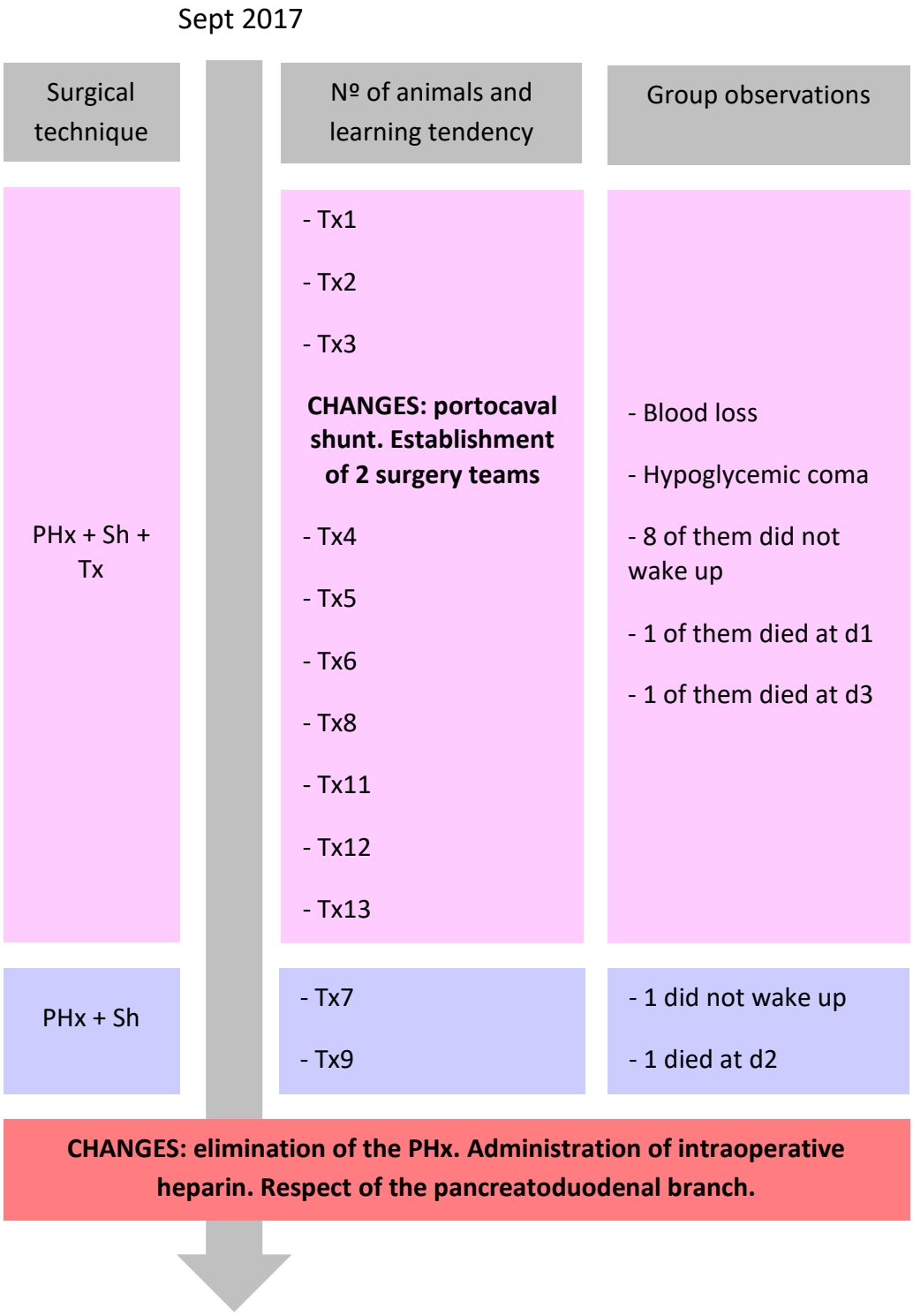

Sh	- Tx10 - Tx14 - Tx15 - Tx16 - Tx17	- Longer survival rates: 3 euthanized at d30 2 euthanized by HEP at days 12 and 24 - Swollen stomachs

CHANGES: intraoperative glucose control. Gastrostomy. Post-surgical glucose control.

Sh + Tx	- Tx18: SEP at d7 - Tx19: reached d30 - Tx20: SEP d21 **CHANGES: graft survival is our caused of end point** - Tx21: bad echo at d8 - Tx23: bad echo at d17 -Tx24: SEP d8 **CHANGES: HA anastomosis from GD to AA. SVC probe implantation** - Tx25: SEP at d7 - Tx26: bad angiography at d7 **CHANGES: blood coagulation control**	- Increased animal survival rates but grafts were necrotic - Graft size increased in some cases - Our goal changed from animal surviving up to 30d to avoid graft necrosis

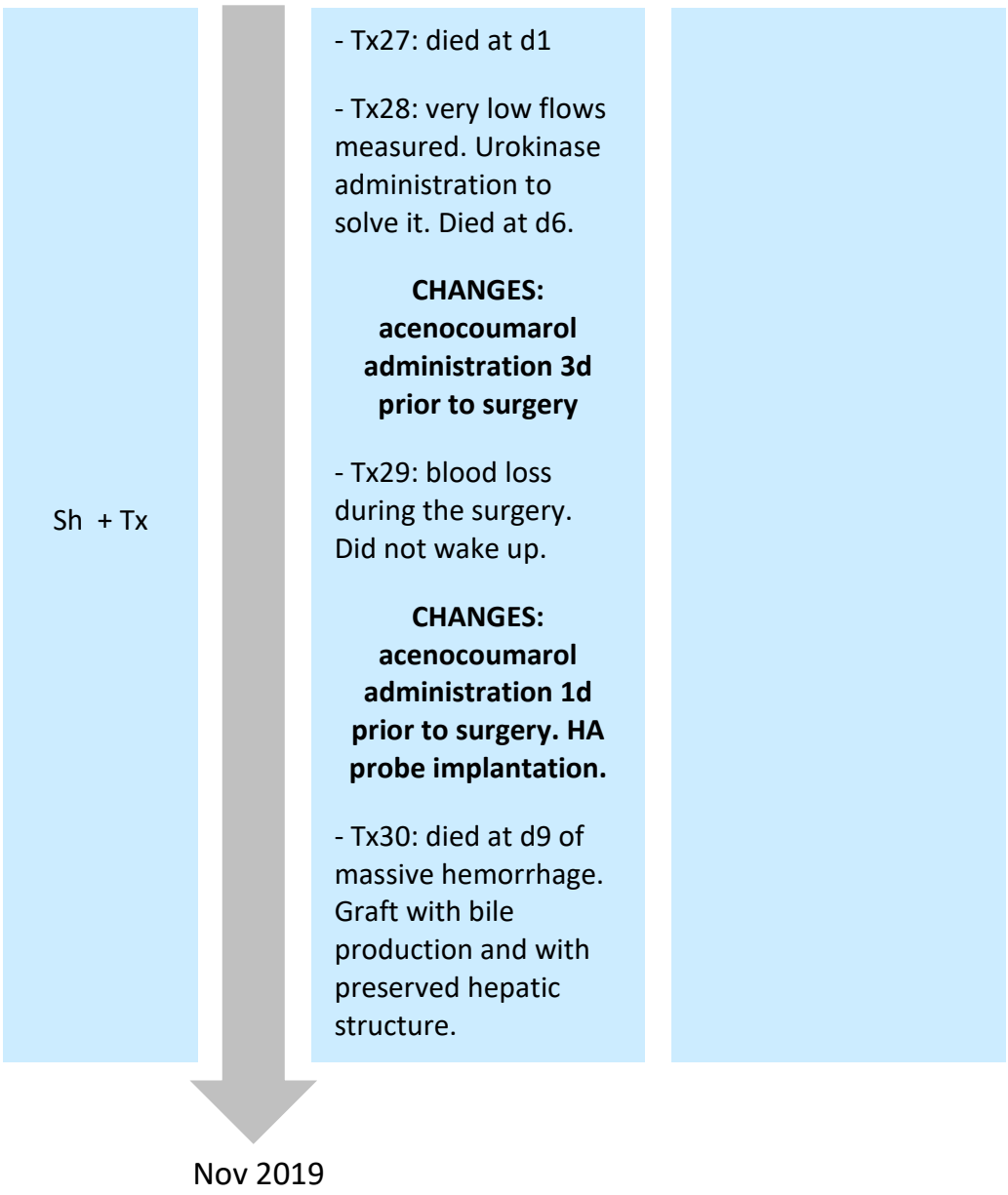

Figure 3. Summary of knowledge/technical improvement in the generation of the porcine animal model.

A total of 6 out of 12 animals of this group resulted in graft size increase (Table 1 and Fig.4).

Table 2. Graft size increase in animals with portocaval shunt and graft transplantation.

Group 4. Sh + Tx				
Animal	**Graft weight before transplantation (gr)**	**Animal survival (days)**	**Graft weight after transplantation (gr)**	**Graft mass fold increase**
Tx18	70	17	180	2,57
Tx21	149	8	154	1,03
Tx25	95,4	7	273	2,86
Tx26	123,6	7	219,6	1,77
Tx28	127,2	6	276	2,17
Tx30	119,7	9	175,5	1,46

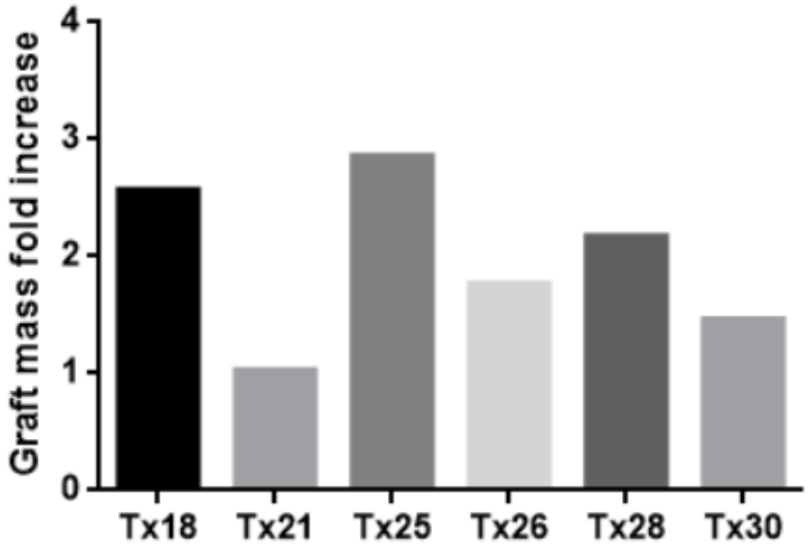

Figure 4.Graft mass fold increase representation of each recipient animal.

Furthermore, these transplanted animals presented normal values of the different biochemical parameters examined. Only some of them presented GOT values a bit off the standards, particularly the first days after the surgery (Fig. 5).

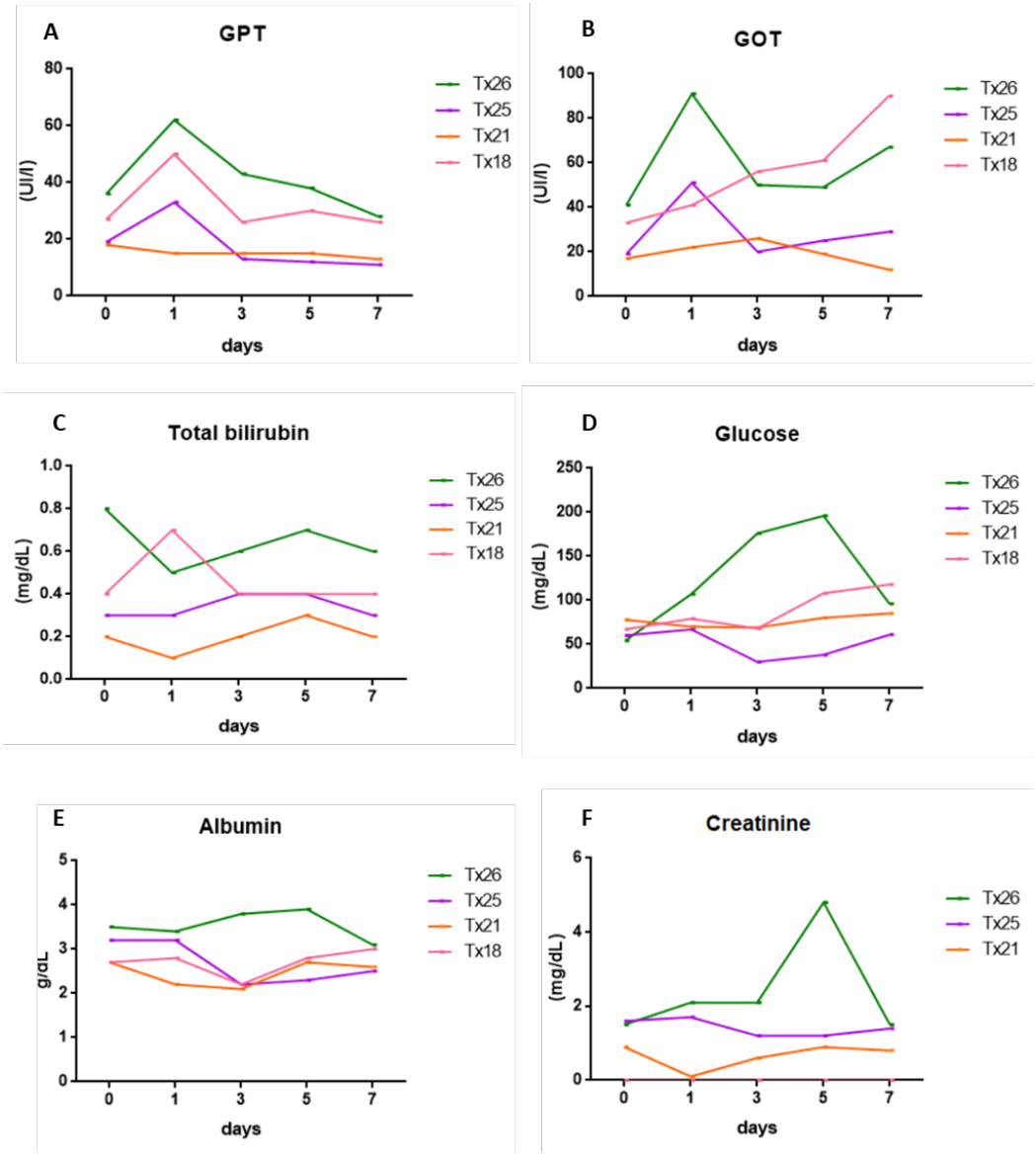

Figure 5. Biochemical panel of different parameters from some Tx that showed graft regeneration. Reference values: **A)** <70 UI/l; **B)** <40 UI/l; **C)** 0-0,6 mg/dL; **D)** 58-150 mg/dL; **E)** 1,8-3,3 g/dL; **F)** 1-2,7 mg/dL..

Comparative macroscopic and microscopic view of native liver and graft tissues are reflected in Fig.6. Native liver is shown as control (Fig. 6 A and B), which reveals a preserved parenchymal architecture, with no inflammatory changes or signs of congestion. Graft's H&Es show our progression in graft survival: graft from Tx19 (Fig.6 C and D), presented massive ischemic necrosis, with no parenchymal preservation; graft from Tx26 (Fig. 6 E and F) also presented some parts with ischemic necrosis and inflammatory infiltrates (arrow), however it also presented some areas with preserved liver parenchyma (asterisk). Finally, graft from Tx30 presented a preserved hepatic architecture (Fig. 6 G and H).

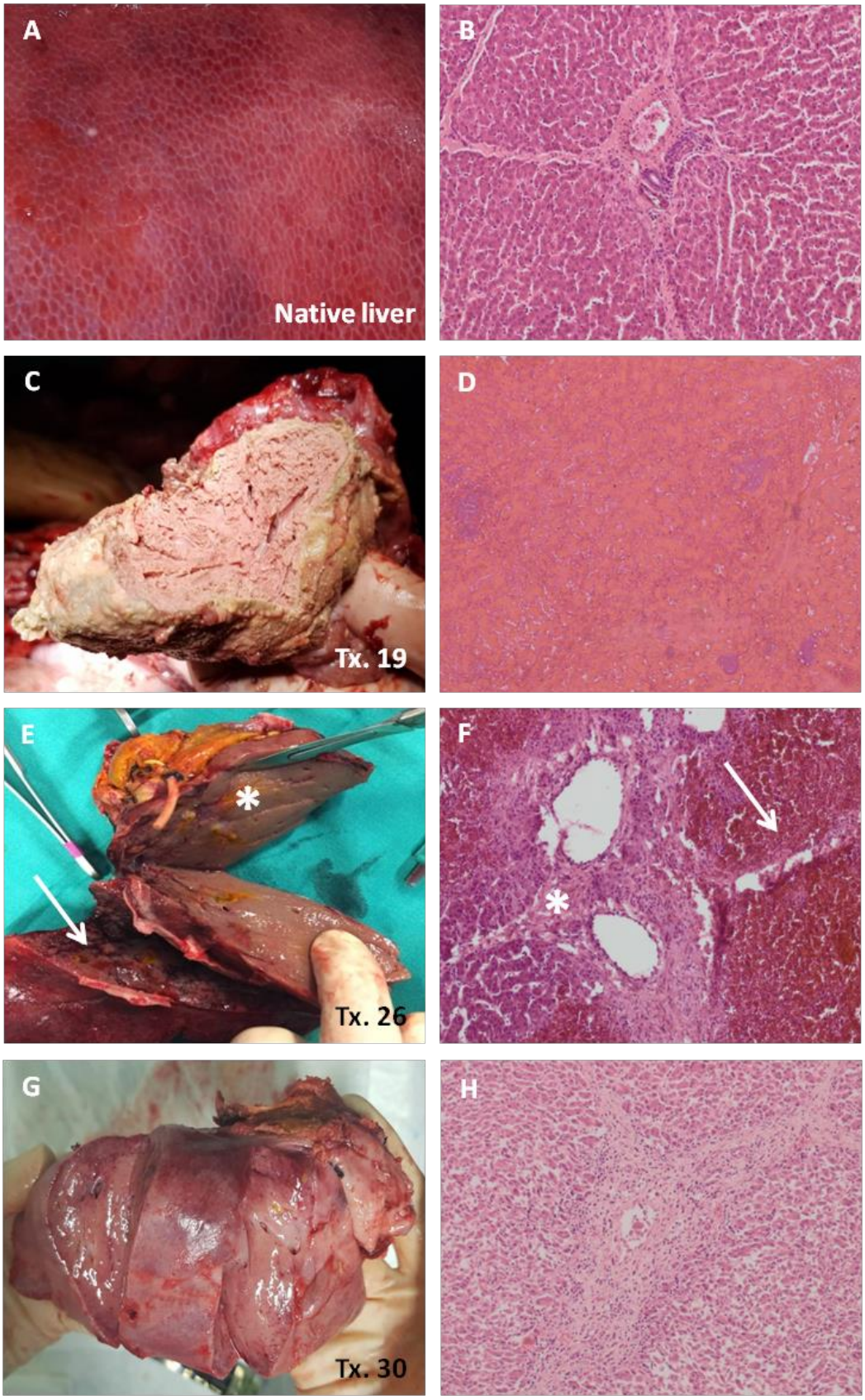

Figure 6. Graft status of different recipient animals, showing our learning in preserving graft survival after transplantation. A) macroscopic view of a native (intact) liver; **B)** H&E

staining of a native liver, where a preserved liver architecture is observed: portal triad delimiting different liver lobules; **C)** Graft macroscopic view of Tx19 showing parenchymal necrosis; **D)** H&E staining of Tx19, showing an almost total loss of hepatocytes; **E)** Graft macroscopic view from Tx26, where two clear zones could be observed: arrow determines a hemorrhagic necrosis zone, with ischemic centrolobular necrosis; asterisk determinates a hepatic zone with partially preserved architecture; **F)** H&E staining from Tx26, where this two zones are clearly determined; **G)** Graft macroscopic view from Tx30, where no apparent necrosis signs are appreciated; **H)** H&E staining from Tx30, where a preserved hepatic architecture is observed. H&E pictures at 10x.

The progress in our ability of maintaining blood perfusion in the SVC and HA within the graft is represented in Fig 7.

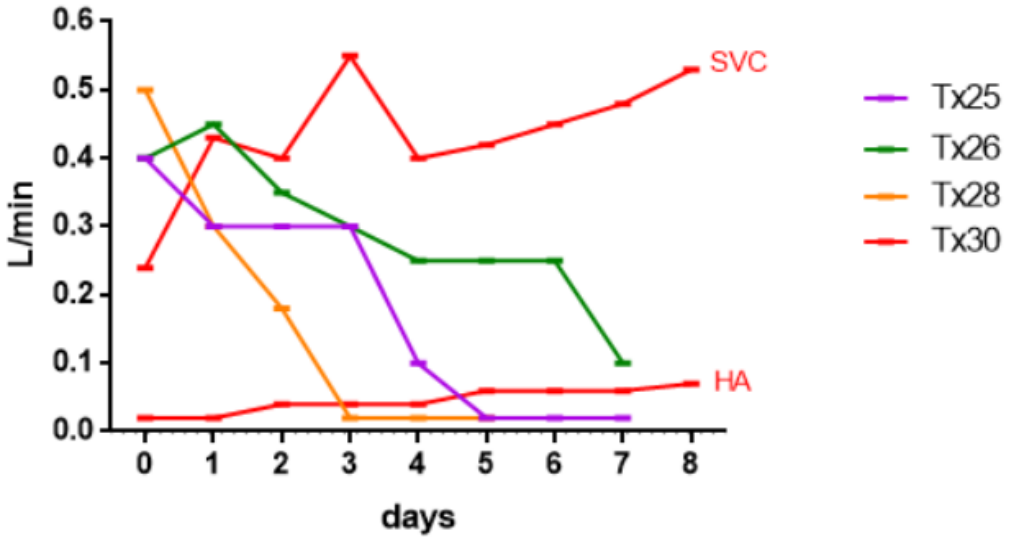

Figure 7. SVC and HA flows registered in different recipients during post-surgery days. Tx25, 26 and 28 were implanted with only one sensor, located in the SVC; Tx30 could have been implanted with two flow sensors, located in the SVC and HA**.**

Tx25 and Tx26 were examples of recipients in which blood coagulation analysis were not yet performed. A constant decrease in the SVC blood

flow could be observed, due to graft thrombosis. Tx28 received two urokinase doses in an attempt of degrading the blood clot, which we assumed it had due to the decrease in blood flow monitoring from the SVC and from the coagulation results; however it died due to a hemorrhage derived from this systemic urokinase administration. Finally, in Tx30 we were able to have more controlled blood anticoagulation values, allowing graft blood perfusion up to 8 days, both in SCV and HA. Despite the more accurate blood coagulation control, the recipient also suffered from an internal bleeding and perished due to this. This status of graft preservation was also contrasted with bile production, which, unlike previous recipients, was produced continuously until day 7, with a mean production of 100ml/24h. Other animals presented scarce bile production with a mean secretion, in the best of cases, of 10ml/24h, being bloody sometimes (data not shown).

These good results in terms of bile secretion and graft survival was possible to our constant learning during the surgical techniques (Fig.8).

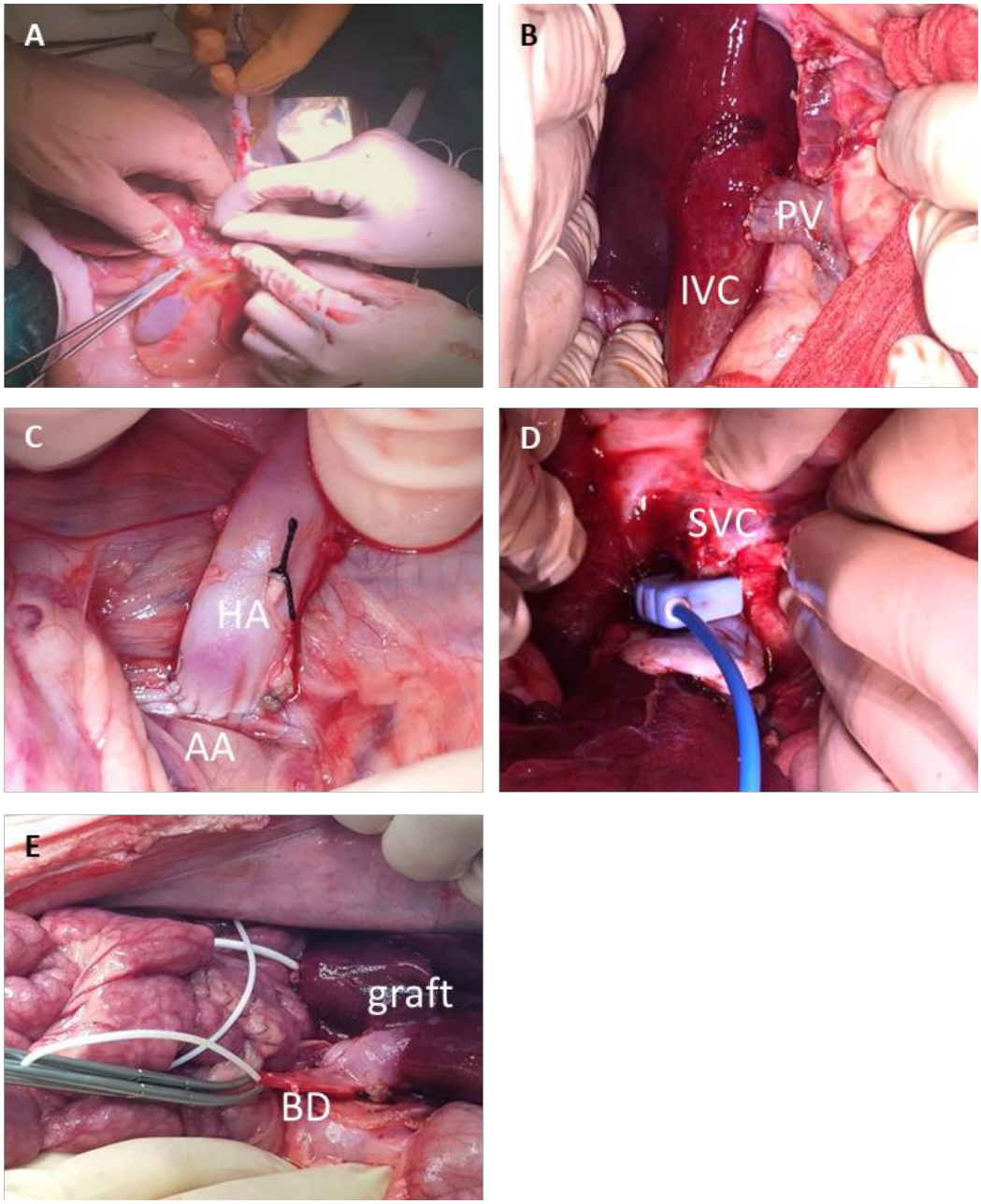

Figure 8. Results from the different procedures carried out during the surgery. A) Back table graft preparation; **B)** Latero-terminal portocaval shunt; **C)** Arterial anastomosis; **D) F**flow probe implantation in the graft's SVC; **E)** Graft's bile duct externalization.

B) GROUP 2 (NEGATIVE CONTROL)

In this group, our results revealed that scaffold graft could be easily handled and anastomosed to the recipient's vasculature. After

unclamping, graft scaffold was perfused with blood without complications (Fig. 9 A and B).

Fig. 9 C shows the macroscopic view of graft's status at the necropsy day (15d post-surgery), where only blood cells were observed, as expected.

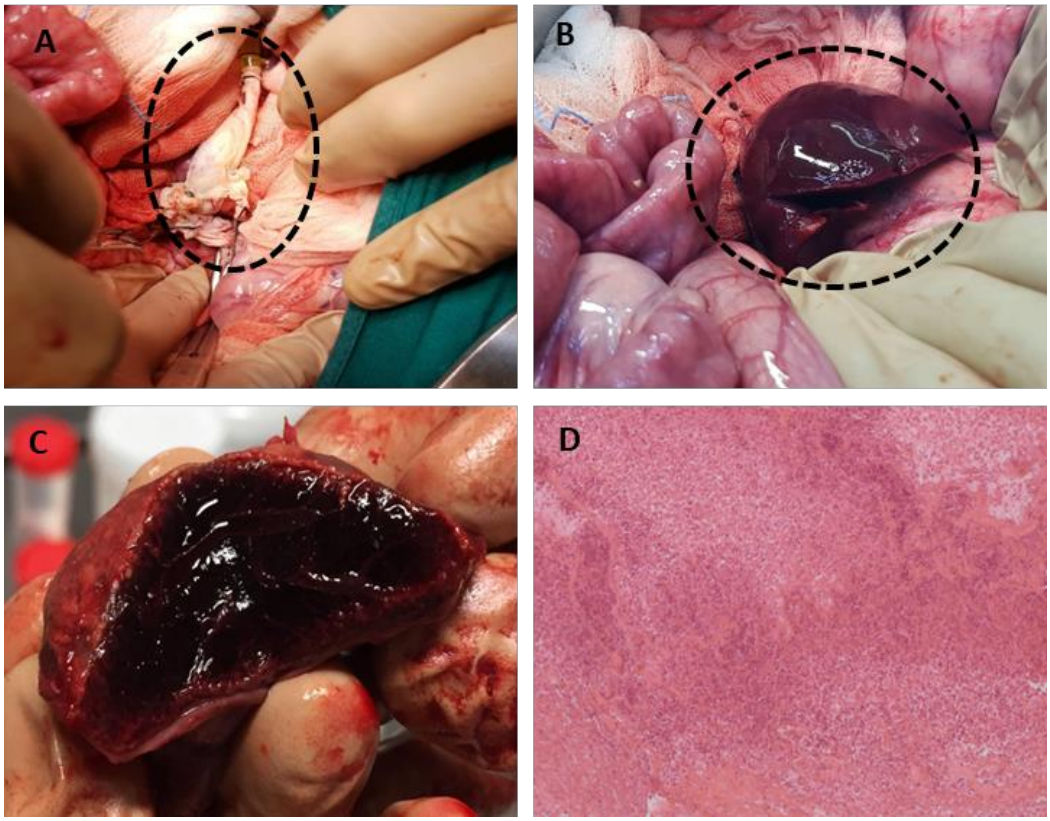

Figure 9. Results from scaffold transplantation into the recipient animal. A) Graft during the vascular anastomosis; **B)** Graft blood perfusion after vessel unclamping; **C)** Macroscopic view of graft aspect after 15d post-surgery**; D)** H&E staining microscopic view of the graft. H&E picture at 10x.

DISCUSSION

The animal model developed in this thesis work represents a novel strategy for liver regeneration. The set-up of our designed porcine model has been a constant learning process in which we have been working for the last 2 years.

Despite advanced necrotic status in several grafts from group 1 was observed, some recipients presented also graft hypertrophy, what would suggest that our defined porcine animal model is suitable for triggering liver regeneration bypassing the native liver. Our main problem was controlling blood coagulation and anticoagulation; however, our last surgery (Tx30) displayed very promising results, with a more efficient blood anticoagulation control, which allowed the survival of a functional graft up to 8 days. Another probe of the suitability of this model are the results obtained from the biochemical analyses, suggesting that our technical procedure is compatible with the preservation of recipient's hepatic functions after suffering the portocaval shunt and graft transplantation (Fig.5).

Results from the surgery performed in group 2 also displayed excellent results, because the resultant scaffold obtained after liver decellularization preserved an optimal texture/consistency to be properly anastomosed to the recipient's host vasculature. This is an important step to take into account because future porcine bioengineered grafts' texture/consistency would be more similar to that of a decellularized scaffold than that of native liver tissue, so surgical conditions for transplantation needed to be considered too.

Finally, there is still work to do on the accurate control of blood anticoagulation, to extend graft survival for a longer period of time after transplantation. Ultimately, we believe we were able to develop a novel porcine model of liver transplantation amenable to liver regeneration, which enables the ultimate test of human size bioengineered livers *in vivo*.

CONCLUSIONS

1. We have established an adequate porcine model for the transplantation of bioengineered liver grafts and allow them to regenerate.
    a. Partial hepatectomy did not help our model and added surgical complications. Latero-terminal portocaval shunt and portal blood inflow calibration after transplantation are sufficient parameters to avoid SFSS and allow graft hypertrophy.
    b. More surgeries are need to finally control porcine anticoagulation in order to avoid graft thrombosis and necrosis.
2. Our resultant scaffolds from porcine liver decellularization have an adequate texture to be anastomosed to recipient's vasculature.

BIBLIOGRAPHY

1. Michalopoulos, G.K. Liver regeneration. *J Cell Physiol* **213**, 286-300 (2007).
2. Tao, Y., Wang, M., Chen, E. & Tang, H. Liver Regeneration: Analysis of the Main Relevant Signaling Molecules. *Mediators Inflamm* **2017**, 4256352 (2017).
3. Sun, G. & Irvine, K.D. Control of growth during regeneration. *Curr Top Dev Biol* **108**, 95-120 (2014).
4. Alison, M.R., Poulsom, R. & Forbes, S.J. Update on hepatic stem cells. *Liver* **21**, 367-373 (2001).
5. Michalopoulos, G.K. Liver regeneration: alternative epithelial pathways. *Int J Biochem Cell Biol* **43**, 173-179 (2011).
6. Prior, N., Inacio, P. & Huch, M. Liver organoids: from basic research to therapeutic applications. *Gut* **68**, 2228-2237 (2019).

7. Francavilla, A., Porter, K.A., Benichou, J., Jones, A.F. & Starzl, T.E. Liver regeneration in dogs: morphologic and chemical changes. *J Surg Res* **25**, 409-419 (1978).
8. Sigel, B. Partial Hepatectomy in the Dog. A Revised Technique Based on Anatomic Considerations. *Arch Surg* **87**, 788-791 (1963).
9. Court, F.G.*, et al.* Subtotal hepatectomy: a porcine model for the study of liver regeneration. *J Surg Res* **116**, 181-186 (2004).
10. Court, F.G.*, et al.* Segmental nature of the porcine liver and its potential as a model for experimental partial hepatectomy. *Br J Surg* **90**, 440-444 (2003).
11. Michalopoulos, G.K. Liver regeneration after partial hepatectomy: critical analysis of mechanistic dilemmas. *Am J Pathol* **176**, 2-13 (2010).
12. Skov Olsen, P.*, et al.* Influence of epidermal growth factor on liver regeneration after partial hepatectomy in rats. *Hepatology* **8**, 992-996 (1988).
13. Hou, C.T.*, et al.* Portal venous velocity affects liver regeneration after right lobe living donor hepatectomy. *PLoS One* **13**, e0204163 (2018).
14. Thomson, R.Y. & Clarke, A.M. Role of portal blood supply in liver regeneration. *Nature* **208**, 392-393 (1965).
15. Moolten, F.L. & Bucher, N.L. Regeneration of rat liver: transfer of humoral agent by cross circulation. *Science* **158**, 272-274 (1967).
16. Lorenz, L.*, et al.* Mechanosensing by beta1 integrin induces angiocrine signals for liver growth and survival. *Nature* **562**, 128-132 (2018).
17. Asakura, T.*, et al.* Portal vein pressure is the key for successful liver transplantation of an extremely small graft in the pig model. *Transpl Int* **16**, 376-382 (2003).
18. Kelly, D.M.*, et al.* Porcine partial liver transplantation: a novel model of the "small-for-size" liver graft. *Liver Transpl* **10**, 253-263 (2004).
19. Lo, C.M.*, et al.* Minimum graft volume for successful adult-to-adult living donor liver transplantation for fulminant hepatic failure. *Transplantation* **62**, 696-698 (1996).
20. Maema, A.*, et al.* Impaired volume regeneration of split livers with partial venous disruption: a latent problem in partial liver transplantation. *Transplantation* **73**, 765-769 (2002).
21. Kiuchi, T.*, et al.* Small-for-size graft in living donor liver transplantation: how far should we go? *Liver Transpl* **9**, S29-35 (2003).

22. Troisi, R. & de Hemptinne, B. Clinical relevance of adapting portal vein flow in living donor liver transplantation in adult patients. *Liver Transpl* **9**, S36-41 (2003).
23. Troisi, R.*, et al.* Effects of hemi-portocaval shunts for inflow modulation on the outcome of small-for-size grafts in living donor liver transplantation. *Am J Transplant* **5**, 1397-1404 (2005).
24. Demetris, A.J.*, et al.* Pathophysiologic observations and histopathologic recognition of the portal hyperperfusion or small-for-size syndrome. *Am J Surg Pathol* **30**, 986-993 (2006).
25. Rajekar, H. Small-for-size syndrome in adult liver transplantation: A review. *Indian Journal of Transplantation* **7**, 53-58 (2013).
26. Couinaud, C. [Liver lobes and segments: notes on the anatomical architecture and surgery of the liver]. *Presse Med* **62**, 709-712 (1954).
27. Athanasiou, A.*, et al.* Extended hepatectomy using the bipolar tissue sealer: an experimental model of small-for-size syndrome in pigs. *J BUON* **21**, 1403-1409 (2016).
28. Chari, R.S.*, et al.* Brief report: treatment of hepatic failure with ex vivo pig-liver perfusion followed by liver transplantation. *N Engl J Med* **331**, 234-237 (1994).
29. Spetzler, V.N.*, et al.* Technique of porcine liver procurement and orthotopic transplantation using an active porto-caval shunt. *J Vis Exp*, e52055 (2015).
30. Vogel, T.*, et al.* Successful transplantation of porcine liver grafts following 48-hour normothermic preservation. *PLoS One* **12**, e0188494 (2017).
31. Wittauer, E.M.*, et al.* Porcine model for the study of liver regeneration enhanced by non-invasive 13C-methacetin breath test (LiMAx test) and permanent portal venous access. *PLoS One* **14**, e0217488 (2019).
32. Kahn, D., Hickman, R., Terblanche, J. & von Sommoggy, S. Partial hepatectomy and liver regeneration in pigs--the response to different resection sizes. *J Surg Res* **45**, 176-180 (1988).
33. Nagashima, I., Bergmann, L., Alsina, A.E. & Schweizer, R.T. Auxiliary heterotopic partial liver transplantation in pigs with acute ischemic liver failure. *Hepatogastroenterology* **44**, 1426-1431 (1997).
34. Marubayashi, S.*, et al.* Auxiliary heterotopic partial liver transplantation in pigs with acute liver failure. *Surg Today* **25**, 429-432 (1995).

35. Cuschieri, A., Baker, P.R., Holley, M.P. & Hanson, C. Portacaval shunt in the pig 1. Effect on survival, behavior, nutrition, and liver function. *J Surg Res* **17**, 387-396 (1974).
36. Gonzalez, H.D., Liu, Z.W., Cashman, S. & Fusai, G.K. Small for size syndrome following living donor and split liver transplantation. *World J Gastrointest Surg* **2**, 389-394 (2010).

FINAL CONCLUSIONS

1. We were able to establish a protocol for rat liver ECM revascularization, controlling pressure conditions and culture media, which allowed the generation of a complete vascular tree *in vitro* where large, intermediate and small vessels were created *de novo*.

2. Our collaboration with the research group of Dr. Bart Spee and Dr. Hans Clevers from Utrecht University showed a novel strategy for the generation of hepatocyte-like cells *in vitro*, paving the way for the generation of large amounts of these cells that are required for liver recellularization.

3. We have established a novel porcine model adequate for the transplantation and regeneration of bioengineered liver grafts.

CONCLUSIONES FINALES

1. Pudimos establecer un protocolo para la revascularización de *ECM* de hígado de rata, controlando las condiciones de presión y los medios de cultivo, lo que permitió la generación *in vitro* de un árbol vascular completo, donde se crearon *de novo* vasos grandes, intermedios y pequeños.

2. Nuestra colaboración con el grupo de investigación del Dr. Bart Spee y el Dr. Hans Clevers de la Universidad de Utrecht mostró una estrategia novedosa para la generación *in vitro* de células similares a hepatocitos, allanando así el camino para generar las grandes cantidades de estas células que se requieren para la recelularización de hígado.

3. Hemos establecido un nuevo modelo porcino adecuado para el trasplante y la regeneración de injertos hepáticos de bioingeniería.